Award Number: W81XWH-12-2-0035

TITLE: Gram-Negative Bacterial Wound Infections

PRINCIPAL INVESTIGATOR: Luis A. Actis

CONTRACTING ORGANIZATION: Miami University
Oxford, OH 45056

REPORT DATE: July 2016

TYPE OF REPORT: Final

PREPARED FOR: U.S. Army Medical Research and Materiel Command
Fort Detrick, Maryland 21702-5012

DISTRIBUTION STATEMENT: Approved for Public Release;
Distribution Unlimited

The views, opinions and/or findings contained in this report are those of the author(s) and should not be construed as an official Department of the Army position, policy or decision unless so designated by other documentation.

REPORT DOCUMENTATION PAGE

Form Approved
OMB No. 0704-0188

1. REPORT DATE	2. REPORT TYPE	3. DATES COVERED
July 2016	Final	1May2012 – 30Apr2016

4. TITLE AND SUBTITLE

Gram-Negative Bacterial Wound Infections

5a. CONTRACT NUMBER
W81XWH-12-2-0035

5b. GRANT NUMBER

5c. PROGRAM ELEMENT NUMBER

6. AUTHOR(S)
Luis A. Actis

E-Mail: actisla@miamioh.edu

5d. PROJECT NUMBER

5e. TASK NUMBER

5f. WORK UNIT NUMBER

7. PERFORMING ORGANIZATION NAME(S) AND ADDRESS(ES)
University of Miami
Oxford, OH 45056

8. PERFORMING ORGANIZATION REPORT NUMBER

9. SPONSORING / MONITORING AGENCY NAME(S) AND ADDRESS(ES)

U.S. Army Medical Research and Materiel Command
Fort Detrick, Maryland - 21702-5012

10. SPONSOR/MONITOR'S ACRONYM(S)

11. SPONSOR/MONITOR'S REPORT NUMBER(S)

12. DISTRIBUTION / AVAILABILITY STATEMENT

Approved for Public Release; Distribution Unlimited

13. SUPPLEMENTARY NOTES

14. ABSTRACT

Experimental data collected during the studies supported by this award showed that all tested *Acinetobacter baumannii*, *Escherichia coli, Klebsiella pneumoniae and Pseudomonas aeruginosa* military wound isolates are iron-uptake proficient and form biofilms on plastic surfaces found in medical elements and settings. In the case of *A. baumannii*, the finding that the virulence of the AB5075 MRSN model isolate depends on the expression of active iron acquisition functions supports the hypothesis that these functions could be used as an antimicrobial target. Accordingly, our data indicate that Ga-PPIX is the most effective antibacterial agent we tested because of its negative effects on bacterial iron metabolism. Although this non-ferric metalloporphyrin derivative displayed variable activity against *E. coli*, *K. pneumoniae* and *P. aeruginosa*, it showed antibacterial activity against all *A. baumannii* tested strains, including MRSN and non-MRSN isolates under standard bacteriological conditions, independently of their time and site of isolation, multi drug resistance phenotypes and iron content of the media. Furthermore, *ex vivo* and *in vivo* studies using the A549 human alveolar epithelial cells as well as the *G. mellonella* and mouse wound infection models showed that Ga-PPIX has significant antibacterial activity by inhibiting the metabolism of iron *A. baumannii* could scavenge from host's extracellular and intracellular sources. The role of the latter sources is supported by the observation that all *A. baumannii* MRSN tested isolates express iron-regulated phospholipase C (PLC) activity, the inactivation of which negatively affects virulence. Furthermore, the PLC activity and virulence responses were significantly reduced by the presence of the competitive inhibitor miltefosine. These findings suggest that treatment of infections with Ga-PPIX and miltefosine, a combination that would affect iron metabolism and the availability of host iron sources, respectively, could be an effective approach to treat *A. baumannii* infections, including those associated with severe wounds. Regarding the possibility of using biofilm biogenesis as an antimicrobial target, our studies using compounds already described as antibiofilm/antivirulence agents for other pathogens showed not only moderate inhibitory effects, but also the capacity of some of the tested compounds to either enhance *A. baumannii*'s capacity to form biofilms on the surface of human epithelial cells or even increase virulence. These responses could be due to the expression of unique uncharacterized cellular functions, which could be identified by conducting comparative genomic analyses of the MRSN strains we have sequenced during this project.

15. SUBJECT TERMS
Nothing listed

16. SECURITY CLASSIFICATION OF:			17. LIMITATION OF ABSTRACT	18. NUMBER OF PAGES	19a. NAME OF RESPONSIBLE PERSON
a. REPORT	b. ABSTRACT	c. THIS PAGE			USAMRMC
Unclassified	Unclassified	Unclassified	Unclassified	112	19b. TELEPHONE NUMBER *(include area code)*

Standard Form 298 (Rev. 8-98)
Prescribed by ANSI Std. Z39.18

Table of Contents

Page

1. Introduction

The overall purpose of this research effort is to determine the role iron acquisition and biofilm functions expressed by Gram-negative pathogens play in the pathogenesis of severe infections in the Wounded Warrior because of polytrauma and blast injuries. The information collected with these studies will be used to explore the efficacy of different chemical and biological agents to block these potential virulence functions using appropriate experimental infection models. These studies have the potential of providing not only new basic information on the pathobiology of bacteria that cause serious infections, but also facilitating the development of new and more effective therapeutics to treat severe Gram-negative infections in wounded military personnel.

2. Body

Targeting iron uptake functions

Siderophore-mediated iron acquisition functions as antibacterial targets

Work done throughout this project has shown that *Acinetobacter baumannii*, *Pseudomonas aeruginosa*, *Klebsiella pneumoniae* and *Escherichia coli* military wound isolates are able to acquire essential iron under limiting conditions when tested using laboratory conditions. The *A. baumannii* tested strains included 29 isolates selected from the Multidrug-Resistant Organism Repository and Surveillance Network (MRSN) strain collection at the Walter Reed Army Institute of Research (WRAIR). These strains were selected because of their isolation site, antibiotic resistance phenotypes and pulse field gel electrophoresis (PFGE) characteristics. The clinical type strains ATCC 19606^T, ATCC 17978, and AYE, which we purchased from the American Type Culture Collection (ATCC), as well as the strain ACICU, which was provided to us by Dr. Daniel V. Zurawski from WRAIR, were included in these studies. These four strains, which are not MRSN isolates, were used as controls since their iron acquisition and biofilm formation properties were reported previously (1-6).

Overall, biological assays, HPLC and chemical analyses of iron-chelated culture supernatants showed that the iron uptake capacity of the *A. baumannii* MRSN isolates is mainly due to the production of catechol-derived siderophores, some of which could be different from the acinetobactin siderophore initially described in the ATCC 19606^T strain (1), while others are potentially similar or identical to acinetobactin. Interestingly, all tested strains were able to promote the growth an ATCC 19606^T *basD* acinetobactin-deficient mutant when cultured under iron-chelated conditions, independently of their capacity to produce proteins involved in acinetobactin biosynthesis or active transport of ferric acinetobactin complexes. All these observations indicate that unrelated *A. baumannii* isolates produce different iron chelators that can be used by other strains as xenosiderophores to grow under iron limitation. This outcome implies that selecting a particular siderophore-mediated iron acquisition system as an antibacterial target may not be effective in the case of infections caused by more than one *A. baumannii* strain or polymicrobial infections caused by different siderophore-producing pathogens. Furthermore, our preliminary flow-cytometry assays using polyclonal antibodies against surface proteins, including the acinetobactin outer membrane receptor protein BauA, did not produce definite results showing the interaction of polyclonal antibodies against surface exposed *A. baumannii* proteins, some of which could be involved in iron acquisition.

The collection of *A. baumannii* tested strains included the wound isolate AB5075, which was selected as a model strain to study the virulence of this pathogen because of its high virulence and multidrug resistance (MDR) phenotypes as proposed in our report (7) (see Appendix 1). Functional and mutagenesis analyses showed that the ability of this strain to grow under iron-chelated laboratory conditions depends on the active expression of the acinetobactin-mediated iron acquisition system as we described for the ATCC 19606^T strain (1). AB5075 isogenic transposon insertion derivatives, which were selected from an ordered transposon mutant library generated by Dr. C. Manoil (University of Washington) containing insertions in most non-essential genes (8), affected in the expression of the *entA* and *entB* acinetobactin biosynthetic genes and the *bauA* coding for the acinetobactin outer membrane protein BauA, showed a significant growth impairment when cultured in bacteriological media containing the iron chelator 2,2'-dipyridyl (DIP) (data not shown). Furthermore, insertion inactivation of these genes also affected the virulence of AB5075. The data displayed in figures 1 and 2 show that AB5075 causes infection and kills invertebrate and vertebrate hosts only when fully expressing the acinetobactin system; inactivation of the *entA, entB* and *bauA* genes resulted in a significant reduction in animal mortality. These observations supported our decision of using AB5075 at the model MRNS strain to conduct further studies exploring the value of iron-acquisition/metabolism inhibitors as antibacterial agents.

Since most *A. baumannii* MRSN isolates produce dihydroxybenzoic-(DHBA)-based siderophores, we decided to explore the effect of salicylic acid derivatives on the iron utilization capacity of these clinical isolates because of their potential inhibitory effects on the biosynthesis of DHBA derivatives (9). Unfortunately, compounds such as sodium salicylate, 5-chlorosalicylic acid, salicylamide, diflunisal, 5-sulfosalicylic acid, 2-hydroxy-5-nitrobenzoic acid, 5-aminosalicylic acid, and 4-aminosalicylic acid were non-inhibitory or showed inhibitory effects only at high concentrations (in the micromolar to millimolar range), which most likely do not have therapeutic values. Attempts made by other investigators to target specific acinetobactin biosynthetic enzymes, such as BasE, also failed. Although a non-nucleoside inhibitor showed high affinity to this enzyme, it did not display antimicrobial effects when tested using *A. baumannii* cells cultured under iron-chelated conditions (10). We also considered the possibility of testing antibiotics conjugated to siderophore moieties, compounds that are known as sideromycins (11), which could have an enhanced antimicrobial activity when compared to the native antibiotic. However, we decided not to pursue this avenue because of the recent report showing that a siderophore-conjugated monobactam derivative, which displayed a significant minimal inhibitory concentration (MIC) reduction when compared to the unconjugated antibiotic when tested under standard laboratory conditions, failed as an antimicrobial agent against *P. aeruginosa* when tested in animal infection models (12). Such a failure could be due to a competition between the monobactam-catechol derivative and the natural siderophore produced by *P. aeruginosa* during infection. Based on this observation, it is possible to speculate that a similar negative outcome could be attained with a β-lactam sideromycin derivative recently developed as an effective antibiotic against *A. baumannii* (13). This possibility is supported by the investigators' report showing that this sideromycin is also antagonized by the natural siderophore produced by the strain ATCC 17961, which most likely is acinetobactin, when tested using standard laboratory conditions.

All the results collected with the *A. baumannii* MRSN isolates together with our observation that strains such as AYE produce the hydroxamate siderophore baumannoferrin but not a catechol siderophore (3), indicate that targeting particular siderophore-mediated iron acquisition functions may be more challenging and less effective than predicted. This is due not only because of the insensitivity of siderophore biosynthetic enzymes to specific inhibitors by unknown mechanisms, but also to the production of structurally different siderophores and the ability of different isolates to use xenosiderophores produced by different bacterial pathogens during polymicrobial infections.

Iron utilization functions as antibacterial targets

The observations reported above prompted us to explore other Fe-based antibacterial alternatives, which could effectively affect the ability of *A. baumannii* to acquire and use this essential metal during host-pathogen interactions. For this purpose, we tested the effect of gallium nitrate [$Ga(NO_3)_3$] since this compound is currently used in human medicine to treat serious illnesses, such as cancer (14), because of its inability to be reduced under physiological conditions. Standard sensitivity assays showed that all *A. baumannii*, *P. aeruginosa*, *K. pneumonia* and *E. coli* MRSN and non-MRSN tested isolates are sensitive to this compound. However, bacterial sensitivity to gallium nitrate is significantly variable among strains and highly dependent on the iron-free content of the culture medium. These observations seriously affect the antimicrobial predictability of this compound when tested under standard laboratory conditions normally used to determine the MIC of antimicrobial agents used in human medicine. Furthermore, it was recently reported that the *A. baumannii* LAC-4 hyper-virulent isolate displays high tolerance to gallium nitrate (15), an outcome that could be observed with some of the *A. baumannii* MRSN isolates including AB5075, which also displays high virulence MDR phenotypes (7). These observations prompted us to determine the antimicrobial effect of Ga-protoporphyrin IX (Ga-PPIX) on all MRSN and non-MRSN strains we have in our collection. This approach was based on the report that this metalloporphyrin derivative has antimicrobial activity when tested with other pathogens (16-18). Analysis of 42 *A. baumannii* strains, including non-military and military strains, as well as strains representing different clonal lineages and isolates classified as susceptible or MDR showed that Ga-PPIX inhibits the growth of all tested strains when cultured in cation-adjusted Mueller-Hinton broth, with a MIC of 20 µg/ml. This concentration significantly reduced bacterial viability, while 40 µg/ml killed all bacteria after 24-h incubation. The antibacterial activity of Ga-PPIX was independent of the antimicrobial resistance phenotype, clone lineage, and time and site of isolation of strains causing these infections. The report we published in the journal Antimicrobial Agents and Chemotherapy (see Appendix 2) describes the results of this study in more detail.

We also tested the susceptibility of extended-spectrum β-lactamase (ESBL)-producing *E. coli* strains isolated from wounded soldiers and provided to us by Dr. Zurawski (Table 1). Disk diffusion assays showed that not all strains displayed the same susceptibility to Ga-PPIX when cultured on LB agar in the presence or absence of DIP. For example, strains 105438, 105454, 105547 and 109497 were more sensitive to Ga-PPIX than strains 105433 and 108191 only when tested under iron-chelated conditions. Further analysis showed that with the exception of the *K. pneumoniae* 4640 isolate, which showed variable results, all *K. pneumoniae* and *P. aeruginosa* MRSN tested strains were not sensitive to Ga-PPIX independently of the presence or absence of DIP (Table 1). Taken together, these results indicate that not all bacterial pathogens have a comparable Ga-PPIX susceptibility response, an observation that indicates that differences in iron metabolism, particularly those associated with the uptake and utilization of heme, may play a critical role in the antibacterial activity of this non-ferric metalloporphyrin derivative. This observation also questions the potential wide spectrum antibacterial activity of Ga-PPIX, although it seems to be an effective narrow spectrum antibiotic agent for the treatment of *A. baumannii* infections.

The *ex vivo* A549 human alveolar epithelial cell infection model, which we used before to examine the role of the acinetobactin-mediated siderophore system in *A. baumannii*'s virulence (19), was used to further test the antibacterial activity of Ga-PPIX. Tissue culture assays using **submerged** A549 human alveolar epithelial monolayers showed that the recovery of bacteria from infected monolayers was significantly decreased when the medium was supplemented with Ga-PPIX, particularly at a 40-µg/ml concentration as we recently reported (see Fig. 5A and 5B in Appendix 2). We further tested the Ga-PPIX antibacterial activity with an A549 **polarized** cell system, which we developed in our laboratory using the MRSN AB5075 strain because of the role iron acquisition plays in its virulence. This particular experimental infection model mimics more closely the interaction of this pathogen with the host during respiratory infections since the polarized cells have their apical surfaces exposed to air and covered by the surfactant layer normally found in human alveoli. Briefly, A549 cells were seeded from a frozen stock and passaged three times using standard tissue culture medium and dishes. During passaging, A549 cells were maintained in a 5% CO_2 incubator at 37°C in DMEM supplemented with 10% heat inactivated fetal bovine serum and 1% ampicillin and streptomycin. After the third passage, approximately 10^5 A549 cells were seeded into a 24-well trans-well membrane support plate (Corning). Fresh DMEM was exchanged above and below the membrane every day for one week. After the first week, media was aspirated from above and below the membrane and fresh media was replaced below the membrane, but not above to begin the polarization process. Fresh DMEM was exchanged below the membrane for two weeks until the cell layer was confluent, watertight and secreting surfactant as determined by visual inspection. After the last week of polarization, the cells were infected with 10^6 bacteria/ml and maintained with DMEM free of antibiotics until the end of the experiment. After the first 24 h of infection, some of the polarized cell samples were incubated with complete DMEM containing 40 µg/ml of Ga-PPIX, added from a stock solution made with DMSO underneath of the trans-well membranes holding the monolayers. Alternatively, approximately 1-2 µg of Ga-PPIX powder was sprinkled on top of the polarized cell surface. The infected and treated monolayers as well as the sterile untreated and treated samples were then incubated for an additional 24 h before they were prepared for analysis by scanning electron microscopy as we described before (4). This approach showed that feeding from the bottom (Fig. 3B) or adding Ga-PPIX powder on the surface (Fig. 3C) of sterile polarized monolayers cause neither detectable cell damage nor drastic effects on the production of the surfactant layer covering the surface of the A549 cells when compared with the untreated non-infected negative control (Fig. 3A). The infection of the A549 polarized monolayers with AB5075 bacteria resulted in significant cell damage as well as a drastic reduction of the surfactant layer (compare panels A and D of Fig. 3). In contrast, the presence of Ga-PPIX in the DMEM medium underneath the membrane insets or on top of the A549 monolayer significantly reduced the damage AB5075 causes to the epithelial cells as well as the surfactant layer when compared with the untreated infected sample (compare panels E and F with D of Fig. 3). Furthermore, the addition of Ga-PPIX resulted in an increased presence of bacteria attached either to the surfactant layer or the A549 cell surface. These results, which were obtained with an approach that has not been reported so far, strongly indicate that the effect Ga-PPIX on bacterial iron metabolism impairs host-pathogen interactions that could be critical for the pathogenesis of *A. baumannii* human infections, such as severe cases of pneumonia.

The antibacterial activity of Ga-PPIX against *A. baumannii* was further examined using the *Galleria mellonella in vivo* model, which we adapted to confirm the virulence role of the acinetobactin-mediated iron acquisition system (19). The data we recently published showed that infection of larvae with a bacterial inoculum

containing 20 µg/ml and 40 µg/ml Ga-PPIX significantly increased animal survival independently of the time and site of isolation and the MDR phenotypes of the tested strains (see Fig. 5C and 5D in Appendix 2).

The antibacterial activity of Ga-PPIX was also tested using a murine cutaneous wound infection model recently described by Dr. Zurawski and his collaborators to study *A. baumannii* virulence and evaluate the action of antimicrobial agents (20). Considering the results we have obtained with Ga-PPIX using *in vitro* (laboratory conditions using bacteriological media), *ex vivo* (A549 tissue culture assays) and *in vivo* (*G. mellonella* infection) assays and the observation that Ga-PPIX must be dissolved in dimethyl sulfoxide (DMSO), an organic solvent that has potential anti-inflammatory and toxic effects on the host that could affect the outcome of the assays, the objectives of the mouse wound infection studies were to:

1. assess the efficacy of Ga-PPIX treatment on AB5075-infected wounds,
2. determine if DMSO has an effect on AB5075-infected wounds, and
3. determine if Ga-PPIX treatment has an effect on uninfected wounds.

To achieve these goals, mice were treated with cyclophosphamide 4 (Day -4) and 1 (Day -1) day before infection with $5x10^4$ colony forming units (CFU) immediately following surgery (Day 0). For objective #3, mice were injected with the same volume of sterile PBS at Day 0. All mice were treated 4 h and then twice a day (AM/PM) on Day 1 and Day 2 post-infection. Treatments were done by inoculating 50 µl of sterile PBS (PBS control), 20% DMSO (DMSO control) or 60 µg Ga-PPIX solubilized in 20% DMSO under the Tegaderm dressing. The 60 µg Ga-PPIX dose was chosen based on previous animal infection experiments in which a lower dose (20 µg) and a higher dose (100 µg) did not effectively prevent infection or had potential toxicity effects, respectively. All animals were infected with a derivative of the *A. baumannii* AB5075 strain that harbors a chromosomal insertion of the *lux* operon (AB5075::lux), which was constructed during this project and can be detected by its luminescence with the IVIS system to determine bacterial burden. Infection experiments were done twice at different times using nine animals per group. Animals were followed daily after infection. The experimental data was analyzed using the Mann-Whitney t-test.

To assess the efficacy of Ga-PPIX treatment on AB5075-infected wounds (objective #1), all tested animals were examined for changes in *clinical signs*, *body weight*, *bacterial burden* and *wound size/time of wound closure*. Regarding *clinical signs*, on Day 2, only 2 out of 9 infected mice (22%) in the DMSO-control group had made nests. In contrast, 9 out of 9 mice (100%) in the Ga-PPIX-treated group had made nests. These results indicate that that mice treated with Ga-PPIX are feeling well and are mobile after infection when compared with those treated with 20% DMSO. Two and one mice for the control and Ga-PPIX-treated groups were euthanized because they were moribund, respectively. Regarding *body weight*, Ga-PPIX-treated infected animals lost significantly less weight during the course of infection compared to the control group treated with 20% DMSO (Fig. 4). Regarding the effect of Ga-PPIX on *bacterial burden* of infected tissues, the presence of this non-ferric metalloporphyrin derivative significantly reduced the number of bacteria in the wounds by Day 1 as determined using either the IVIS system (Fig. 5A and 5C) or standard CFU counts (Fig. 5B). These two detection systems showed a positive correlation in the determination of bacteria present in wounded tissues. However, all panels of figure 5 show that by Day 3 after infection, animals produced comparable bacterial wound counts independently of their treatment with 20% DMSO or 60 µg Ga-PPIX dissolved in 20% DMSO. Regarding *wound size/time of wound closure*, Ga-PPIX treatment prevented wounds from increasing in size compared to the control group (Fig. 6). While not all differences were statistically significant, there were significant differences in wound sizes among control and treated animals between Day 7 and Day 10 post infection. In the case of the experiments conducted on February 19, 2016 (Fig. 6B), the wounds of all tested animals were closed by Day 17 after infection. This observation indicates that Ga-PPIX treatment, as administered in this experiment, did not significantly decrease wound closure time compared to control-treated mice (data not shown). All these observations indicate that Ga-PPIX appears to provide a benefit to mice, at least early on during treatment since the infected animals displayed fewer clinical signs of illness and lose less weight when compared to the infected control group treated only with 20% DMSO. However, by Day 3, one day after the last treatment with Ga-PPIX, the responses of both animal groups were comparable. These outcomes could be due to the quick metabolism of Ga-PPIX, a problem that could be addressed by extending the Ga-PPIX treatment beyond Day 2, although it may cause undesirable toxic symptoms. The poor solubility of Ga-PPIX in an aqueous environment is another explanation for the observations described above. To address this issue, we have investigated the possibility of using alternative delivery methods in collaboration

with Dr. Justin Saul, a member of the Miami University Department of Chemical, Paper and Biomedical Engineering who has experience and expertise with methods and techniques used to effectively deliver therapeutic agents including antimicrobial agents. Our preliminary studies showed that the combination of Ga-PPIX with the lipids dipalmitoylphosphatidylcholine (DPPC) or 1,2-distearoyl-*sn*-glycero-3-phosphocholine (DSPC) resulted in the formation of liposomes that contained this metalloporphyrin derivative as determined by methods normally used to detect the formation of liposomes. Biological tests showed that DPPC and DSPC liposomes are effective tools to deliver Ga-PPIX. We plan to continue this work and explore the use of hydrogels as a tool to treat wound infections with Ga-PPIX in a research project independent of this award we hope will be supported by extramural funds.

To determine if 20% DMSO has an effect on AB5075-infected wounds (objective #2), all tested animals were examined for changes in *body weight*, *bacterial burden* and *wound size/closure*. For this purpose, mice were infected and then treated with either sterile PBS or 20% DMSO as described above. These studies showed that there was no statistical difference in weight loss, bacterial bioluminescence (burden), or wound size between infected animals treated with sterile PBS or 20% DMSO (Fig. 7). These observations suggest that treatment of infected animals with 20% DMSO does not have any detectable negative effects on the animal responses and bacterial burden of infected wounds.

Based on the data collected with the infected animals, we hypothesize that Ga-PPIX dissolved in 20% DMSO is not toxic when compared to the vehicle 20% DMSO since treatment of infected animals with Ga-PPIX resulted in better outcomes than those observed with animals treated with 20% DMSO. To test this hypothesis, wounded uninfected animals were treated with either 20% DMSO or 60 µg Ga-PPIX/wound dissolved in 20% DMSO (objective #3). Figure 8A shows that there was no statistical difference in weight loss between the two animal groups, an indication that DMSO has no detectable effect on the host. However, we were a bit surprised to see that all the 20% DMSO-treated wounds closed by Day 8, while most of the Ga-PPIX-treated wounds did not close until Day 13 (Fig. 8B), with only one of the Ga-PPIX wounds closed by Day 8. These data would suggest that Ga-PPIX may be hindering healing in some way compared to 20% DMSO, even though we see the opposite result in the AB5075-infected mice. It should be noted that for these experiments, the animal groups were smaller – 5 rather than 9 mice per group – when compared to the AB5075::lux infection studies described above, an experimental condition that may have an effect on the measured outcomes.

Overall, the data collected using the mouse wound infection model indicate that treatment of infected animals with 60 µg Ga-PPIX per wound for two days after infection with *A. baumannii* AB5075 is beneficial, at least early on during treatment. Infected mice display fewer clinical signs of illness and lose less weight. Accordingly, Ga-PPIX treatment significantly reduced wound bacterial burden on Day 1 post infection. However, no significant differences were observed between the control and test animals by Day 3, one day after Ga-PPIX treatment was discontinued. As mentioned before, this outcome could reflect a significant reduction in the amount of Ga-PPIX available in the wounds, which could be due to its fast metabolism by the host by unknown mechanisms or problems associated with the poor solubility of this non-ferric metalloporphyrin derivative in an aqueous environment such as that found in the wounds. Ga-PPIX treatment also prevents wounds from getting as large as control-treated wounds, although it does not appear to decrease wound closure time. The latter outcome could also be due to issues related to Ga-PPIX concentration and solubility. Importantly, the control experiments showed that the antibacterial benefits of Ga-PPIX dissolved in 20% DMSO are due to the presence of this non-ferric metalloporphyrin derivative and not to the vehicle used to deliver it to the wounds, without affecting the overall fitness of uninfected animals. Although these observations are encouraging, the overall outcomes of these animal experiments do not warrant the implementation of the porcine wound model, which is a more costly and involving model, until some of the aforementioned issues related to the solubility of Ga-PPIX solubility and metabolism are properly addressed. Because of these considerations, the porcine wound model was not implemented during this project.

Targeting biofilm biogenesis functions

The initial screening of all MRSN isolates showed that they form biofilms on abiotic surfaces, such as glass and polystyrene, when cultured statically 37°C in LB broth. However, we observed a significant variation in the amount of biofilms formed by these strains on these surfaces, which are normally found in medical settings and devices that could serve as reservoirs and facilitate the development of nosocomial infections. This outcome

was apparent among the *A. baumannii* tested strains, which included MRSN and non-MRSN isolates. Table 2 shows the amount of biofilm formed by these isolates is variable independently of the nature of the solid substratum, the iron-chelated culture conditions as well as the production of the CsuA/BABCDE usher-chaperone mediated pili, which plays a critical role in the adherence and biofilm biogenesis capacity of the *A. baumannii* ATCC 19606^T isolate (4). A similar outcome was observed when these strains were tested for surface (Table 2) and twitching (data not shown) motility, cell responses that could play a role in the virulence of this pathogen. Interestingly, we noticed that the *A. baumannii* AB5075 MRSN isolate, which was selected because its high virulence and MDR phenotypes (7), formed limited amount of biofilms only on plastic under non-chelated conditions and displayed moderate twitching and surface motility, although it did not produce the CsuAB-mediated pili we detected in the ATCC 19606^T type isolate. Taken together, these observations, most of which are in line with our report showing the same lack of correlation among strains of a different set of clinical isolates (21), indicate that different *A. baumannii* isolates, as well as other MRSN pathogens, could use different cellular mechanisms to interact with and persist on different hydrophobic or hydrophilic surfaces. Clearly, this is a challenge for the development of an effective wide- or even a narrow-spectrum biofilm inhibitor.

In spite of the results described above, we decided to test the antibiofilm activity of Virstatin, LED209 and the 2-aminoimidazole compound 1 (2AI-1), which were described as antibiofilm agents for different bacterial pathogens. Virstatin affects virulence regulation in *Vibrio cholerae* by inhibiting the transcriptional regulator ToxT (22). Inhibition of ToxT prevents the expression of the cholera toxin and the toxin co-regulated pilus (TCP). A similar effect was recently shown with *A. baumannii,* incubation with virstatin resulted in decreased biofilm formation in 70% of the tested isolates (23). LED209 has been shown to inhibit QseC, a conserved bacterial membrane histidine sensor kinase that recognizes epinephrine and norepinephrine produced by a host as well as the bacterial autoinducer-3 (AI-3) leading to the increased expression of virulence genes (24). LED209-mediated inhibition of QseC resulted in the inhibition of biofilm formation by pathogenic *E. coli* strains (25). Collaborative work with Dr. J. Cavanagh from North Carolina State University resulted in the observation that 2AI-1 targets bacterial response regulators, specifically BfmR, the master regulator for biofilm formation in *A. baumannii* and significantly affects biofilm biogenesis when tested with the ATCC 19606^T isolate (26).

The ability of the aforementioned compounds to reduce biofilm formation on polystyrene was tested by incubating a selected group of MRSN isolates, which were cultured statically for 24 h at 37°C in polystyrene culture tubes containing LB broth and 0 µM or 25 µM of 2AI-1, LED209 or Virstatin. Biofilm formation was then determined by assessing the retention of crystal violet by bacterial biofilms using the $580_{nm}/600_{nm}$ ratio to normalize the amount of biofilm formed to the cell density of each sample, as previously described (4). Unfortunately, neither LED209 nor Virstatin, which did not affect bacterial growth, significantly reduced the amount of biofilm formed by the tested strains. In contrast, incubation of the MRSN strains listed in Table 3 in LB medium supplemented with 0 µM, 25 µM, 50 µM, 75 µM or 100 µM of 2-AI over a 24-h timeframe in a shaking incubator at 37ºC showed that the effect of 2AI-1 on bacterial growth is diverse within and among genera. Based on the growth inhibitory effects, we classified the strains into 4 categories, with class 1 not being significantly affected by the presence of this compound when compared with unsupplemented medium. Strains belonging to the class 2 response reached significantly lower OD_{600} values, when compared to the response obtained with plain LB broth. Strains belonging to the class 3 response showed a dose-dependent inhibitory effect with a clear delay in bacterial growth, although all cultures showed comparable final growth rates independently of the presence or absence of 2AI-1. Strains belonging to the class 4 response showed a significant increase in the lag phase and almost no growth as the concentration of 2AI-1 added to the medium increased. Overall, our results suggest that the 2AI-1 compound has either a modest or no effect on bacterial growth (class 1), causes the bacterial culture to reach a lower OD_{600} when compared to bacteria incubated in the absence of 2AI-1 (class 2), causes increases in lag phase in a dose-dependent fashion (class 3) or causes increases in lag phase in a dose-dependent fashion with higher doses being bactericidal (class 4). Furthermore, the class 3 response seems to prevail among all tested isolates when compared with the other 2AI-1 growth responses detected in this preliminary study, with class 4 responses being the second most common type. It is interesting to note that incubation of the *bfmR* mutant of the *A. baumannii* ATCC 19606^T type strain, which does not produce the BfmR regulator that controls the pili needed for attachment and biofilm formation (27) and is the target of 2AI-1 (26), in the presence of all 2AI-1 tested concentrations resulted in complete growth inhibition. We are evaluating the significance of this unexpected observation since the ATCC

19606^T *bfmR* mutant produces long filaments that could be more sensitive to 2AI-1, a possibility that seems to be supported by the recent observation that this compound could affect cell membrane permeability and/or stability (28). This observation suggests this compound acts not only by inhibiting the BfmR regulator, but also affects cell viability. Considering these effects on bacterial growth, it is difficult to conclude at this time whether 2AI-1 acts as an antibiofilm or as an antimicrobial agent until more work is done to understand the overall effects of this compound on bacterial physiology. We expect to provide some insights into these issues with the collaborative work we are conducting with Dr. Cavanagh, which we predict will produce enough preliminary data to submit a NIH grant proposal to continue this interesting research avenue.

We further investigated the effect of 2AI-1, LED209 and Virstatin on the interaction of *A. baumannii* AB5075 with the polarized A549 human alveolar epithelial cell model described above. For this purpose, polarized cells were infected with AB5075 and then treated with either 100 µM 2AI-1, 100 µM LED209, or 100 µg/ml Virstatin added to the tissue culture medium used to feed to the polarized cells from underneath the insert membrane. Uninfected untreated and infected untreated polarized cells were used as controls. All samples were then fixed after 72 h of infection and prepared for scanning electron microscopy as we described before (4). This approach showed that when left untreated, AB5075 is able to form robust biofilms and cause significant damage to the surfactant layer on the polarized cells and to the A549 alveolar epithelial cells themselves after 72 h of infection (Fig. 9B) when compared with the uninfected control (Fig. 9A). Treatment of the infected polarized cells with 2AI-1 results in a detectable reduction of biofilms formed on the surface of A549 cells and cell damage (Fig. 9D) when compared with the untreated infected control sample (Fig. 9B). Treatment of the infected A549 with LED209 caused an appreciable increase in biofilm formation on top of the polarized cell layer (Fig. 9F). However, damage to the surfactant and cell layers was hard to evaluate due to the amount of biofilm formed on top of the polarized cells (compare panels F and B of Fig. 9). Finally, treatment of the infected polarized cells with Virstatin caused a drastic effect on the samples. There was no detectable mucin layer and most of the A549 cells were absent (Fig. 9H), and the epithelial cells were lysed or detached from the membranes and therefore lost during sample preparation. The few A549 cells that remained attached to the trans-well membranes showed bacteria adhered on their surfaces (Fig. 9H inset). It is important to note that the addition of 2AI-1, LED 209 or Virstatin to uninfected A549 polarized samples did not cause significant changes when compared with uninfected untreated samples (compare panels A, C, E and G of Fig. 9).

In conclusion, 2AI-1, LED209, and Virstatin treatment not only did not prevent biofilm formation on abiotic and biotic surfaces as well as damage to the mucin layer and the epithelial cells, but also resulted either in an increase of biofilms on the surface of the epithelial cells or a drastic detrimental effect on the A549 cells when the samples were treated with LED209 and Virstatin, respectively. The observation that Virstatin did not have a significant effect on the ability of *A. baumannii* 4795, 5075 and 5711 to form biofilms may also reflect the observation that only 70% of the tested strains are susceptible to this antibiofilm agent (23), an outcome that questions the wide antimicrobial spectrum of this compound. Alternatively, differences in the experimental conditions used in our work when compared with the referenced work could explain the different outcomes observed with these potential antimicrobial agents. Considering the fact that Virstatin inhibits the activity of the *Vibrio cholerae* ToxT transcriptional factor (22), it is possible to speculate that the enhanced damage we detected with this chemical agent is due to the inactivation of an *A. baumannii* AB5075 ToxT related factor that may negatively control the virulence of this strain. If this is the case, the possibility that the application of this antivirulence agent to bacterial pathogens other than *V. cholerae* may cause undesired results should be carefully considered and investigated.

Targeting phospholipases

Since the overall goal of my research program is to understand the cellular and molecular factors involved in the virulence of *A. baumannii*, we have been testing the capacity of this pathogen to lyse vertebrate/human cells as a mechanism that not only causes host cell damage, but also serves as a mean to obtain essential nutrients including iron. Consequently we have investigated the capacity of *A. baumannii* to produce hemolysins since these enzymes have been described as important virulence factors for a wide range of pathogens, including *P. aeruginosa* where the production of phospholipase C has been linked to tissue destruction and pathologies reminiscent of burn infections (29). Since the majority of iron in a vertebrate host is intracellular, the availability of intracellular iron-containing molecules to bacterial pathogens is dependent on the lysis of host cells and subsequent release of these molecules due to cell and tissue damage found in

wounds (30, 31). Analysis of *A. baumannii* representative strains, including MRSN isolates, grown in Chelex 100-treated medium for hemolytic activity demonstrated that this pathogen is increasingly hemolytic to sheep, human and horse erythrocytes, which interestingly contain increasing amounts of phosphatidylcholine in their membranes. Bioinformatic, genetic and functional analyses of 19 *A. baumannii* isolates showed that the genome of each strain contained two phosphatidylcholine-specific phospholipase C (PC-PLC) genes, which were named *plc1* and *plc2*, and their culture supernatants tested positive for PC-PLC activity. Further analyses showed that the transcriptional expression of *plc1* and *plc2* and the production of phospholipase activity increased when bacteria were cultured under iron-chelated conditions, which also affected the expression of the acinetobactin-mediated iron acquisition system. Testing of the *A. baumannii* ATCC 19606^T *plc1*::*aph-FRT*, *plc2*::*aph* and *plc1*::*ermAM/plc2*::*aph* isogenic insertion derivatives demonstrated that only the double *plc1*::*ermAM/plc2*::*aph* PC-PLC mutant expressed significantly reduced cytolytic and hemolytic activity. However, only *plc1* contributed significantly to *A. baumannii* virulence using the *G. mellonella* infection model. Taken together, our data demonstrate that both PLC1 and PLC2, which have diverged from a common ancestor, play a concerted role in hemolytic and cytolytic activities; although PLC1 seems to play a more critical role in *A. baumannii*'s virulence when tested in an animal model. These activities would provide access to intracellular iron stores this pathogen could use during growth in the infected host. Thus, simultaneously targeting bacterial iron metabolic functions with Ga-PPIX, as we reported before, and cytolytic activities, which could provide essential iron, could be a practical and effective approach to treat *A. baumannii* infections, particularly those caused by MDR strains. These results are described in detail in the working draft of a manuscript that will be submitted for publication before the end of the summer of 2016 (see Appendix 3).

Miltefosine is an alkylphosphocholine derivative that has activity against cancer cells; parasites, mainly *Leishmania*; fungi and some pathogenic bacteria (32). In the case of the latter infective agents, miltefosine proved to be an effective antibacterial agent against *P. aeruginosa*; its administration protected animals infected with this pathogen, which also produces phospholipase C (33). Therefore, we decided to test the effect of miltefosine on the hemolytic activity produced by the ATCC 19606^T strain by adding this inhibitor to Fe-depleted trypticase soy broth (TSBD) in concentrations ranging from 0 µM to 12 µm. This approach showed that miltefosine competitively inhibits the hemolytic activity of ATCC 19606^T against horse red blood cells in a dose dependent manner (Fig. 10). The effect of miltefosine was also tested using A549 cells infected or not with *A. baumannii*. Interestingly, incubation of uninfected A549 submerged monolayers with miltefosine ranging in concentration from 0 µM to 50 µM showed that this compound causes a statistically significant ($P < 0.0001$) decrease in the number of viable A549 cells at concentrations at and above 390 nM (Fig. 11A). This is not surprising however considering the use of miltefosine as an anticancer drug and the fact that A549 cells are adenocarcinoma cells isolated from lung tissue (34). Due to this inherent limitation and the lack of a significant impact on the viability of A549 cells below 390 nM, 300 nM miltefosine was chosen as the experimental dosage to determine the feasibility of using miltefosine against *A. baumannii*. Miltefosine significantly decreases cytolysis of A549 submerged monolayers as a result of *A. baumannii* ATCC 19606^T ($P < 0.05$), ATCC 17978 ($P < 0.05$), AYE ($P < 0.05$) and AB5075 ($P < 0.05$) infections highlighting the potential use of this compound as an effective therapeutic agent (Fig. 11B). It is important to note that the addition of miltefosine at a final concentration of 300 nM does not cause significant cytolysis of A549 cells when tested with the Amplex Red Phosphatidylcholine-Specific Phospholipase C Assay Kit (Molecular Probes) using lecithin as a substrate and following the conditions suggested by the manufacturer's protocol (Fig. 11A). We further tested the effect of the addition of 300 nM miltefosine in the interaction of *A. baumannii* AB5075 with A549 polarized human alveolar epithelial cells. Figure 12 shows that infection of the polarized cells with AB5075 bacteria results in extensive cell damage with almost no epithelial cells present at the site of the infection (panel B), an outcome we have consistently observed when using this *ex vivo* experimental approach. In contrast, the presence of 300 nM miltefosine in the culture medium resulted in the presence of polarized cells covered with a layer of surfactant on the surface, where bacteria adhered and formed biofilms without causing the extensive cell damage detected in untreated infected samples (compare panels B and E of Fig. 12). Furthermore, the testing of the ATCC 19606^T strain (Fig. 12, panels C and F), which produced similar results, indicates that the antibacterial activity of miltefosine is not strain specific and independent of the time and site isolation as well as the MDR phenotypes of the clinical isolates.

Bacterial Genomes

With the assistance of a grant-in-aid from Illumina, because the Miami University Center for Bioinformatics and Functional Genomics (CBFG) purchased a MiSeq next generation nucleotide sequencer, we initially sequenced the genomes of one *P. aeruginosa* and three *K. pneumoniae* MRSN isolates provided to us by Dr. Zurawski from WRAIR. We also sequenced the genome of the *K. pneumoniae* ATCC 13883 stain which is being used by other investigators to study different aspects of the pathobiology of this microorganism. This work included not only the proper preparation of the genomic libraries to be sequenced and collection of nucleotide sequence data, but also the utilization of an improved and more convenient gene annotation process that combined the RAST annotation tool with Prokka (35), a software package designed to annotate bacterial genomes (http://www.vicbioinformatics.com/software.prokka.shtml). All this bioinformatics work, which was done in-house in collaboration with Dr. I. Friedberg and his graduate student David Ream, facilitated the overall gene annotation process and produced the properly and conveniently formatted files that were submitted to GenBank to obtain the cognate accession numbers needed to report these sequences in the Genome Announcements manuscript we already published (see Appendix 4). Using the same experimental and bioinformatic approach we also sequenced the genome of *A. baumannii* A155, one of the first CC109 isolates from Argentina that includes a AbaR-type island inserted within *comM*, and the *aac(6')-Ib* gene, which confers resistance to numerous aminoglycosides (36-38). This work resulted in a second Genome Announcements publication (see Appendix 5). We have extended these genome-sequencing efforts to all isolates obtained from WRAIR and Fort Sam that were provided to us by Dr. Zurawski. As shown in Table 3, a total of 41 strains, including 24, 5, 6 and 6 *A. baumannii*, *P. aeruginosa*, *K. pneumoniae* and *E. coli* isolates, respectively, were sequenced using paired-end libraries. The data collected from the 24 *A. baumannii* isolates listed in Table 3 is reported in a manuscript accepted for publication in the journal Genome Announcements (see Appendix 6). The genomic data collected from the *E. coli* and *P. aeruginosa* isolates listed in Table 3 are also reported in manuscripts accepted for publication in the journal Genome Announcements (see Appendix 7 and 8). This genomic information will be useful to us as well as other investigators interested in the pathobiology of these pathogens. As a matter of fact, two investigators interested in the study of *K. pneumoniae* have already contacted us and another colleague of mine, Dr. A. Hauser (Northwestern University, Chicago, IL), has expressed interest in the *A. baumannii* genome sequence data since he is conducting comparative genomic studies with the ultimate goal of understanding the nature of the virulence factors produced by this pathogen. Comparative genomic analyses have the potential for providing a better understanding of the genetic traits associated with the virulence of these pathogens. In the particular case of *A. baumannii*, having this set of genomes will allow us as well as others to examine critical genetic variations among different isolates. For example, we are examining the presence and expression of different operons that potentially code for different pili assembly systems, which could be involved in bacterial adherence and biofilm biogenesis. It has been reported that in addition to the CsuA/BABCDE pili assembly system we described before (4), different *A. baumannii* isolates have the capacity to code for and produce alternative Type I and poorly characterized Type III pili (39), which could be differentially produced in response to unknown extracellular signals. Furthermore, this report (39) indicates that some of the operons may not be expressed because potential single nucleotide polymorphisms. Although interesting and puzzling, the value of the report by Eijkelkamp *et al.* (39) is limited since they analyzed only seven *A. baumannii* isolates. Thus, having the genomes we have sequenced together with others reported by different investigators will facilitate a more comprehensive comparative genomic analysis to determine not only the presence or absence of potentially four or five pili assembly operons, but also how different extracellular signals control their differential expression. A similar rationale could be applied to understand the potential of different isolates to express different iron acquisition functions. Our recent report showed that *A. baumannii* produces and uses the acinetobactin-mediated or the baumannoferrin-mediated siderophore systems to acquire iron (1, 3). Currently, it is not known whether clinical isolates can express both systems at the same time and whether they could use siderophores produced by other strains (xenosiderophores). All this information will be critical to better understand the mechanisms *A. baumannii* uses to interact with the environment and the human host and design proper therapeutics, which would effectively target these bacterial functions that play a critical role in the pathobiology of *A. baumannii*.

3. Key Research Accomplishments

- Demonstration of the capacity of all MRSN tested strains to grow under iron limitation and produce biofilms on abiotic surfaces.

- Demonstration of the key role the acinetobactin-mediated iron acquisition system plays in the ability of *A. baumannii* AB5075 MRSN strain to persist and cause disease and death when tested using invertebrate and vertebrate hosts.
- Demonstration of the ability of AB5075 to use xenosiderophores under iron-chelated conditions, a response that may reflect a potentially negative outcome of poly-microbial wound infections.
- Detection of variable and medium-dependent responses to $Ga(NO_3)_3$ by all MRSN tested strain.
- Observation that although *E. coli*, *P. aeruginosa* and *K. pneumoniae* MDR isolates showed limited sensitivity to Ga-PPIX, all *A. baumannii* tested strains (including MRSN and non-MRSN isolates) showed sensitivity to this metalloporphyrin derivative that inhibits iron metabolism when tested under standard laboratory conditions.
- Demonstration that sensitivity of *A. baumannii* to Ga-PPIX is independent of the site and time of isolation of the strains, their MDR phenotype and the iron content of the medium.
- Detection of effective antibacterial activity by Ga-PPIX against *A. baumannii* when tested *in vivo* using the *G. mellonella* experimental model without causing detectable host effects.
- Detection of antibacterial effect of Ga-PPIX treatment when tested using a wound infection model, although solubility and metabolic issues remain to be elucidated to confirm its role as an effective antibiotic to treat *A. baumannii* wound infections.
- Observation of variable antibacterial effects of Ga-PPIX against tested *E. coli*, *K. pneumoniae* and *P. aeruginosa* MRSN isolates.
- Observation of lack of significant effect of antibiofilm agents used with other pathogens when tested with selected MRSN strains using *in vitro* laboratory conditions and abiotic surfaces.
- Detection of undesirable responses to antibiofilm/antivirulence agents successfully used against other pathogens when AB5075 was tested using the *ex vivo* A549 polarized cell infection model. Presence of LED209 and Virstatin increased AB5075 biofilm formation of the surface of the epithelial cells and caused a potential hyper-virulence response against this human epithelial cell line, respectively.
- Detection of potential virulence role and target value of phospholipases that could provide iron because of the cell/tissue damage they cause during infection.
- Report of MRSN isolates genome sequences that would facilitate comparative genomic studies and the better understanding of genes and gene product potentially involved in their virulence and interaction with the host.

4. Reportable Outcomes

Publications

1. Jacobs, A., M. Thompson, C. Black, J. Kessler, L. Clark, C. McQueary, H. Gancz, J. Moon, Y. Si, M. Owen, J. Hallock, Y. Kwak, A. Summers, C. Li, D. Rasko, W. Penwell, C. Honnold, M. Wise, P. Waterman, E. Lesho, R. Stewart, **L. A. Actis**, T. Palys, D. Craft and D. Zurawski. AB5075, a highly virulent isolate of *Acinetobacter baumannii*, as a model strain for the evaluation of pathogenesis and antimicrobial treatments. mBio, 5, e01076-14, 2014. Acknowledgement of federal support.
2. Arivett, B. A, D. C. Ream, S. E. Fiester, K. Mende, C. K. Murray, M. G. Thompson, S. Kanduru, A. M. Summers, A. L. Roth, D. V. Zurawski, and **L. A. Actis**. Draft genome sequences of *Klebsiella pneumoniae* clinical type strain ATCC 13883 and three multidrug-resistant clinical isolates. Genome Announcements, 3, e01385-14, 2015. Acknowledgement of federal support.
3. Arivett, B., S. Fiester, D. Ream, D. Centrón, M. S. Ramirez, M. Tolmasky, and **L. A. Actis**. Draft genome of the multidrug-resistant *Acinetobacter baumannii* A155 clinical isolate. Genome Announcements, 3, e00212-15, 2015. Acknowledgement of federal support.
4. Arivett, B. A., S. E. Fiester, E. J. Ohneck, W. F. Penwell, C. M. Kaufman, R. F. Relich and **L. A. Actis**. Antimicrobial activity of gallium protoporphyrin IX against *Acinetobacter baumannii* strains displaying different antibiotic resistance phenotypes. Antimicrobial Agent and Chemotherapy, **59**, 7657-7665, 2015. Acknowledgement of federal support.
5. Arivett, B., D. Ream, S. E. Fiester, D. Kidane, and **L. A. Actis**. Draft genomes of *Acinetobacter baumannii* isolates from wounded military personnel. Genome Announcements. Genome Announcements, accepted for publication, 2016. Acknowledgement of federal support.
6. Arivett, B., D. Ream, S. E. Fiester, D. Kidane, and **L. A. Actis**. Draft Genomes of *Escherichia coli* isolates from wounded military personnel. Genome Announcements, accepted for publication, 2016. Acknowledgement of federal support.

7. Arivett, B., D. Ream, S. E. Fiester, D. Kidane, and **L. A. Actis**. Draft Genomes of *Pseudomonas aeruginosa* isolates from wounded military personnel. Genome Announcements, accepted for publication, 2016. Acknowledgement of federal support.
8. Fiester, S. E., B. A. Arivett, R. E. Schmidt, A. C. Beckett, T. Ticak, M. V. Carrier, E. J. Ohneck, M. L. Metz, M. K. Sellin Jeffries and **L. A. Actis.** Iron-regulated phospholipase C activity contributes to the cytolytic activity and virulence of *Acinetobacter baumannii*. Manuscript in preparation. Acknowledgement of federal support.

Books or other non-periodical, one-time publications

Nothing to report.

Conferences and presentations

Podium presentations

1. Shedding light on *Acinetobacter baumannii* virulence. Annual meeting, Ohio Branch American Society for Microbiology, Ashland University, Ashland, Ohio, 2013.
2. Understanding the pathophysiology of Acinetobacter: light at the end of the tunnel. *Acinetobacter* 2013. 9th International Symposium on the Biology of *Acinetobacter*. Cologne, Germany, June 2013.
3. Gram-negative Bacterial Wound Infections. JPC-2 MIDRP In-Progress Review (IPR). Fort Dietrich, Frederick, MD, March 2016.

Poster presentations

1. Fiester, S. E, B. A. Arivett, M. V. Carrier, A. C. Beckett and **L. A. Actis**. Hemolytic activity of *Acinetobacter baumannii.* 19th Annual Midwest Microbial Pathogenesis Conference, Milwaukie, Wisconsin, 2012.
2. Metz, M. L., B. A. Arivett, A. C. Beckett, M. V. Carrier, W. F. Penwell, S. E. Fiester and **L. A. Actis**. Examining hemolytic activity in *Acinetobacter baumannii*. 19th Annual Undergraduate Research Forum, Miami University, April 2013.
3. Metz, M. L., B. A. Arivett, A. C. Beckett, M. V. Carrier, W. F. Penwell, S. E. Fiester and **L. A. Actis**. Phosphatidylcholine-specific phospholipase C activity is responsible for the hemolytic activity of *A. baumannii*. Annual meeting, Ohio Branch American Society for Microbiology, Ashland University, Ashland, Ohio, 2013.
4. Penwell, W.F., D. L. Zimbler, A. C. Beckett, B. A. Arivett, S. E. Fiester, Zurawski, D. V. and **L. A. Actis**. Variability of virulence factors among *Acinetobacter baumannii* isolates obtained from wounded military personnel. 20th Annual Midwest Microbial Pathogenesis Conference, Columbus, Ohio, 2013.
5. Geiger, S. C, B. A. Arivett and **L. A. Actis**. Determining the antimicrobial mode of action of Ga-PPIX on *Acinetobacter baumannii*. Annual meeting, Ohio Branch American Society for Microbiology, The Ohio State University, Columbus, Ohio, 2014.
6. Fiester, S. E., C. C. Nwugo, W. F. Penwell, J. Neary, A. C. Beckett, M.L. Metz, B. A. Arivett, P. L. Connerly, S. M. Menke, A. P. Tomaras and **L. A. Actis**. Iron-regulated cytolytic activity plays a role in the virulence of the human pathogen *Acinetobacter baumannii*. Ohio Branch American Society for Microbiology, The Ohio State University, Columbus, Ohio, 2014.
7. Arivett, B. A., W. F. Penwell, C. M. Kaufman, R. F. Relich, S. E. Fiester and **L. A. Actis**. Gallium protoporphyrin IX inhibits growth of multidrug- resistant *Acinetobacter baumannii.* 114th General Meeting of the American Society for Microbiology, Boston, Massachusetts, 2014.
8. Singh, S., J. C. Luka, I. Soojhawon, E. J. Ohneck, A. C. Jacobs, M. G. Thompson, Y. Alamneh, R. Abu-Taleb, P. Rajaguru, S. M. Noble, **L. A. Actis**, S. D. Tyner, and D. V. Zurawski. A multivalent monoclonal antibody cocktail to prevent and treat Gram-negative skin and soft tissue infections. Poster to be presented at the 2016 Military Health System Research Symposium, Orlando, Florida, 2016.

Patents and licenses

Nothing to report.

Obtained degrees

Nothing to report.

Development of cell lines, tissue, serum repositories or animal models

Nothing to report.

Databases

Genome sequences of the *A. baumannii*, *E. coli*, *K. pneumoniae* and *P. aeruginosa* military and non-military isolates were deposited into GenBank under Bioproject ID PRJNA261239 with the accession numbers reported in the five manuscripts published or submitted for publication in Genome Announcements (see Appendices 4-8).

Funding applied for based on work supported by this award

Nothing to report.

Employment or research opportunities applied for and/or received based on experience/training supported by this award

Dr. W. Penwell, who was a graduate student during this award, was hired by AstraZeneca in part because oh his work with different *A. baumannii* wound isolates and the analysis of the iron acquisition systems they express, particularly that of the AB5075 strain.

Mr. B. Arivett, who was a Senior Research Technician during the entire project and supported by this award, was able to join the graduate program at Middle Tennessee State University to pursue doctoral studies because of the experience and expertise he gained working on this project.

5. Conclusions

The experimental data indicate that all MRSN wound infection isolates are iron uptake proficient and capable of forming biofilms on plastic surfaces normally found in medical elements and settings. Regarding the value of iron acquisition as a therapeutic target, which could be used to treat wound infections caused by MDR strains, the observation that the virulence of the *A. baumannii* AB5075 MRSN model isolate depends on the expression of the acinetobactin-mediated iron acquisition system supports this possibility. Accordingly, our data show that Ga-PPIX is the most effective antibacterial agent we tested because of its negative effects on bacterial iron metabolism. Although this non-ferric metalloporphyrin derivative displayed variable activity against *E. coli*, *K. pneumoniae* and *P. aeruginosa*, it showed antibacterial activity against all *A. baumannii* strains including MRSN and non-MRSN isolates under standard bacteriological conditions. This activity was independent of their time and site of isolation, MDR phenotypes and the iron content of the media. Furthermore, *ex vivo* and *in vivo* studies using the A549 human alveolar epithelial cells as well as the *G. mellonella* and mouse wound experimental infection models showed that Ga-PPIX has significant antibacterial activity against AB5075. All these observations support our hypothesis that targeting iron uptake functions is a logical approach to treat *A. baumannii* infections caused by MDR isolates. Our studies on the role of iron-regulated phospholipase C activity expressed by all *A. baumannii* MRSN tested isolates, which could provide intracellular iron during infection because of tissue and cell damage, further supports the role of iron in wound infections. Furthermore, the observation that miltefosine inhibits this enzymatic activity and affects bacterial virulence suggests that treatment of infections with Ga-PPIX and miltefosine, a combination that would affect iron metabolism and the availability of host iron sources, respectively, could be an effective approach to effectively treat *A. baumannii* infections, including those associated with severe wounds. Regarding the possibility of using biofilm biogenesis as an antimicrobial target, our studies with compounds already described as antibiofilm/antivirulence agents for other pathogens showed not only moderate inhibitory effects, but also the capacity of some of the compounds to either enhance biofilm formation on the surface of human epithelial cells or even increase virulence. These responses could be due to the expression of unique and potentially novel cellular functions, which could be identified by conducting comparative genomic analysis of the *A. baumannii* MRSN strains we have sequenced during this project.

6. References

1. Dorsey CW, Tomaras AP, Connerly PL, Tolmasky ME, Crosa JH, Actis LA. 2004. The siderophore-mediated iron acquisition systems of *Acinetobacter baumannii* ATCC 19606 and *Vibrio anguillarum* 775 are structurally and functionally related. Microbiology **150:**3657-3667.

2. Penwell WF, Arivett BA, Actis LA. 2012. The *Acinetobacter baumannii entA* gene located outside the acinetobactin cluster is critical for siderophore production, iron acquisition and virulence. PLoS One **7:**e36493.
3. Penwell WF, DeGrace N, Tentarelli S, Gauthier L, Gilbert CM, Arivett BA, Miller AA, Durand-Reville TF, Joubran C, Actis LA. 2015. Discovery and characterization of new hydroxamate siderophores, Baumannoferrin A and B, produced by *Acinetobacter baumannii*. Chembiochem **16:**1896-1904.
4. Tomaras AP, Dorsey CW, Edelmann RE, Actis LA. 2003. Attachment to and biofilm formation on abiotic surfaces by *Acinetobacter baumannii*: involvement of a novel chaperone-usher pili assembly system. Microbiology **149:**3473-3484.
5. Zimbler DL, Park TM, Arivett BA, Penwell WF, Greer SM, Woodruff TM, Tierney DL, Actis LA. 2012. Stress response and virulence functions of the *Acinetobacter baumannii* NfuA Fe-S scaffold protein. J Bacteriol **194:**2884-2893.
6. Zimbler DL, Penwell WF, Gaddy JA, Menke SM, Tomaras AP, Connerly PL, Actis LA. 2009. Iron acquisition functions expressed by the human pathogen *Acinetobacter baumannii*. Biometals **22:**23-32.
7. Jacobs AC, Thompson MG, Black CC, Kessler JL, Clark LP, McQueary CN, Gancz HY, Corey BW, Moon JK, Si Y, Owen MT, Hallock JD, Kwak YI, Summers A, Li CZ, Rasko DA, Penwell WF, Honnold CL, Wise MC, Waterman PE, Lesho EP, Stewart RL, Actis LA, Palys TJ, Craft DW, Zurawski DV. 2014. AB5075, a highly virulent isolate of *Acinetobacter baumannii*, as a model strain for the evaluation of pathogenesis and antimicrobial treatments. MBio **5:**e01076-01014.
8. Gallagher LA, Ramage E, Weiss EJ, Radey M, Hayden HS, Held KG, Huse HK, Zurawski DV, Brittnacher MJ, Manoil C. 2015. Resources for genetic and genomic analysis of emerging pathogen *Acinetobacter baumannii*. J Bacteriol **197:**2027-2035.
9. Miethke M, Marahiel MA. 2007. Siderophore-based iron acquisition and pathogen control. Microbiol Mol Biol Rev **71:**413-451.
10. Neres J, Engelhart CA, Drake EJ, Wilson DJ, Fu P, Boshoff HI, Barry CE, 3rd, Gulick AM, Aldrich CC. 2013. Non-nucleoside inhibitors of BasE, an adenylating enzyme in the siderophore biosynthetic pathway of the opportunistic pathogen *Acinetobacter baumannii*. J Med Chem **56:**2385-2405.
11. Braun V, Pramanik A, Gwinner T, Koberle M, Bohn E. 2009. Sideromycins: tools and antibiotics. Biometals **22:**3-13.
12. Tomaras AP, Crandon JL, McPherson CJ, Banevicius MA, Finegan SM, Irvine RL, Brown MF, O'Donnell JP, Nicolau DP. 2013. Adaptation-based resistance to siderophore-conjugated antibacterial agents by *Pseudomonas aeruginosa*. Antimicrob Agents Chemother **57:**4197-4207.
13. Wencewicz TA, Miller MJ. 2013. Biscatecholate-monohydroxamate mixed ligand siderophore-carbacephalosporin conjugates are selective sideromycin antibiotics that target *Acinetobacter baumannii*. J Med Chem **56:**4044-4052.
14. Kelson AB, Carnevali M, Truong-Le V. 2013. Gallium-based anti-infectives: targeting microbial iron-uptake mechanisms. Curr Opin Pharmacol **13:**707-716.
15. de Leseleuc L, Harris G, KuoLee R, Xu HH, Chen W. 2014. Serum resistance, gallium nitrate tolerance and extrapulmonary dissemination are linked to heme consumption in a bacteremic strain of *Acinetobacter baumannii*. Int J Med Microbiol **304:**360-369.
16. Boch J, Nau-Wagner G, Kneip S, Bremer E. 1997. Glycine betaine aldehyde dehydrogenase from *Bacillus subtilis*: characterization of an enzyme required for the synthesis of the osmoprotectant glycine betaine. Arch Microbiol **168:**282-289.
17. Bozja J, Yi K, Shafer WM, Stojiljkovic I. 2004. Porphyrin-based compounds exert antibacterial action against the sexually transmitted pathogens *Neisseria gonorrhoeae* and *Haemophilus ducreyi*. Int J Antimicrob Agents **24:**578-584.
18. Stojiljkovic I, Kumar V, Srinivasan N. 1999. Non-iron metalloporphyrins: potent antibacterial compounds that exploit haem/Hb uptake systems of pathogenic bacteria. Mol Micro **31:**429-442.
19. Gaddy JA, Arivett BA, McConnell MJ, Lopez-Rojas R, Pachon J, Actis LA. 2012. Role of acinetobactin-mediated iron acquisition functions in the interaction of *Acinetobacter baumannii* ATCC 19606^T with human lung epithelial cells, *Galleria mellonella* caterpillars and mice. Infect Immun **80:**1015-1024.
20. Thompson MG, Black CC, Pavlicek RL, Honnold CL, Wise MC, Alamneh YA, Moon JK, Kessler JL, Si Y, Williams R, Yildirim S, Kirkup BC, Jr., Green RK, Hall ER, Palys TJ, Zurawski DV. 2014. Validation of a novel murine wound model of *Acinetobacter baumannii* infection. Antimicrob Agents Chemother **58:**1332-1342.

21. McQueary CN, Actis LA. 2011. *Acinetobacter baumannii* biofilms: variations among strains and correlations with other cell properties. J Microbiol **49:**243-250.
22. Hung DT, Shakhnovich EA, Pierson E, Mekalanos JJ. 2005. Small-molecule inhibitor of *Vibrio cholerae* virulence and intestinal colonization. Science **310:**670-674.
23. Chabane YN, Ben Mlouka M, Alexandre S, Nicol M, Marti S, Pestel-Caron M, Vila J, Jouenne T, De E. 2014. Virstatin inhibits biofilm formation and motility of *Acinetobacter baumannii*. BMC Microbiol **14:**62.
24. Rasko DA, Moreira CG, Li de R, Reading NC, Ritchie JM, Waldor MK, Williams N, Taussig R, Wei S, Roth M, Hughes DT, Huntley JF, Fina MW, Falck JR, Sperandio V**.** 2008. Targeting QseC signaling and virulence for antibiotic development. Science **321:**1078-1080.
25. Curtis MM, Russell R, Moreira CG, Adebesin AM, Wang C, Williams NS, Taussig R, Stewart D, Zimmern P, Lu B, Prasad RN, Zhu C, Rasko DA, Huntley JF, Falck JR, Sperandio V. 2014. QseC inhibitors as an antivirulence approach for Gram-negative pathogens. MBio **5:**e02165.
26. Thompson RJ, Bobay BG, Stowe SD, Olson AL, Peng L, Su Z, Actis LA, Melander C, Cavanagh J. 2012. Identification of BfmR, a response regulator involved in biofilm development, as a target for a 2-aminoimidazole-based antibiofilm agent. Biochemistry **51:**9776-9778.
27. Tomaras AP, Flagler MJ, Dorsey CW, Gaddy JA, Actis LA. 2008. Characterization of a two-component regulatory system from *Acinetobacter baumannii* that controls biofilm formation and cellular morphology. Microbiology **154:**3398-3409.
28. Stowe SD, Thompson RJ, Peng L, Su Z, Blackledge M, Draughn GL, Coe WH, Johannes E, Lapham VK, Mackenzie J, Melander C, Cavanagh J. 2014. Membrane-permeabilizing activity of reverse-amide 2-aminoimidazole antibiofilm agents against *Acinetobacter baumannii*. Curr Drug Deliv. **12:** 223-230.
29. Schmiel DH, Miller VL. 1999. Bacterial phospholipases and pathogenesis. Microbes Infect **1:**1103-1112.
30. Fiester SE, Actis LA. 2013. Stress responses in the opportunistic pathogen *Acinetobacter baumannii*. Future Microbiol **8:**353-365.
31. Yeoh-Ellerton S, Stacey MC. 2003. Iron and 8-isoprostane levels in acute and chronic wounds. J Invest Dermatol **121:**918-925.
32. Dorlo TP, Balasegaram M, Beijnen JH, de Vries PJ. 2012. Miltefosine: a review of its pharmacology and therapeutic efficacy in the treatment of leishmaniasis. J Antimicrob Chemother **67:**2576-2597.
33. Wargo MJ, Gross MJ, Rajamani S, Allard JL, Lundblad LK, Allen GB, Vasil ML, Leclair LW, Hogan DA. 2011. Hemolytic phospholipase C inhibition protects lung function during *Pseudomonas aeruginosa* infection. Am J Respir Crit Care Med **184:**345-354.
34. Eibl H, Unger C. 1990. Hexadecylphosphocholine: a new and selective antitumor drug. Cancer Treat Rev **17:**233-242.
35. Seemann T. 2014. Prokka: rapid prokaryotic genome annotation. Bioinformatics **30:**2068-2069.
36. Lin DL, Tran T, Alam JY, Herron SR, Ramirez MS, Tolmasky ME. 2014. Inhibition of aminoglycoside 6'-N-acetyltransferase type Ib by zinc: reversal of amikacin resistance in *Acinetobacter baumannii* and *Escherichia coli* by a zinc ionophore. Antimicrob Agents Chemother **58:**4238-4241.
37. Ramirez MS, Tolmasky ME. 2010. Aminoglycoside modifying enzymes. Drug Resist Updat **13:**151-171.
38. Ramirez MS, Vilacoba E, Stietz MS, Merkier AK, Jeric P, Limansky AS, Marquez C, Bello H, Catalano M, Centron D. 2013. Spreading of AbaR-type genomic islands in multidrug resistance *Acinetobacter baumannii* strains belonging to different clonal complexes. Curr Microbiol **67:**9-14.
39. Eijkelkamp BA, Stroeher UH, Hassan KA, Paulsen IT, Brown MH. 2014. Comparative analysis of surface-exposed virulence factors of *Acinetobacter baumannii*. BMC Genomics **15:**1020.

7. Appendices

Publications

Appendix 1. Jacobs, A. C., M. G. Thompson, C. C. Black, J. L. Kessler, L. P. Clark, C. N. McQueary, H. Y. Gancz, B. W. Corey, J. K. Moon, Y. Si, M. T. Owen, J. D. Hallock, Y. I. Kwak, A. Summers, C. Z. Li, D. A. Rasko, W. F. Penwell, C. L. Honnold, M. C. Wise, P. E. Waterman, E. P. Lesho, R. L. Stewart, L. A. Actis, T. J. Palys, D. W. Craft, and D. V. Zurawski. AB5075, a highly virulent isolate of *Acinetobacter baumannii*, as a model strain for the evaluation of pathogenesis and antimicrobial treatments. mBio, 5, e01076-14, 2014

Appendix 2. Arivett, B. A., S. E. Fiester, E. J. Ohneck, W. F. Penwell, C. M. Kaufman, R. F. Relich and L. A. Actis. Antimicrobial activity of gallium protoporphyrin IX against *Acinetobacter baumannii* strains

displaying different antibiotic resistance phenotypes. Antimicrobial Agent and Chemotherapy, **59**, 7657-7665, 2015.

Appendix 3. Fiester, S. E., B. A. Arivett, R. E. Schmidt, A. C. Beckett, T. Ticak, M. V. Carrier, E. J. Ohneck, M. L. Metz, M. K. Sellin Jeffries and L. A. Actis**.** Iron-regulated phospholipase C activity contributes to the cytolytic activity and virulence of *Acinetobacter baumannii*. Manuscript in preparation.

Appendix 4. Arivett, B. A, D. C. Ream, S. E. Fiester, K. Mende, C. K. Murray, M. G. Thompson, S. Kanduru, A. M. Summers, A. L. Roth, D. V. Zurawski, and L. A. Actis. Draft genome sequences of *Klebsiella pneumoniae* clinical type strain ATCC 13883 and three multidrug-resistant clinical isolates. Genome Announcements, 3, e01385-14, 2015.

Appendix 5. Arivett, B., S. Fiester, D. Ream, D. Centrón, M. S. Ramirez, M. Tolmasky, and L. A. Actis. Draft genome of the multidrug-resistant *Acinetobacter baumannii* A155 clinical isolate. Genome Announcements, 3, e00212-15, 2015.

Appendix 6. Arivett, B., D. Ream, S. E. Fiester, D. Kidane, and L. A. Actis. Draft genomes of *Acinetobacter baumannii* isolates from wounded military personnel. Genome Announcements. Genome Announcements, accepted for publication, 2016.

Appendix 7. Arivett, B., D. Ream, S. E. Fiester, D. Kidane, and L. A. Actis. Draft Genomes of *Escherichia coli* isolates from wounded military personnel. Genome Announcements, accepted for publication, 2016.

Appendix 8. Arivett, B., D. Ream, S. E. Fiester, D. Kidane, and L. A. Actis. Draft Genomes of *Pseudomonas aeruginosa* isolates from wounded military personnel. Genome Announcements, accepted for publication, 2016.

8. Supporting data
Tables

Table 1. Ga-PPIX sensitivity of *E. coli*, *K. pneumoniae* and *P. aeruginosa* MRSN isolates

Genus/Species	WRAIR	Sensitivity[a] - LB	Sensitivity - LB+DIP
E. coli	105433	-	-
	105438	-	+
	105454	-	+
	105547	-	+
	108191	-	-
	109497	-	+
K. pneumoniae	4640	-	?
	101436	-	-
	101488	-	-
	101712	-	-
	101731	-	-
	105371	-	-
P. aeruginosa	105738	-	-
	105777	-	-
	105819	-	-
	105857	-	-
	105880	-	-

[a]Sensitivity to Ga-PPIX was determined by disk diffusion assays. Each strain was swabbed onto LB plates with and without 100 µM DIP. Sterile disks with 50, 20, and 10 µg Ga-PPIX were applied to the plates. Zones of growth inhibition were assessed after 24 h incubation at 37°C.

Table 2. Production of biofilms, CsuA/B protein and motility of selected MRSN *A. baumannii* isolates

Strain	Plastic[a]		Glass[a]		Production of CsuA/B protein[b]	Motility on 0.3% agarose[c]
	LB	LB +DIP	LB	LB +DIP		
967	++	+	+	++	-	-
2828	++	++	++	++	-	-
3340	++	++	+	-	-	+
3560	++	++	+	-	-	-
3638	++	++	++	+++	-	-
3785	+++	++	-	+	+	-
3806	++	+++	+++	++	-	+
3927	++	++	-	+	-	+
4025	+++	++	+	+	+	+
4026	+++	+++	-	++	+	+
4027	+++	++	+	-	+	+
4052	++	+++	+++	-	+	-
4269	++	+++	+	++	+	-
4448	+	+	+	+	-	+
4456	+	++	+	+	-	+
4490	+	+	++	-	-	+
4498	+++	++	+	++	+	+
4795	++	++	-	-	-	-
4857	+	++	+++	+	-	-
4878	++	+++	+	+	+	-
4932	++	+++	+++	+	+	-
4957	++	+++	+++	+++	+	+
4991	+	++	++	+	-	-
5001	++	+++	+++	+++	+	-
5075	+	-	-	-	-	+
5197	+	+	+	+	-	-
5256	++	+++	+++	++	-	+
5674	+	++	+	++	+	-
5711	++	++	++	++	+	-
19606[§]	+++	+++	+	+++	+	-
17978[§]	++	-	+	-	-	+
ACICU[§]	+	++	+	-	-	-
AYE[§]	+	+	+	+	-	+
19606-BfmR[§]	-	-	-	-	-	-

[a]Biofilm formation was classified as negative (-), weak (+), moderate (++) and strong (+++) when compared with biofilms formed by the ATCC 19606^T and BfmR strains, which were used as positive and negative controls, respectively. [b]Detection of the CsuA/B pilin protein in total bacterial cell lysates using anti-CsuA/B antiserum; (+), positive reaction; (-), negative reaction. [c]Detection of bacterial motility on the surface of 0.3% agarose plates after overnight incubation at 37°C. [§]Control strains. Strain 19606-BfmR is an isogenic derivative of ATCC 19606^T that does not produce pili and does not make biofilms on abiotic surfaces (27).

Table 3. Genome sequencing of military isolates

Sample Name	Organism	Collected by	Collected Date	Isolation source	2 x 250 PE[a]	2 x 75 Mate-PE[b]
AB967	*A. baumannii*	WRAMC Staff	9/23/03	Blood	✔	✔
AB2828	*A. baumannii*	WRAMC Staff	3/28/06	Blood	✔	✔
AB3340	*A. baumannii*	WRAMC Staff	10/22/06	Blood	✔	✔
AB3560	*A. baumannii*	WRAMC Staff	12/14/06	Blood	✔	✔
AB3638	*A. baumannii*	WRAMC Staff	1/10/07	Severe trauma site	✔	✔
AB3785	*A. baumannii*	WRAMC Staff	3/18/07	Blood	✔	✔
AB3806	*A. baumannii*	WRAMC Staff	3/19/07	Severe trauma site	✔	✔
AB3927	*A. baumannii*	WRAMC Staff	5/18/07	Severe trauma site	✔	✔
AB4025	*A. baumannii*	WRAMC Staff	6/24/07	Wound	✔	✔
AB4026	*A. baumannii*	WRAMC Staff	6/26/07	Wound	✔	✔
AB4027	*A. baumannii*	WRAMC Staff	6/26/07	Wound	✔	✔
AB4052	*A. baumannii*	WRAMC Staff	7/16/07	War wound	✔	✔
AB4448	*A. baumannii*	WRAMC Staff	12/25/07	War wound	✔	✔
AB4456	*A. baumannii*	WRAMC Staff	12/30/07	Trach aspirate	✔	✔
AB4490	*A. baumannii*	WRAMC Staff	1/12/08	War wound	✔	✔
AB4498	*A. baumannii*	WRAMC Staff	1/13/08	Blood	✔	✔
AB4795	*A. baumannii*	WRAMC Staff	5/5/08	Severe trauma site, bone	✔	✔
AB4878	*A. baumannii*	WRAMC Staff	6/6/08	War wound	✔	✔
AB4932	*A. baumannii*	WRAMC Staff	7/4/08	Sputum	✔	✔
AB4957	*A. baumannii*	WRAMC Staff	7/17/08	Severe Trauma Site	✔	✔
AB4991	*A. baumannii*	WRAMC Staff	8/3/08	War wound	✔	✔
AB5001	*A. baumannii*	WRAMC Staff	8/5/08	Blood	✔	✔
AB5197	*A. baumannii*	WRAMC Staff	10/15/08	Severe trauma site	✔	✔
AB5674	*A. baumannii*	WRAMC Staff	5/22/09	Blood	✔	✔
105777	*P. aeruginosa*	Fort Sam Staff	4/21/2007	Wound	✔	✔
105819	*P. aeruginosa*	Fort Sam Staff	11/12/2007	Wound	✔	✔
105880	*P. aeruginosa*	Fort Sam Staff	3/26/2008	Thigh	✔	✔
105857	*P. aeruginosa*	Fort Sam Staff	1/28/2008	Right knee	✔	✔
105738	*P. aeruginosa*	Fort Sam Staff	10/7/2006	Chest tube	✔	✔
101436	*K. pneumoniae*	Fort Sam Staff	5/17/06	Wound	✔	✔
101712	*K. pneumoniae*	Fort Sam Staff	10/7/07	Wound	✔	✔
105371	*K. pneumoniae*	Fort Sam Staff	5/22/08	Blood	✔	✔
101488	*K. pneumoniae*	Fort Sam Staff	11/11/06	Wound	✔	✔
101731	*K. pneumoniae*	Fort Sam Staff	1/25/08	Wound	✔	✔
4640	*K. pneumoniae*	WRAMC Staff	Not Collected	Severe trauma site	✔	✔
105454	*E. coli*	Fort Sam Staff	4/12/08	Urine	✔	✔
105547	*E. coli*	Fort Sam Staff	2/4/09	Wound	✔	✔
109497	*E. coli*	Fort Sam Staff	1/20/10	Urine	✔	✔
108191	*E. coli*	Fort Sam Staff	2/17/09	Urine	✔	✔
105433	*E. coli*	Fort Sam Staff	11/14/07	Wound	✔	✔
105438	*E. coli*	Fort Sam Staff	12/17/07	Wound, right thigh	✔	✔

[a]2 x 250 Paired-End sequencing performed with MiSeq v3 reagent

[b]2 X 75 Mate-Pair Paired-End sequencing performed with MiSeq v3 reagent

Figures

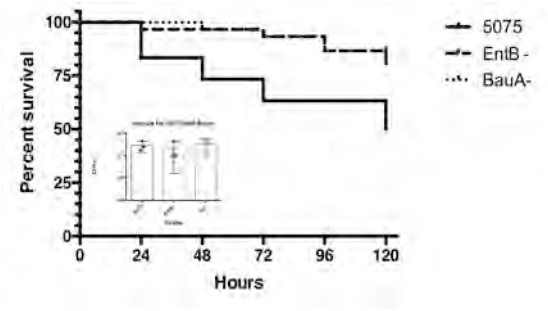

Figure 1. Survival of *G. mellonella* larvae injected with AB5075 and isogenic derivatives affected in iron acquisition functions. *G. mellonella* were assayed every 24 h after injection with 10^5 CFU/ml of *A. baumannii* AB5075 or isogenic derivatives *bauA*::Tn (BauA$^-$) or *entB*::Tn (EntB$^-$) in PBS. Inset shows inocula for each infection. These experiments were done three times using fresh biological samples and 10 caterpillars per bacterial strain each time.

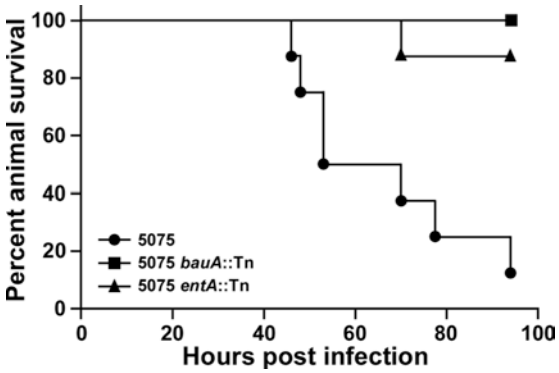

Figure 2. Survival of mice injected with AB5075 and isogenic derivatives affected in iron acquisition functions. Cyclophosphamide-treated mice were intranasally infected with AB 5075 cells (1.4 x 10^6) or cells of the *bauA*::Tn (1.6 x 10^6) or *entA*::Tn (1.3 x 10^6) isogenic derivatives. Animal mortality was scored twice daily for 5 days. Animal experimental procedures were approved by the Institutional Animal Care and Use Committee at WRAIR.

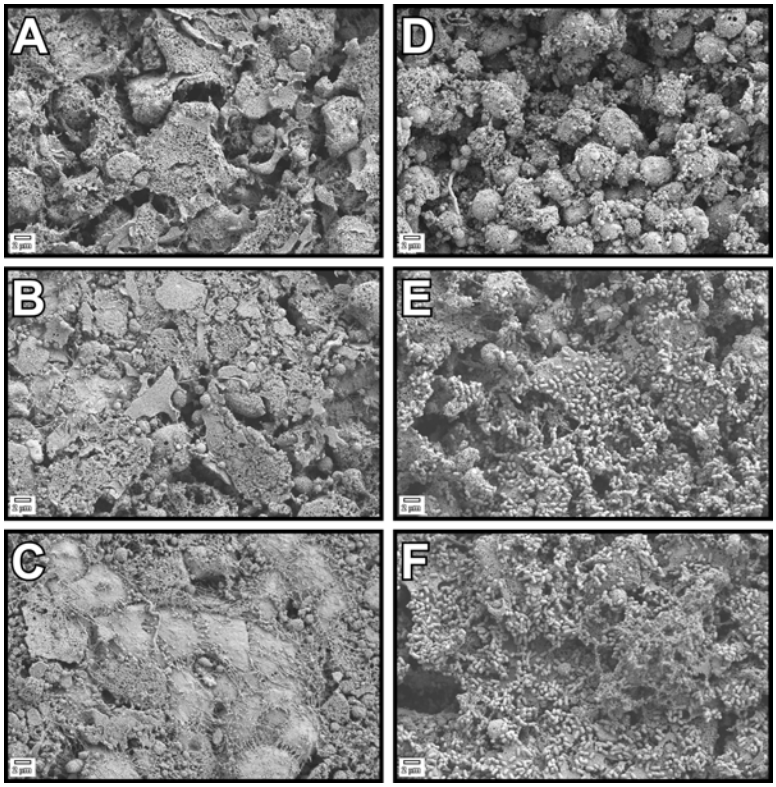

Figure 3. Effects of Ga-PPIX on the interaction of AB5075 with polarized A549 human alveolar epithelial cells. Polarized monolayers were infected with AB5075 either in the absence of Ga-PPIX (D) or the presence of Ga-PPIX that was added to the DMEM medium underneath of the trans-well membranes holding the monolayers (E) or sprinkled as powder on top of the monolayers (F). Uninfected monolayers cultured in the absence (A) or the presence of Ga-PPIX that was added to the DMEM medium underneath of the trans-well membranes holding the monolayers (B) or sprinkled as powder on top of the monolayers (C) were used as negative controls. Samples were treated with Ga-PPIX after 24 h infection and then incubated for an additional 24 h. Uninfected control samples were incubated for 48 h. All samples were fixed and prepared for analysis using scanning electron microscopy.

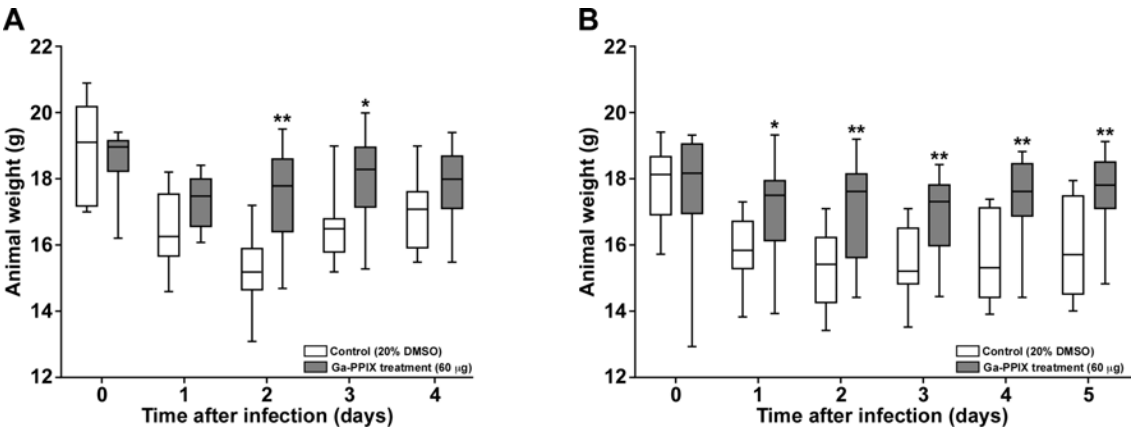

Figure 4. Effect of Ga-PPIX treatment on animal weight. Animals were infected with the AB5075::lux derivative and then treated with either 20% DMSO (control group) or Ga-PPIX (treatment group). The body weight of the animals was monitored daily up to five days after infection. Animal experiments were conducted on January 29, 2016 (A) and February 19, 2016 (B). *$P < 0.05$, **$P < 0.01$.

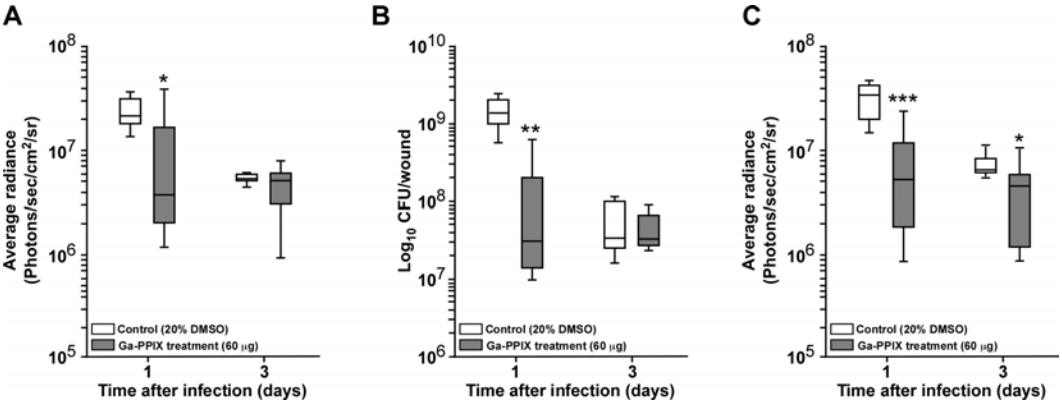

Figure 5. Effect of Ga-PPIX treatment on animal infection. Bacterial wound burden was determined by detecting bioluminescence produced by the AB5075::lux derivative using the IVIS system (A and C) or CFU counts after tissue removal and standard plate counting (B). Animal experiments were conducted on January 29, 2016 (A and B) and February 19, 2016 (C). *$P < 0.05$, **$P < 0.01$, ***$P < 0.001$.

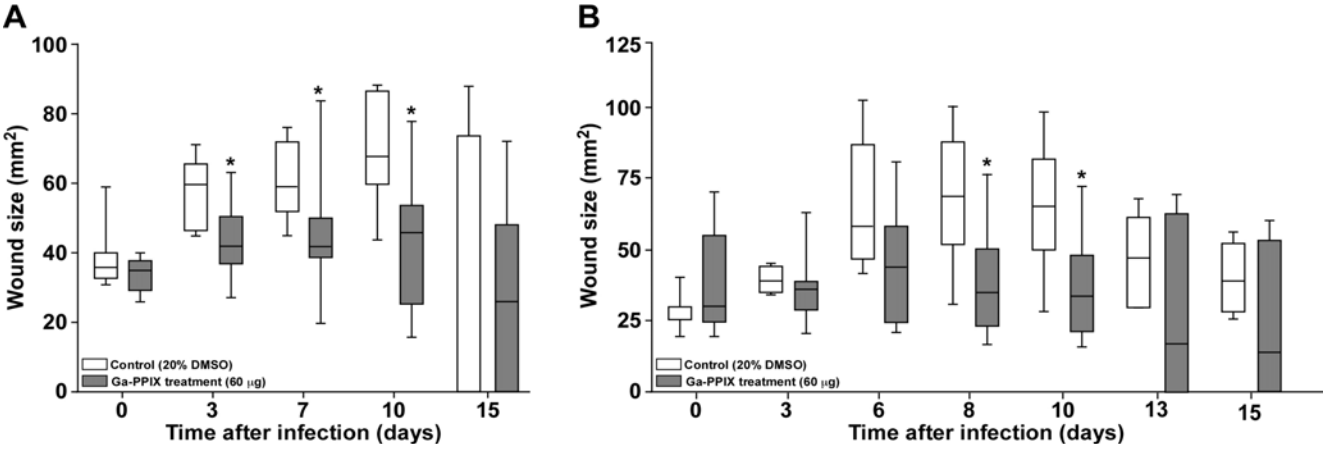

Figure 6. Effect of Ga-PPIX treatment on wound size and closure. Wound size and closure were determined in infected animals treated with 20% DMSO or Ga-PPIX dissolved in 20% DMSO. Animal experiments were conducted on January 29, 2016 (A) and February 19, 2016 (B). *$P < 0.05$.

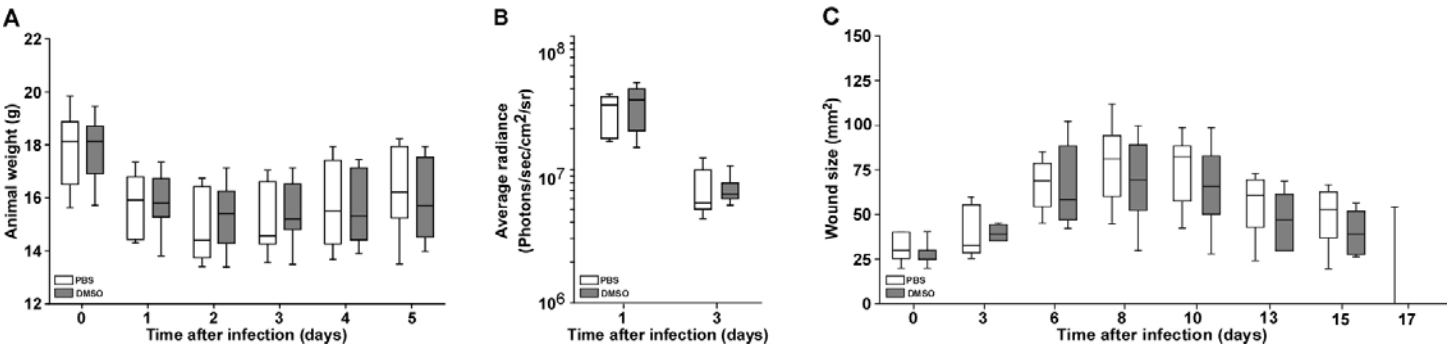

Figure 7. Effect of DMSO on wound infected animals. Animals infected with AB5075 were treated with either sterile PBS or 20% DMSO to determine the potential effect of DMSO in the responses of infected animals by determining body weight (A), bacterial wound burden (B) and wound size/closure (C).

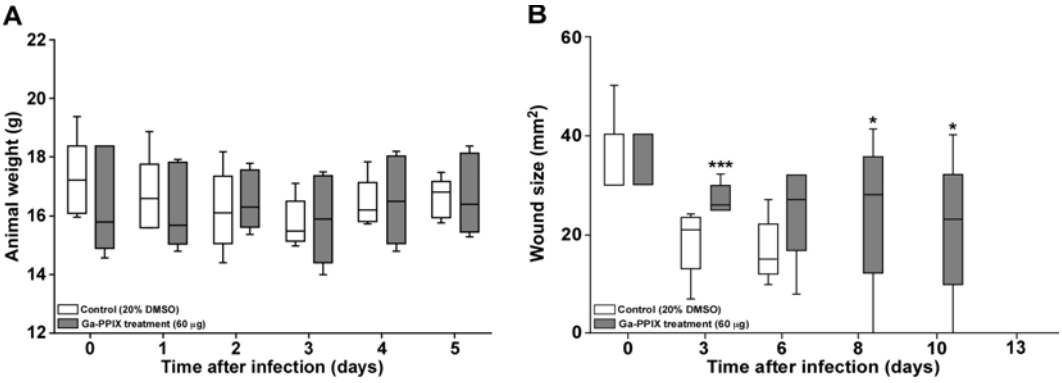

Figure 8. Effect of DMSO on wounded uninfected animals. Animals were wounded and immediately inoculated with sterile PBS. The wounded uninfected animals were then treated with either 20% DMSO or Ga-PPIX dissolved in 20% DMSO. Animal weights (A) and wound sizes (B) were determined at the indicate times. **P* < 0.05, ****P* < 0.001.

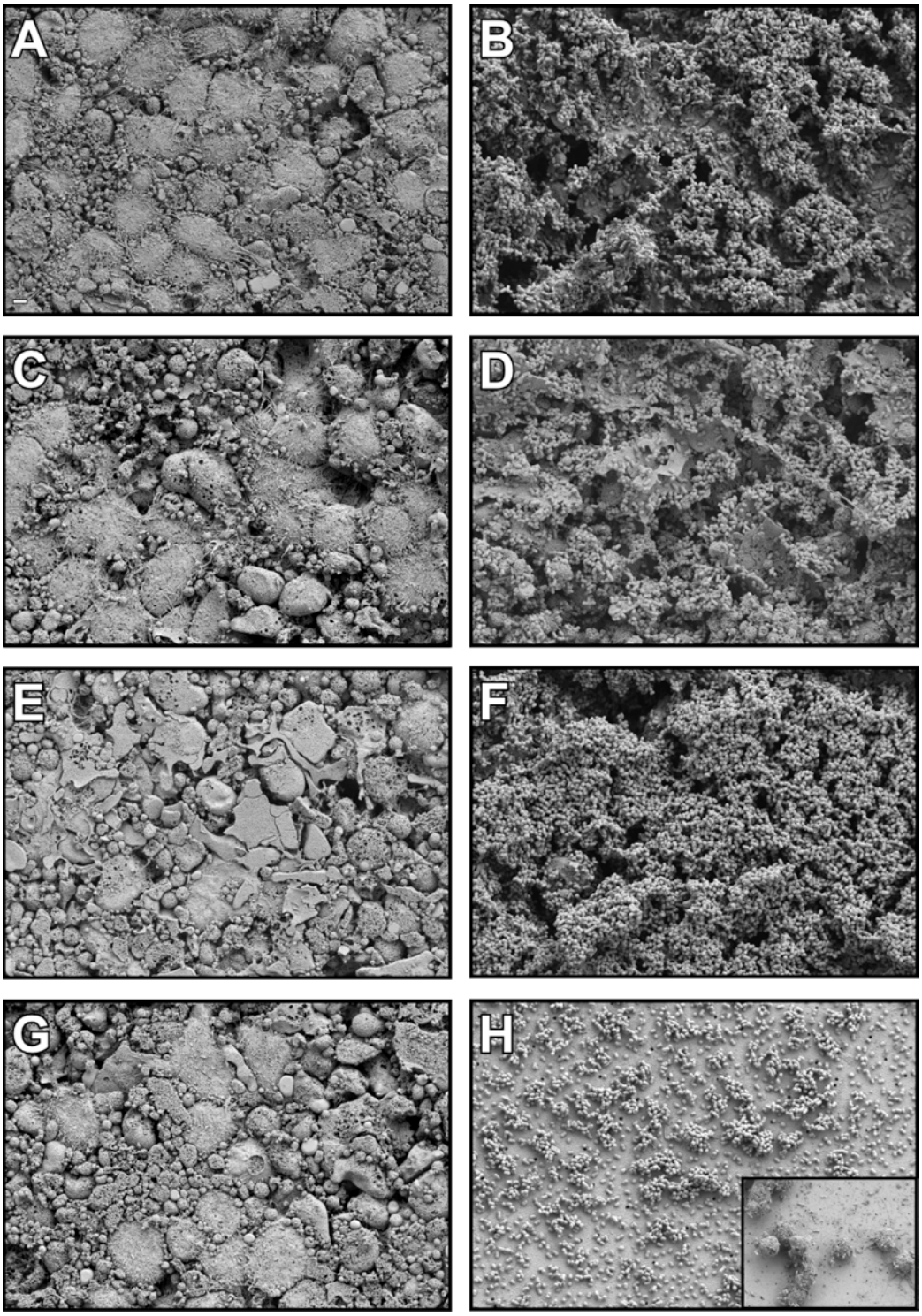

Figure 9. Effect of 2AI-1, LED209 and Virstatin on polarized A549 epithelial cells. Uninfected monolayers were incubated in the absence (A) or presence of 2AI-1 (C), LED209 (E) or Virstatin (G). Infected monolayers were incubated in the absence (B) or presence of 2AI-1 (C), LED209 (E) or Virstatin (H). Inset in H shows the presence of few A549 cells that remained attached to trans-well membranes with bacteria adhered to their surfaces after treatment with Virstatin. All images were collected at the same magnification and the white bar at the bottom left corner of panel A represents 2 µm.

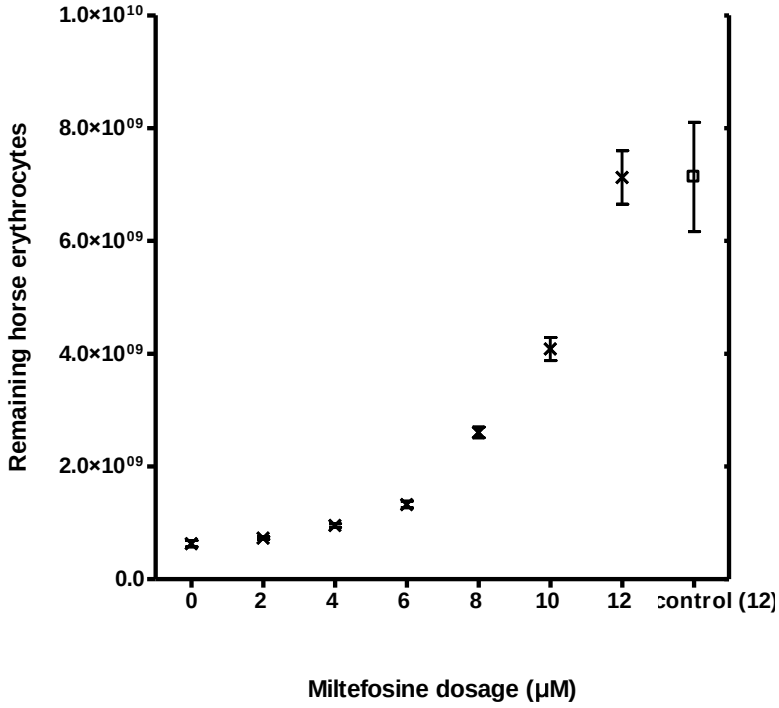

Figure 10. Hemolytic activity of *A. baumannii* ATCC 19606^T in the presence of increasing doses of miltefosine. Enumeration of intact horse erythrocytes remaining after incubation with ATCC 19606^T in TSBD supplemented with increasing dosages of miltefosine ranging in concentration from 0 µM to 12 µM at 37°C for 20 h with shaking at 200 rpm. Error bars represent the standard error (SE) of the mean.

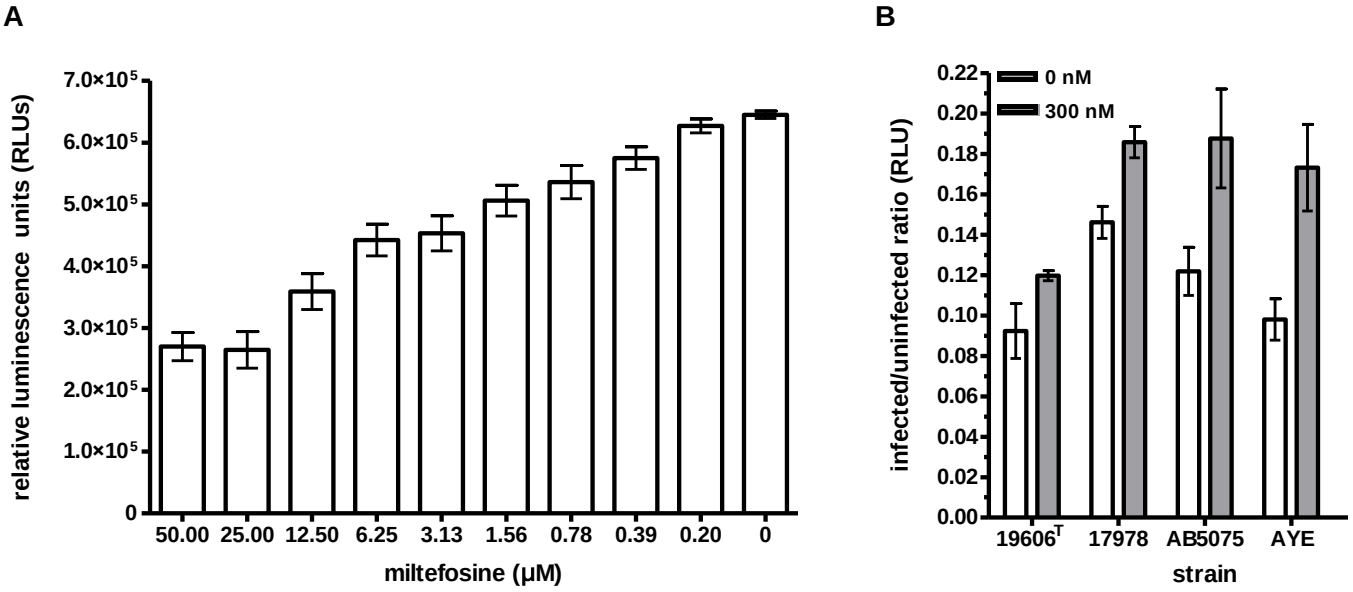

Figure 11. Cytolytic activity of *A. baumannii* strains on A549 human alveolar epithelial cells in the presence of miltefosine. (A) Cytolytic activity of increasing doses of miltefosine ranging from 0 µM to 50 µM on A549 cells after 24 h incubation at 37°C in the presence of 5% CO_2. (B) Relative number of A549 cells remaining after incubation with *A. baumannii* strains and 0 nM or 300 nM miltefosine. Relative luminescence units (RLU) were determined as the ratio between the number of A549 cells present in uninfected samples and each sample infected with a different bacterial strain. Error bars represent the standard error (SE) of the mean.

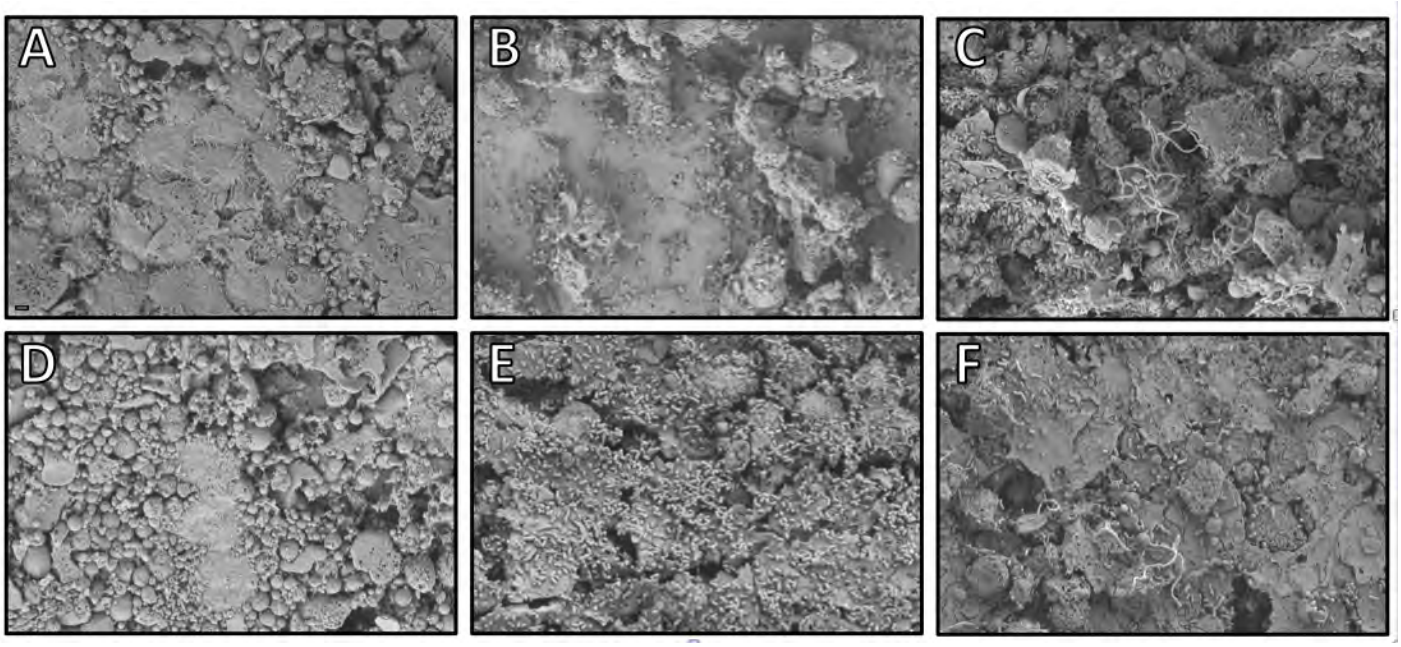

Figure 12. Antimicrobial effect of the phospholipase C activity inhibitor miltefosine against bacteria infecting polarized A549 epithelial cells. Uninfected cells were incubated in the absence (A) or the presence (D) of 300 nM miltefosine. Polarized cells infected with AB5075 (B and E) or ATCC 19606^{T} (C and F) bacteria were incubated in the absence (B and C) or the presence (E and F) of 300 nM miltefosine.

Appendix 1

RESEARCH ARTICLE

AB5075, a Highly Virulent Isolate of *Acinetobacter baumannii*, as a Model Strain for the Evaluation of Pathogenesis and Antimicrobial Treatments

Anna C. Jacobs,[a] Mitchell G. Thompson,[a] Chad C. Black,[a] Jennifer L. Kessler,[a] Lily P. Clark,[a] Christin N. McQueary,[a] Hanan Y. Gancz,[a] Brendan W. Corey,[a] Jay K. Moon,[a] Yuanzheng Si,[a] Matthew T. Owen,[b] Justin D. Hallock,[b] Yoon I. Kwak,[c] Amy Summers,[a] Charles Z. Li,[a] David A. Rasko,[d] William F. Penwell,[e] Cary L. Honnold,[f] Matthew C. Wise,[f] Paige E. Waterman,[c] Emil P. Lesho,[c] Rena L. Stewart,[b] Luis A. Actis,[e] Thomas J. Palys,[a] David W. Craft,[a] Daniel V. Zurawski[a]

Department of Wound Infections, Walter Reed Army Institute of Research, Silver Spring, Maryland, USA[a]; Division of Orthopaedics, University of Alabama at Birmingham, Birmingham, Alabama, USA[b]; Multidrug-resistant Organism and Surveillance Network, Walter Reed Army Institute of Research, Silver Spring, Maryland, USA[c]; Institute for Genome Sciences, University of Maryland School of Medicine, Baltimore, Maryland, USA[d]; Department of Microbiology, Miami University, Oxford, Ohio, USA[e]; Department of Pathology, Walter Reed Army Institute of Research, Silver Spring, Maryland, USA[f]

D.W.C. and D.V.Z. contributed equally to this article.

ABSTRACT ***Acinetobacter baumannii* is recognized as an emerging bacterial pathogen because of traits such as prolonged survival in a desiccated state, effective nosocomial transmission, and an inherent ability to acquire antibiotic resistance genes. A pressing need in the field of *A. baumannii* research is a suitable model strain that is representative of current clinical isolates, is highly virulent in established animal models, and can be genetically manipulated. To identify a suitable strain, a genetically diverse set of recent U.S. military clinical isolates was assessed. Pulsed-field gel electrophoresis and multiplex PCR determined the genetic diversity of 33 *A. baumannii* isolates. Subsequently, five representative isolates were tested in murine pulmonary and *Galleria mellonella* models of infection. Infections with one strain, AB5075, were considerably more severe in both animal models than those with other isolates, as there was a significant decrease in survival rates. AB5075 also caused osteomyelitis in a rat open fracture model, while another isolate did not. Additionally, a Tn*5* transposon library was successfully generated in AB5075, and the insertion of exogenous genes into the AB5075 chromosome via Tn*7* was completed, suggesting that this isolate may be genetically amenable for research purposes. Finally, proof-of-concept experiments with the antibiotic rifampin showed that this strain can be used in animal models to assess therapies under numerous parameters, including survival rates and lung bacterial burden. We propose that AB5075 can serve as a model strain for *A. baumannii* pathogenesis due to its relatively recent isolation, multidrug resistance, reproducible virulence in animal models, and genetic tractability.**

IMPORTANCE **The incidence of *A. baumannii* infections has increased over the last decade, and unfortunately, so has antibiotic resistance in this bacterial species. *A. baumannii* is now responsible for more than 10% of all hospital-acquired infections in the United States and has a >50% mortality rate in patients with sepsis and pneumonia. Most research on the pathogenicity of *A. baumannii* focused on isolates that are not truly representative of current multidrug-resistant strains isolated from patients. After screening of a panel of isolates in different *in vitro* and *in vivo* assays, the strain AB5075 was selected as more suitable for research because of its antibiotic resistance profile and increased virulence in animal models. Moreover, AB5075 is susceptible to tetracycline and hygromycin, which makes it amenable to genetic manipulation. Taken together, these traits make AB5075 a good candidate for use in studying virulence and pathogenicity of this species and testing novel antimicrobials.**

Received 27 March 2014 **Accepted** 10 April 2014 **Published** 27 May 2014

Citation Jacobs AC, Thompson MG, Black CC, Kessler JL, Clark LP, McQueary CN, Gancz HY, Corey BW, Moon JK, Si Y, Owen MT, Hallock JD, Kwak YI, Summers A, Li CZ, Rasko DA, Penwell WF, Honnold CL, Wise MC, Waterman PE, Lesho EP, Stewart RL, Actis LA, Palys TJ, Craft DW, Zurawski DV. 2014. AB5075, a highly virulent isolate of *Acinetobacter baumannii*, as a model strain for the evaluation of pathogenesis and antimicrobial treatments. mBio 5(3):e01076-14. doi:10.1128/mBio.01076-14.

Editor Howard Shuman, University of Chicago

Address correspondence to Daniel V. Zurawski, daniel.v.zurawski.ctr@mail.mil.

Acinetobacter baumannii is an opportunistic, Gram-negative pathogen that thrives in clinical settings and is often multidrug resistant (MDR), factors which earn it a place among the ESKAPE (*Enterococcus faecium*, *Staphylococcus aureus*, *Klebsiella pneumoniae*, *Acinetobacter baumannii*, *Pseudomonas aeruginosa*, and *Enterobacter* species) pathogens of clinical importance (1). Some recent isolates are resistant to all typically used antibiotics except colistin and tigecycline and thus are called extensively or extremely drug-resistant (XDR) *A. baumannii* (2). MDR/XDR *A. baumannii* strains are a worldwide problem for clinicians and caregivers in the hospital setting, particularly in the intensive care unit (ICU) (3). *A. baumannii* is also often isolated from infections of severe wounds sustained in military combat. These infections are responsible for increased morbidity, with prolonged wound

healing and amputations of extremities when limbs cannot be salvaged (4, 5). *A. baumannii* was a predominant isolate from wounded soldiers serving in Iraq (4, 5) and was associated with wartime polytrauma injuries in the past (6). Additionally, there may be a link between *A. baumannii* and crush injuries, as *A. baumannii* infections were also prevalent after the recent large earthquakes in Haiti (7) and China (8).

Another disturbing development that has increased the clinical importance of *A. baumannii* infections is that many strains have become highly antibiotic resistant. For example, in previous decades, *A. baumannii* isolates obtained from both military and civilian settings were often carbapenem sensitive. Now, the majority of U.S. military isolates are carbapenem resistant (9). This trend has also been mirrored in civilian hospitals around the world (10). Recently, even colistin-resistant strains have emerged in the military health care system (11). The latter development is deeply troubling, as colistin is considered the last line of defense against these MDR isolates. Exacerbating this problem is the lack of new treatments in the pharmaceutical pipeline (12); therefore, research on *A. baumannii* virulence factors is urgently needed, as they could constitute potentially novel targets for future antimicrobials.

While previous studies attempted to examine the virulence of different clinical *A. baumannii* strains utilizing *in vivo* model systems (13, 14), the majority of *A. baumannii* researchers still use two American Type Culture Collection (ATCC) strains, ATCC 19606^T and ATCC 17978, which were isolated more than 50 years ago and are not significantly antibiotic resistant. These strains are certainly more amenable to genetic manipulation than most clinical isolates (15, 16) and share considerable genome homology (>90%) to current *A. baumannii* isolates (17), but they are not representative of contemporary isolates of this rapidly evolving pathogen. Some researchers, recognizing that the ATCC isolates are dated, have performed studies with more recent clinical isolates; however, genetic manipulation of such isolates has depended on susceptibility to aminoglycosides (18–20), which is often not found in clinical strains (21). Therefore, our goal was to carry out a systematic study of our own contemporary clinical strains isolated from patients in the U.S. military health care system to identify a strain that is more representative of current clinical isolates, that is highly virulent in established model infections, and that can be genetically manipulated without a potential sacrifice with respect to virulence and antibiotic resistance. Not only does identifying such a strain account for more recent clinical outcomes, but the increased virulence in animal models allows greater statistical power in screening new therapeutics. Moreover, the ability to manipulate the genome allows the study of virulence factors, some of which may be responsible for the emergence of this pathogen in more recent years.

RESULTS

Defining genetic characteristics of *A. baumannii* isolates. In order to identify potential reference strains, a diverse set of 33 *A. baumannii* isolates was chosen based on genetic, isolation site, and antibiotic resistance differences from more than 200 *A. baumannii* strains isolated between 2004 and 2010 from patients in the U.S. military health care system. AB0057, first isolated in 2004 at Walter Reed Army Medical Center, was also included as a comparator because this strain is well characterized, and its genome was previously sequenced (22).

The diversity set of *A. baumannii* isolates was determined via pulsed-field gel electrophoresis (PFGE) analysis and a multiplex PCR assay previously developed to identify the international clonal complexes (ICC). Separately, antibiograms were determined using two different automated bacterial identification systems. The majority of strains were found to be multidrug resistant, typical of current clinical strains (see Table S1 in the supplemental material). As shown in Fig. 1, the genetic similarity of the strains, as determined by PFGE, ranged from 45 to 100%. PFGE types were considered to represent the same clones when their genetic similarity was >80% (23); based on this cutoff, the 33 strains represent 19 unique clones. When the genetic relatedness of these 19 clones was compared, it was found that the majority of them clustered into three groups, which generally aligned with the ICC designations determined by multiplex PCR (Fig. 1 and Table 1) (24). Exceptions were the isolates AB3560, AB4456, and AB4857, which were determined to be ICC III by the multiplex assay but appeared to be ICC I via PFGE. In this case, we relied on the multiplex data (Table 1) to be definitive. These data were used to select four representative strains for genome sequencing and evaluation in animal models.

Three of the strains chosen each represented one of the three ICC groups, AB5075 (ICC I), AB5711 (ICC II), and AB4857 (ICC III). The fourth strain, AB5256 was an outlier, as the OXA-51 allele from this strain was amplified with group 1 primers (24), while the *csuE* allele was not. The isolates were sequenced (25) and compared to previously sequenced *A. baumannii* genomes using the BLAST score ratio (BSR) approach (26). This method compares putative peptides encoded in each genome based on the ratio of BLAST scores to determine if they are conserved (BSR value $\geq$ 0.8), divergent (0.8 > BSR > 0.4), or unique (BSR < 0.4). The majority of the proteomes were similar among strains, meaning they had a BSR of >0.4; however, each isolate also had a set of unique proteins (see Table S2 in the supplemental material). These results are similar to what has been found previously with MDR *A. baumannii* clinical isolates (17), suggesting that the strains used in this study are not genetic outliers.

Virulence assessed in the *Galleria mellonella* model. Strains were first tested in a *Galleria mellonella* infection model, as this model is well established to assess virulence and novel therapeutics for bacterial pathogens, including *A. baumannii* (27, 28). *G. mellonella* larvae were infected with an approximate dose of 1.0×10^5 CFU with each of the four sequenced *A. baumannii* isolates, AB4857, AB5075, AB5256, and AB5711, as well as control strain AB0057. Worms were observed for 6 days, and death was recorded. Within 24 h postinfection, approximately 25% of AB5075-infected worms remained, while the other four strains had survival rates of 70% or higher (Fig. 2). By the end of the 6-day study, AB5075-infected worms had a survival rate of 16%; strains AB4857 and AB5256 were considered moderately pathogenic in this model, with survival rates of 50% and 35%, respectively. The least lethal strains were AB5711 and AB0057, with survival rates of 85% and 83%, respectively. Phosphate-buffered saline (PBS)-injected control worms displayed 100% survival through the course of the study. Based on these data, it was hypothesized that AB5075 was more virulent than the other four strains tested. Using the Mantel-Cox test with Bonferroni correction for multiple comparisons, Kaplan-Meier curves were compared, and AB5075 was found statistically to be more lethal than AB4857, AB5711, and AB0057 (all P values < 0.0125). While AB5256 had a higher

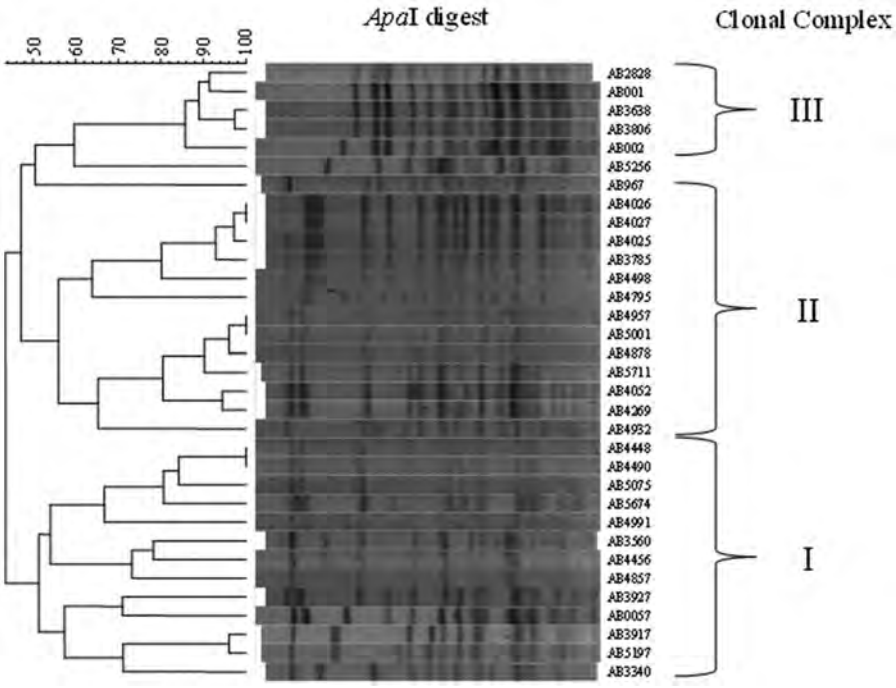

FIG 1 Pulsed-field gel electrophoresis of *A. baumannii* strains. Genomic DNA was isolated from 33 *A. baumannii* clinical isolates, digested with ApaI, and separated by pulsed-field gel electrophoresis (PFGE). Patterns of electrophoresis were compared using BioNumerics 6.0 software. The ICC was determined by multiplex PCR analysis, and brackets delineate the approximate grouping of each strain.

survival rate in this study than AB5075, the difference was not significant after the Bonferroni correction.

Separately, to compare the lethality of AB5075 to that of more commonly utilized *A. baumannii* model strains, the 50% lethal doses (LD_{50}) of AB5075, ATCC 17978, and ATCC 19606^T were determined in *G. mellonella*. The LD_{50} of AB5075 was 1.0×10^4 CFU. In contrast, the LD_{50} of ATCC 17978 and ATCC 19606^T were 5.0×10^5 and 1.0×10^6, respectively.

Virulence assessed in the mouse pulmonary model. *A. baumannii* strains were examined in a murine pulmonary model of infection, because this model is commonly used to assess bacterial virulence and drug efficacy, and survival can be assessed rapidly after an inoculum is delivered (14, 29). The animals were immunocompromised with two doses of cyclophosphamide before inoculation, a treatment that allows *A. baumannii* to establish an infection (14). Mice were inoculated on day 0 with one of the five representative *A. baumannii* strains at a dose of 5.0×10^6 CFU and monitored for 6 days. Consistently, mice infected with AB5075 had a mortality rate of 70% within 48 to 72 h and a 6-day survival rate of 25% (Fig. 3). The other four strains tested, AB0057, AB5711, AB5256, and AB4857, were less lethal than AB5075 in this model, with 6-day survival rates of 65, 80, 80, and 85%, respectively. The log-rank (Mantel-Cox) test with Bonferroni correction determined that AB5075 time-to-death results were statistically significant compared to the other clinical isolates ($P < 0.0125$). The clinical scores of each infected animal also correlated with the survival plots; AB5075-infected mice displayed more severe illness than mice infected with the other strains. In a separate experiment, mice inoculated with 5.0×10^6 cells of ATCC 17978 or ATCC 19606^T resulted in minimal clinical scores and no animal death (data not shown).

Lung bacterial burden in these infections was assessed on days 2 and 3, at the height of illness. The lung CFU/g values for the five infecting strains were compared using a Kruskal-Wallis test followed by a Dunn's multiple comparison test. On day 2, the lungs of AB5256-infected mice had significantly less *A. baumannii* than AB4857-, AB0057-, and AB5075-infected lungs ($P \leq 0.05$) but not AB5711-infected lungs. On day 3, AB5256 displayed a significant decrease in CFU/g compared only to AB5075 (Fig. 4). The four other strains assessed in the model had no significant difference in lung bacterial burden, with the median log CFU/g ranging from 8.5 to 9.3 on day 2 and 8.0 to 8.9 on day 3.

Development of genetic tools in an *A. baumannii* model strain. Our success in establishing AB5075 infections in multiple animal models suggests that the isolate would be an attractive model strain for studying *A. baumannii* virulence. However, in addition to an ideal model strain being highly virulent in animal models, the ability to genetically manipulate the isolate is vital for the study of *A. baumannii* pathogenicity. Because antibiotic resistance determinants are central to many types of genetic manipulations, such as transposon mutagenesis, the antibiotic sensitivity profile of AB5075 was examined in detail. It was observed that AB5075 is susceptible to tetracycline, doxycycline, and related antibiotics (see Table S1 in the supplemental material) and to high levels of erythromycin and hygromycin.

With these known susceptibilities in mind, a method previously developed in *A. baumannii* (30) was adapted for creating AB5075 isogenic mutants by utilizing the *hph* gene, encoding hygromycin resistance, from pMQ300 (31) and the EZ Tn*5* (Epicentre Biotechnologies, Madison, WI) to develop a Tn*5*-based mutagenesis system. This system was used to generate a library of ~6,700 transposon mutants. DNA sequencing of the library was

TABLE 1 *A. baumannii* strains used in this study[a]

Strain	MRSN	Isolation site	Yr isolated	Clonal complex[b]	Source
AB001	1332	ND	ND	ND	C. Murray
AB002	1333	ND	ND	ND	C. Murray
AB0057	1311	Blood/sepsis	2004	I	This study
AB967	1308	Blood/sepsis	2003	III	This study
AB2828	846	Blood/sepsis	2006	III	This study
AB3340	847	Blood/sepsis	2006	I	This study
AB3560	848	Blood/sepsis	2006	III	This study
AB3638	849	Posterior wound	2007	III	This study
AB3785	853	Blood/sepsis	2007	II	This study
AB3806	854	Leg wound	2007	III	This study
AB3917	1309	Blood/sepsis	2007	ND	This study
AB3927	856	Tibia/osteomyelitis	2007	I	This study
AB4025	858	Femur/osteomyelitis	2007	II	This study
AB4026	859	Fibula/osteomyelitis	2007	II	This study
AB4027	860	Femur/osteomyelitis	2007	II	This study
AB4052	863	War wound	2007	II	This study
AB4269	877	War wound	2007	II	This study
AB4448	899	War wound	2007	I	This study
AB4456	903	Tracheal aspirate	2007	III	This study
AB4490	906	War wound	2008	I	This study
AB4498	907	Blood	2008	II	This study
AB4795	930	Bone/osteomyelitis	2008	II	This study
AB4857	939	Ischial/osteomyelitis	2008	III	This study
AB4878	941	War wound	2008	II	This study
AB4932	949	Sputum	2008	II	This study
AB4957	951	Sacral/osteomyelitis	2008	II	This study
AB4991	953	War wound	2008	I	This study
AB5001	954	Blood/sepsis	2008	II	This study
AB5075	959	Tibia/osteomyelitis	2008	I	This study
AB5197	960	STS/tissue	2008	I	This study
AB5256	961	Blood/sepsis	2009	NA	This study
AB5674	963	Blood/sepsis	2009	I	This study
AB5711	1310	Blood/sepsis	2009	II	This study
ATCC 19606^T	NA	Urine	1948	ND	ATCC
ATCC 17978	NA	Spinal meningitis	1951	ND	ATCC
RUH134	NA	Urine	1982	II	L. Dijkshoorn
RUH875	NA	Urine	1984	I	L. Dijkshoorn
RUH5875	NA	Unknown, Netherlands	1997	III	L. Dijkshoorn
ACICU	NA	Outbreak isolate, Rome, Italy	2005	II	M. Tolmasky

[a] MRSN, The Multidrug-resistant Organism Repository and Surveillance Network; ND, no data; NA, not applicable; STS, sterile swab site (most likely from an infected wound).
[b] As determined by multiplex assay performed in this study. AB5256 was considered NA because only the OXA-51 amplicon was amplified from group 1 primer set (31).

performed as previously described (32), yielding 2,548 unique transposon insertions and 68.5% coverage of the genome.

As a further means of modifying the genome, the same hygromycin cassette was inserted into the pUC18T-mini-Tn*7*T-Zeo vector, and this vector was introduced via conjugation into AB5075. Tn*7* insertion into the chromosome was selected for by growth on 250 μg/ml hygromycin and confirmed by PCR across the *att*Tn*7* site on the 3′ end of the *glmS* gene in the AB5075 chromosome. As proof of concept for the use of Tn*7* for gene insertion in the chromosome, the *lux* operon was inserted into the *att*Tn*7* site. This resulted in bioluminescence of this strain, and subsequent subculturing of AB5075::Tn*7*-*lux* over 7 days without antibiotic selection did not affect the bioluminescent signal (see Fig. S1A in the supplemental material), suggesting that the Tn*7* insertion in the chromosome is stable. Additionally, when this strain was cultured in LB broth, there was no growth defect compared to the wild-type isolate AB5075 (see Fig. S1B in the supplemental material). These methods provide us with a means of interrupting and inserting genes on the chromosome, both of which are essential in studying bacterial pathogenesis.

Evaluation of rifampin as proof of concept. As a proof of concept for the use of AB5075 as a model strain for assessing novel antimicrobials, rifampin treatment against AB5075 was tested in the *G. mellonella* and murine pulmonary models. In *G. mellonella*, 30 min after worms were inoculated with 6.0×10^5 CFU of AB5075, they received a treatment injection of 5 or 10 mg/kg rifampin. By 41 h postinfection, all worms infected with AB5075 and receiving PBS treatment had died (Fig. 5). Conversely, worms treated with 5 or 10 mg/kg rifampin had survival rates of 94 and 100%, respectively, at this time point. At the end of the 4-day study, survival rates were 50 and 78%, respectively. The Mantel-Cox test determined that the time to death for AB5075-infected worms was statistically reduced compared to that for rifampin-treated worms ($P < 0.001$).

To further assess AB5075 as a model strain, the mouse lung model was used to examine the efficacy of rifampin. Mice infected intranasally with 5.0×10^6 CFU of AB5075 were treated once daily intraperitoneally (IP) with 2.5, 5, or 10 mg/kg rifampin, and survival was monitored for 48 h. At time of death, or euthanasia at 48 h postinfection, lungs were collected to determine bacterial

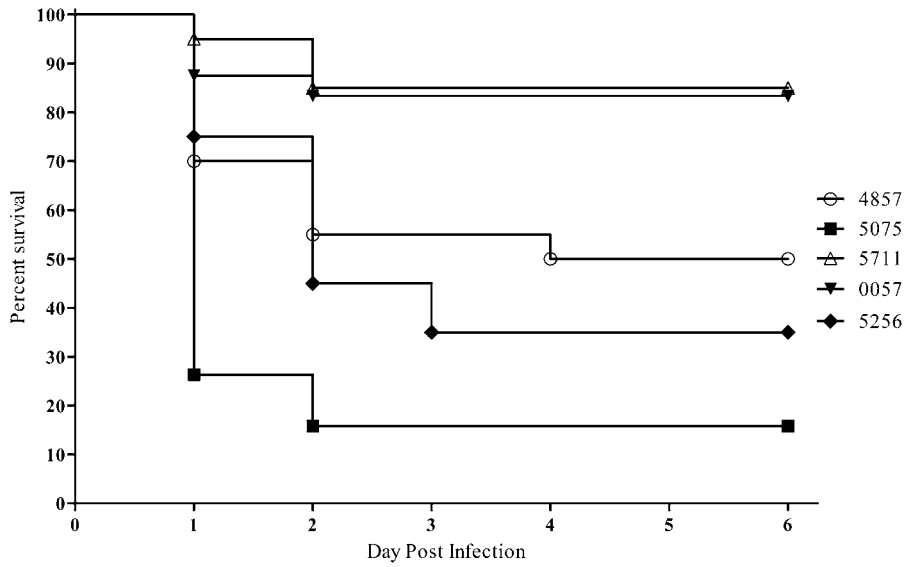

FIG 2 Survival of *Galleria mellonella* larvae infected with *A. baumannii*. Kaplan-Meier survival curves of *G. mellonella* infected with 1.0×10^5 CFU of selected strains of *A. baumannii* are shown. Curves were compared via the Mantel-Cox test with the Bonferroni correction for multiple comparisons. AB5075 showed significantly increased mortality compared to AB4857, AB5711, and AB0057 ($P < 0.0125$).

load. As shown in Fig. 6A, at 48 h after inoculation, only 12.5% of mice infected but not treated with rifampin survived, whereas infected mice receiving 5 and 10 mg/kg rifampin had survival rates of 87.5 and 100%, respectively. These differences in survival were found by the Mantel-Cox test to be statistically significant ($P = 0.0035$ and 0.0008, respectively) compared with mice infected but not treated with rifampin. Mice treated with 2.5 mg/kg rifampin had a 48-h survival rate of 20%, which was not statistically different from that of the control group.

The levels (CFU/g) of bacteria in lung tissue correlated with the survival curves. The median levels in the control and 2.5 mg/kg-treated groups were almost identical, at 9.04 and 9.07 log CFU/g, respectively. Figure 6B shows a decrease in the median log CFU/g for mice treated with 5 and 10 mg/kg rifampin, with values of 8.10 and 4.86, respectively. The Kruskal-Wallis test, followed by Dunn's multiple comparison test, found a statistically significant difference in bacterial burden when the control group was compared to animals treated with 5 or 10 mg/kg rifampin ($P < 0.05$).

DISCUSSION

The goal of the work presented in this report was to identify a model strain of *A. baumannii* that represented current infection

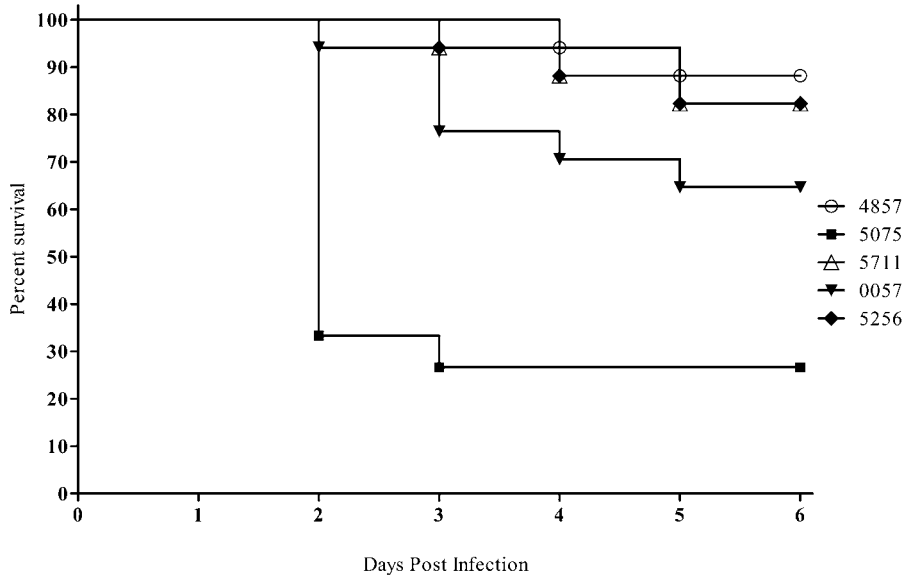

FIG 3 Assessment of *A. baumannii* virulence with the mouse pulmonary model. Kaplan-Meier survival curves of mice infected with 5.0×10^6 CFU of selected *A. baumannii* strains. Curves were compared via the Mantel-Cox test with the Bonferroni correction for multiple comparisons. AB5075 showed significantly increased mortality compared to AB4857, AB5711, AB0057, and AB5256 ($P < 0.0125$).

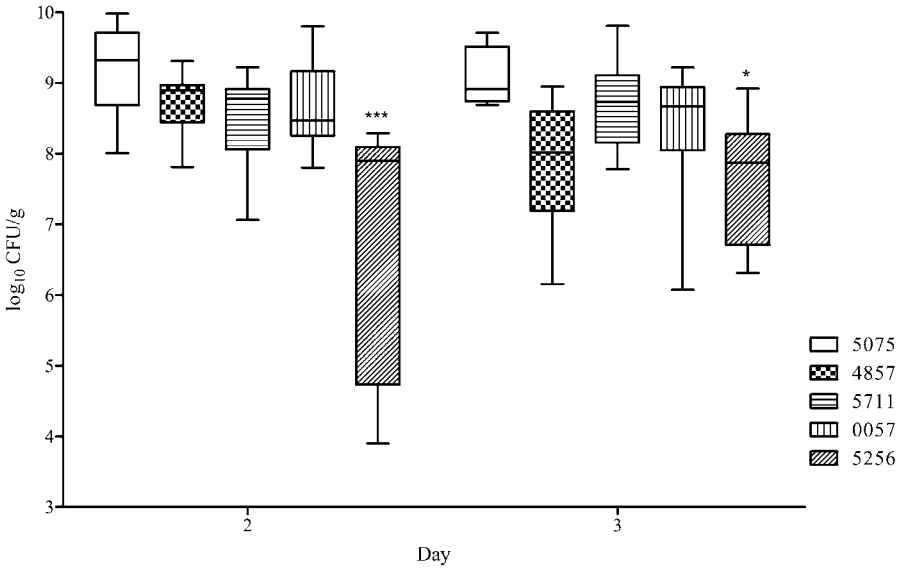

FIG 4 Bacterial levels in lung tissue in the mouse pulmonary model. Box-and-whisker plots of CFU burdens in lungs are shown for days 2 and 3 postinfection. Boxes show median and interquartile ranges, while whiskers represent the 95% confidence interval CI. Strains were compared via the Kruskal-Wallis test followed by Dunn's multiple comparisons posttests. * and ***, $P < 0.05$ and 0.001, respectively.

isolates, was highly virulent in multiple animal models, and was amenable to genetic manipulation. A strain fitting these characteristics would be clinically relevant and could be utilized in various models to study novel therapeutics, and the ability to create isogenic mutants would be critical in investigating genes required for virulence and the pathogenesis of severe infections in the human host. In our comprehensive studies of isolates representative of each major clonal complex group, we identified one such strain, AB5075.

Previous studies compared the virulence of *A. baumannii* strains in single infection models, including a murine pulmonary model (13, 14) and a *G. mellonella* model (33). Other work also compared the virulence of a single strain, ATCC 19606^T, in multiple models *in vivo* (34); however, to our knowledge, this is the first study that used several infection models in parallel to compare multiple strains using representative isolates from each clonal group. Importantly, when we compared infections caused by other *A. baumannii* strains, including the widely used ATCC

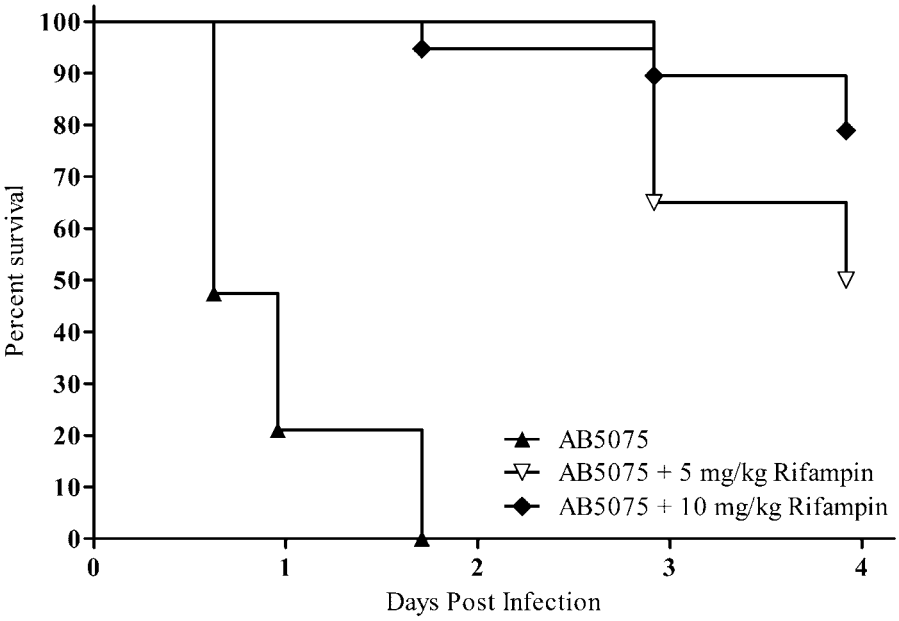

FIG 5 Rifampin as proof of concept in the *G. mellonella* model. Kaplan-Meier survival curves of *G. mellonella* infected with 6.0×10^5 CFU of AB5075 are shown. Worms received a single treatment, 30 min postinfection, of DMSO, 5 mg/kg rifampin, or 10 mg/kg rifampin. Curves were compared via the Mantel-Cox test. The control-treated worms showed significantly increased mortality compared to rifampin-treated worms ($P < 0.001$).

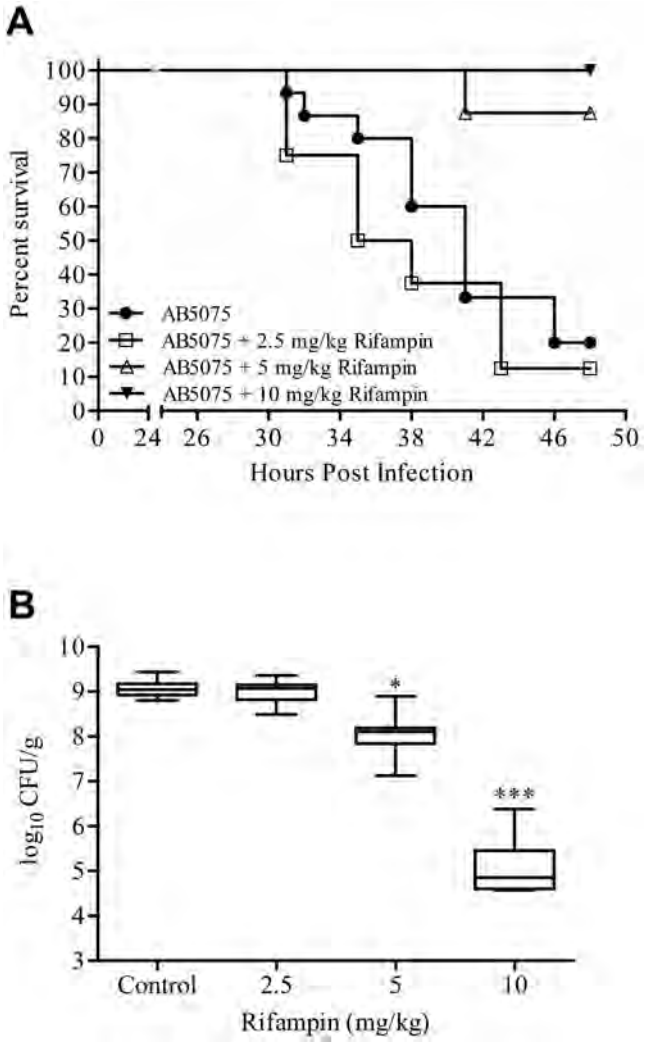

FIG 6 Rifampin as proof of concept in the mouse lung model. (A) Kaplan-Meier survival curves of mice infected with 5.0×10^6 CFU of selected strains of *A. baumannii* are shown. Mice were treated once daily IP with 0, 2.5, 5, or 10 mg/kg rifampin. Curves were compared via the Mantel-Cox test. Rifampin treatments of 5 and 10 mg/kg resulted in significantly increased survival compared to the untreated control ($P = 0.0035$ and 0.0008, respectively). (B) Box-and-whisker plots of CFU burdens within lungs are shown for day 2 postinfection. Boxes show median and interquartile ranges, while whiskers represent 95% CI. Treatments were compared via the Kruskal-Wallis test followed by Dunn's multiple comparisons posttests. * and ***, $P < 0.05$ and 0.001, respectively.

19606^T and ATCC 17978, we did not observe the same severe infection as was consistently observed with AB5075.

In the *G. mellonella* and mouse pneumonia models, AB5075 infection resulted in survival rates consistently below 25%, providing a wide spectrum between infected and uninfected animals to assess novel therapies or genetically mutated strains. Additionally, in the mouse pulmonary model, blood samples and lung histopathology from AB5075-infected mice were consistently positive for the presence of *A. baumannii* (data not shown) and, combined with the high lung bacterial burden observed, offer further means of evaluation in this model. Furthermore, while a recent publication claimed that *A. baumannii* could not cause osteomyelitis in a rat fracture model (35), our data showed that AB5075 could establish an infection in this model and that *A. baumannii* could still be cultured from the bone after 28 days postinfection (see the supplemental material). Recently, we also successfully developed a murine wound model of infection with AB5075, using a small inoculating dose (36). Therefore, the use of AB5075 in additional animal models further demonstrates the great utility of AB5075, as it can serve as a model strain for a variety of studies. The increased virulence of AB5075 in these models also results in larger differences between infected and uninfected animals compared to other tested strains, which allows for less ambiguous results, high statistical power, and thus a requirement for fewer animals to obtain publishable data.

In addition to the successful use of AB5075 in animal models, we were able to exploit the susceptibility of AB5075 to hygromycin to generate a Tn*5* transposon insertion library and use a Tn*7* transposon derivative to insert genes into the genome of this strain. In collaboration with the Manoil laboratory at the University of Washington, we were able to sequence the Tn*5* transposon library using a convenient high-throughput sequencing method. Further, Manoil and his team illustrated the genetic utility of AB5075 by generating a Tn*5* insertion library utilizing a tetracycline-based transposon system (C. Manoil, personal communication). It is expected that these sequenced transposon insertion libraries will be powerful tools for future investigations, as similar libraries have been utilized with success with other bacterial pathogens (37, 38). In the future, the Manoil laboratory will distribute wild-type and mutant derivatives of AB5075 (http://www.gs.washington.edu/labs/manoil/baumannii.htm).

The ability to interrupt or mutate specific genes via transposon insertion and complement mutations via Tn*7*-mediated chromosomal insertion provides a powerful toolkit to answer important questions, such as the nature of specific genes and gene products that are critical for virulence in the host. We believe that AB5075, and the genetic tools and animal models we have designed around this strain, will serve as a platform to readily and reproducibly test mutants in putative virulence factor genes and assess novel antimicrobials. Moreover, we encourage other research groups to use AB5075 as a model strain and to take advantage of the tools we are developing to test their own hypotheses about virulence determinants of *A. baumannii*.

MATERIALS AND METHODS

Bacterial strains, growth media, and clinical microbiology. All work was carried out under biosafety level II or II+ conditions. All the *A. baumannii* strains used in this study can be found in Table 1. Routine growth and strain maintenance was carried out in Luria-Bertani Lennox (LB) broth and agar. Bacterial identification, antibiograms, and MIC were determined using the Vitek 2 (bioMérieux, France) and Phoenix (Becton, Dickinson and Co., Franklin Lakes, NJ) automated systems according to the manufacturer's instructions. Rifampin was obtained from Sigma-Aldrich (St. Louis, MO), prepared in dimethyl sulfoxide (DMSO), and then further diluted in sterile saline.

Pulsed-field gel electrophoresis. The pellet from an overnight broth culture was resuspended in 2 ml 10 mM Tris-HCl, 10 mM EDTA (pH 8.0) to a density equivalent to 0.5 McFarland. Suspensions were mixed with equal volumes of melted 1.6% SeaKem Gold agarose (Lonza, Walkersville, MD), dispensed into wells of a plug mold, and allowed to solidify. The plugs were incubated for 2 h in 20 mg/ml proteinase K and cell lysis buffer (50 mM Tris-HCl, 50 mM EDTA [pH 8.0], 1% *N*-lauroylsarcosine, sodium salt) at 54°C. Subsequently, the plugs were washed four times in TE buffer (10 mM Tris-HCl, 10 mM EDTA [pH 8.0]) and then incubated in a digestion buffer consisting of 50 U of ApaI restriction enzyme, NEBuffer

4, and bovine serum albumin (New England BioLabs, Ipswich, MA) at 25°C for at least 2 h. Electrophoresis was performed at a constant voltage of 200 V by the CHEF-DR II system (Bio-Rad Laboratories, Hercules, CA) with pulse times ramping from 7 to 20 s for 18.5 h. Gels were stained with ethidium bromide and photographed under UV light. PFGE clustering was determined by using the unweighted-pair group method with arithmetic averages (UPGMA) and Dice's coefficient (BioNumerics version 6.0, created by Applied Maths NV).

Multiplex PCR assay. Multiplex PCR methods were followed directly from the work of Turton et al. (24), with modified reaction volume and reagents. Briefly, *A. baumannii* templates were prepared from a single colony grown on Luria-Bertani (LB) agar and resuspended in Lyse-N-Go PCR reagent according to the manufacturer's instructions (Thermo Scientific, Rockford, IL). PCRs were prepared in 20-μl volume using DreamTaq master mix (Thermo Scientific).

Genome sequencing and bioinformatic analysis. Genome analysis was performed as previously described (17), with AB5075, AB5711, AB4857, and AB5256 included in the bioinformatic comparisons. Unique genes were determined using the BLAST score ratio analysis (26). BLAST score ratio (BSR) is an *in silico* approach to conduct comparative proteomic analyses based on proteins predicted to be encoded in a genome (26). BSR was used to compare the proteins encoded in the newly sequenced strains with three isolates from the University of Maryland (17) and eight previously sequenced reference isolates (SDF, AYE, ATCC 17978, ADP1, AB0057, ATCC 19606^T, ACICU, and AB307). The BSRs were calculated as the ratio of raw BLASTP score for the query to the raw BLASTP score of the reference strain. BSR cutoffs of $\geq$0.8, $<$0.8 to $>$0.4, and $<$0.4 were used to determine whether a gene is conserved, divergent, or unique, respectively. A BSR value of 0.8 corresponds to ~85 to 90% identity over 90% of the length of a protein sequence, indicating a highly conserved sequence, while a BSR value of 0.4 corresponds to 30% identity over 30% of the length of a protein sequence, indicating a unique sequence (26).

***Galleria mellonella* infection model.** *A. baumannii* strains were grown overnight in an orbital shaker (37°C, 200 rpm), and overnight cultures were then diluted 100-fold into fresh medium and grown for 3 h. Cells were collected by centrifugation (5 min, 5,000 $\times$ *g*), washed once in phosphate-buffered saline solution (PBS), and resuspended in PBS to a final OD_{600} of 1.0. Further dilutions were done in PBS. The number of bacterial cells in the injected sample was enumerated by plating 10-fold serial dilutions on LB agar plates and counting CFU after overnight incubation.

G. mellonella larvae (Vanderhorst Wholesale, Saint Marys, OH) were used within 10 days of shipment from the vendor. Larvae were kept in the dark at 21°C before infection. Larvae weighing 200 to 300 mg were used in the LD_{50} and survival assays as described previously (28), with slight modifications. Briefly, 5 μl of the sample was injected into the last left proleg of the larvae using a 10-μl glass syringe (Hamilton, Reno, NV) fitted with a 30G needle (Novo Nordisk, Princeton, NJ). Each experiment included control groups of noninjected larvae or larvae injected with 5 μl sterile PBS. For rifampin experiments, approximately 30 min postinfection, worms were injected with 2 μl of rifampin in the second-to-last left proleg using a 10-μl glass syringe. Injected larvae were incubated at 37°C, assessing death at 24 h intervals over 6 days. Larvae were considered dead if they did not respond to physical stimuli. Experiments in which 10% or more of the larvae in either of the control groups died were omitted from the statistical analysis. Experiments were repeated three times using 10 or 20 larvae per experimental group.

The LD_{50} for *A. baumannii* strains AB5075, ATCC 19606^T, and ATCC 17978 were determined by preparing a series of 2-fold dilutions of a PBS suspension of the bacterial strain, starting with a bacterial concentration that caused death of all the larvae within 24 h and going down to a concentration at which no deaths were recorded within this time frame. Twenty larvae were injected with 5 μl of the appropriate dilution, and larvae were determined to be alive or dead after 24 h. Two independent biological repeats of LD_{50} determination were performed. LD_{50} were determined using the Spearman-Karber method.

Murine pulmonary model. The animal experimental procedures were approved by the Institutional Animal Care and Use Committee at the Walter Reed Army Institute of Research (IB02-10). All research was conducted in compliance with the Animal Welfare Act and other federal statutes and regulations relating to animals and experiments involving animals and adhered to principles stated in reference 39. Six-week-old female BALB/c mice (National Cancer Institute, Frederick, MD) were housed at 3 to 4 animals per cage and allowed access to food and water *ad libitum* throughout the experiment. The pulmonary infection model was adapted from reference 14. Briefly, to promote infection, mice were rendered neutropenic via intraperitoneal administration of 150 mg/kg and 100 mg/kg cyclophosphamide in sterile saline on day -4 and day -1 prior to infection (day 0), respectively.

A. baumannii isolates AB4857, AB5075, AB5711, AB0057, and AB5256 were grown overnight in LB broth with aeration at 37°C, subcultured to mid-exponential phase, washed, and resuspended in PBS with optical density at 600 nm (OD_{600}) values corresponding to 2×10^8 CFU/ml. For infection, mice were anesthetized with oxygenated isoflurane immediately prior to intranasal inoculation with 25 μl of bacterial cultures, corresponding to 5×10^6 CFU. For rifampin experiments, mice were injected IP daily, starting at 4 h postinfection. Animal morbidity was scored twice daily for 6 days using a system evaluating mobility, coat condition, and conjunctivitis as previously described (14). As mice became exceedingly moribund based on clinical score, they were humanely euthanized according to protocol.

To assess CFU burden in the lungs, mice were humanely euthanized according to protocol on days 2 and 3 postinfection via an injection of ketamine (100 mg/kg) and xylazine (10 mg/kg). To quantify the pulmonary CFU burden, lungs were homogenized in 1 ml PBS, and serial dilutions were plated using the Autoplate spiral plating system (Advanced Instruments, Norwood, MA) onto LB agar supplemented with 50 μg/ml carbenicillin. Bacterial load was reported as CFU per gram of lung tissue.

Transposon library generation. Transposon mutants were constructed using the EZ-Tn*5* transposon construction vector pMOD-5<R6Kγ*ori*/MCS> (Epicentre, Madison, WI). The transposable element was created by PCR amplifying *hph*, encoding hygromycin resistance, from vector pMQ300 (31) using the primers pMODHygForKPN (AAAA AAGGTACCggaaatgtgcgcggaacccc) and pMODHygRevPST (AAAAAAC TGCAGttggtctgacaatcgatgcgaattgg). The amplicon was then cloned into the multicloning site (MCS) of pMOD-5<R6Kγ*ori*/MCS>. The transposome was constructed according to manufacturer's instructions and introduced into cells via electroporation. The transformed cells were selected for on LB agar supplemented with 250 μg/ml hygromycin. Colonies were picked from plates and grown overnight in 96-well plates containing 100 μl of low-salt LB supplemented with 250 μg/ml hygromycin. After overnight incubation, 100 μl of 50% glycerol was added to each well, and plates were immediately moved to -80°C for storage. The Tn*5* mutant library was subjected to high-throughput sequencing as previously described (32).

Construction of hygromycin mini-Tn*7* vector and insertion onto the chromosome. To make Tn*7*-based genetic tools usable in AB5075, the *hph* gene, coding for hygromycin resistance, was cloned into pUC18T-mini-Tn*7*T-Zeo (40). Briefly, *hph* was amplified from pMQ300 (31) using primers pMOD Hyg For (AAAGCATGCggaaatgtgcgcggaacccc) and pMOD Hyg Rev (AAAGCATGCttggtctgacaatcgatgcgaattgg) (lowercase letters represent the actual primer; capital letters are the restriction site for each primer and a poly-A overhang) and ligated into pUC18T-mini-Tn*7*T-Zeo, which was digested with NcoI and then blunted with the Klenow fragment of the DNA polymerase I (Fermentas). A derivative of the pUC18T-mini-Tn*7*T-*hph* vector containing the *lux* operon was constructed by amplifying the *luxABCDE* operon out of pUC18T-mini-Tn*7*T-Gm-*lux* (40) with the primers Lux For (TCAAGGTTCTGGACCA GTTG) and Lux Rev (AAAAAAAAGCTTGGTGTAGCGTCGTAAGCTA

ATA). The PCR product was digested with BamHI and HindIII and then cloned into the MCS of pUC18T-mini-Tn*7*T-*hph*.

The mini-Tn*7* elements were transposed into the *att*Tn*7* site of AB5075 via the method of Kumar et al. (41). Conjugation mixtures were scraped from LB plates, resuspended in 1 ml of PBS, and plated on LB agar supplemented with 250 μg/ml of hygromycin and 25 μg/ml of chloramphenicol. Insertion into the *att*Tn*7* site was confirmed with the primers AB5075 attTn*7* FWD (AACACAAGTGGAAGTGATTTCT) and AB5075 attTn*7* REV (TGGCTTGCACCAATCATTTATAG), which flanked the *att*Tn*7* site.

Statistical analyses. All statistical analyses were carried out using GraphPad Prism version 5.01 for Windows (GraphPad Software, San Diego, CA). Survival curves were compared via Kaplan-Meier curve analysis with the Bonferroni correction for multiple comparisons. Recovered bacterial burdens were compared via either the Mann-Whitney U test or the Kruskal-Wallis test followed by Dunn's multiple-comparison test. All results were considered significant at a P value of <0.05.

SUPPLEMENTAL MATERIAL

Supplemental material for this article may be found at http://mbio.asm.org/lookup/suppl/doi:10.1128/mBio.01076-14/-/DCSupplemental.

Figure S1A, TIF file, 0.6 MB.
Figure S1B, TIF file, 2.2 MB.
Figure S2, TIF file, 0.5 MB.
Table S1, DOCX file, 0.1 MB.
Table S2, DOCX file, 0.1 MB.
Text S1, DOCX file, 0.1 MB.

ACKNOWLEDGMENTS

We kindly acknowledge Colin Manoil for his collaboration in sequencing the Tn*5* mutant library, his advice, and the critical reading of the manuscript. We thank Lenie Dijkshoorn for providing the clonal complex reference strains that were used as controls for the multiplex PCR assay. We are grateful to Robert Shanks for providing the gift of the pMQ300 plasmid. We thank COL Clint Murray and Mark Shirtliff for providing two additional isolates from Brooke Army Medical Center. We are grateful to Herbert Schweizer for providing the pUC18T-mini-Tn7T-Zeo plasmid, and Anthony Hay for providing the pUC18T-mini-Tn7T-Gm-lux plasmid.

The Zurawski laboratory and the research performed in this study were supported and funded via multiple grants from the Military Infectious Diseases Research Program (MIDRP) and the Defense Medical Research and Development Program (DMRDP).

The findings and opinions expressed herein belong to the authors and do not necessarily reflect the official views of the WRAIR, the U.S. Army, or the Department of Defense.

REFERENCES

1. **Pendleton JN, Gorman SP, Gilmore BF.** 2013. Clinical relevance of the ESKAPE pathogens. Expert Rev. Anti Infect. Ther. **11:**297–308. http://dx.doi.org/10.1586/eri.13.12.
2. **Dizbay M, Tozlu DK, Cirak MY, Isik Y, Ozdemir K, Arman D.** 2010. In vitro synergistic activity of tigecycline and colistin against XDR-*Acinetobacter baumannii*. J. Antibiot. **63:**51–53. http://dx.doi.org/10.1038/ja.2009.117.
3. **Murray CK, Hospenthal DR.** 2008. Acinetobacter infection in the ICU. Crit. Care Clin. **24:**237–248, vii. http://dx.doi.org/10.1016/j.ccc.2007.12.005.
4. **Hujer KM, Hujer AM, Hulten EA, Bajaksouzian S, Adams JM, Donskey CJ, Ecker DJ, Massire C, Eshoo MW, Sampath R, Thomson JM, Rather PN, Craft DW, Fishbain JT, Ewell AJ, Jacobs MR, Paterson DL, Bonomo RA.** 2006. Analysis of antibiotic resistance genes in multidrug-resistant Acinetobacter sp. isolates from military and civilian patients treated at the Walter Reed Army Medical Center. Antimicrob. Agents Chemother. **50:**4114–4123. http://dx.doi.org/10.1128/AAC.00778-06.
5. **Yun HC, Branstetter JG, Murray CK.** 2008. Osteomyelitis in military personnel wounded in Iraq and Afghanistan. J. Trauma **64:**S163–S168. http://dx.doi.org/10.1097/01.ta.0000241143.71274.63.
6. **Tong MJ.** 1972. Septic complications of war wounds. JAMA **219:**1044–1047. http://dx.doi.org/10.1001/jama.219.8.1044.
7. **Potron A, Munoz-Price LS, Nordmann P, Cleary T, Poirel L.** 2011. Genetic features of CTX-M-15-producing *Acinetobacter baumannii* from Haiti. Antimicrob. Agents Chemother. **55:**5946–5948. http://dx.doi.org/10.1128/AAC.05124-11.
8. **Wang T, Li D, Xie Y, Kang M, Chen Z, Chen H, Fan H, Wang L, Tao C.** 2010. The microbiological characteristics of patients with crush syndrome after the Wenchuan earthquake. Scand. J. Infect. Dis. **42:**479–483. http://dx.doi.org/10.3109/00365541003671226.
9. **Keen EF III, Murray CK, Robinson BJ, Hospenthal DR, Co EM, Aldous WK.** 2010. Changes in the incidences of multidrug-resistant and extensively drug-resistant organisms isolated in a military medical center. Infect. Control Hosp. Epidemiol. **31:**728–732. http://dx.doi.org/10.1086/653617.
10. **Evans BA, Hamouda A, Amyes SG.** 2013. The rise of carbapenem-resistant *Acinetobacter baumannii*. Curr. Pharm. Des. **19:**223–238. http://dx.doi.org/10.2174/138161213804070285.
11. **Lesho E, Yoon EJ, McGann P, Snesrud E, Kwak Y, Milillo M, Onmus-Leone F, Preston L, St Clair K, Nikolich M, Viscount H, Wortmann G, Zapor M, Grillot-Courvalin C, Courvalin P, Clifford R, Waterman PE.** 2013. Emergence of colistin-resistance in extremely drug-resistant *Acinetobacter baumannii* containing a novel pmrCAB operon during colistin therapy of wound infections. J. Infect. Dis. **208:**1142–1151. http://dx.doi.org/10.1093/infdis/jit293.
12. **Boucher HW, Talbot GH, Bradley JS, Edwards JE, Gilbert D, Rice LB, Scheld M, Spellberg B, Bartlett J.** 2009. Bad bugs, no drugs: no ESKAPE! An update. Infect. Dis. Soc. Am. Clin. Infect Dis. **48:**1–12. http://dx.doi.org/10.1086/591855.
13. **de Breij A, Eveillard M, Dijkshoorn L, van den Broek PJ, Nibbering PH, Joly-Guillou ML.** 2012. Differences in *Acinetobacter baumannii* strains and host innate immune response determine morbidity and mortality in experimental pneumonia. PLoS One **7:**e30673. http://dx.doi.org/10.1371/journal.pone.0030673.
14. **Eveillard M, Soltner C, Kempf M, Saint-André JP, Lemarié C, Randrianarivelo C, Seifert H, Wolff M, Joly-Guillou ML.** 2010. The virulence variability of different *Acinetobacter baumannii* strains in experimental pneumonia. J. Infect. **60:**154–161. http://dx.doi.org/10.1016/j.jinf.2009.09.004.
15. **Smith MG, Gianoulis TA, Pukatzki S, Mekalanos JJ, Ornston LN, Gerstein M, Snyder M.** 2007. New insights into *Acinetobacter baumannii* pathogenesis revealed by high-density pyrosequencing and transposon mutagenesis. Genes Dev. **21:**601–614. http://dx.doi.org/10.1101/gad.1510307.
16. **Tomaras AP, Dorsey CW, Edelmann RE, Actis LA.** 2003. Attachment to and biofilm formation on abiotic surfaces by *Acinetobacter baumannii*: involvement of a novel chaperone-usher pili assembly system. Microbiology **149:**3473–3484. http://dx.doi.org/10.1099/mic.0.26541-0.
17. **Sahl JW, Johnson JK, Harris AD, Phillippy AM, Hsiao WW, Thom KA, Rasko DA.** 2011. Genomic comparison of multi-drug resistant invasive and colonizing *Acinetobacter baumannii* isolated from diverse human body sites reveals genomic plasticity. BMC Genomics **12:**291. http://dx.doi.org/10.1186/1471-2164-12-291.
18. **Loehfelm TW, Luke NR, Campagnari AA.** 2008. Identification and characterization of an *Acinetobacter baumannii* biofilm-associated protein. J. Bacteriol. **190:**1036–1044. http://dx.doi.org/10.1128/JB.01416-07.
19. **Ramirez MS, Don M, Merkier AK, Bistué AJ, Zorreguieta A, Centrón D, Tolmasky ME.** 2010. Naturally competent *Acinetobacter baumannii* clinical isolate as a convenient model for genetic studies. J. Clin. Microbiol. **48:**1488–1490. http://dx.doi.org/10.1128/JCM.01264-09.
20. **Russo TA, Beanan JM, Olson R, MacDonald U, Luke NR, Gill SR, Campagnari AA.** 2008. Rat pneumonia and soft-tissue infection models for the study of *Acinetobacter baumannii* biology. Infect. Immun. **76:**3577–3586. http://dx.doi.org/10.1128/IAI.00269-08.
21. **Vila J, Pachón J.** 2012. Therapeutic options for *Acinetobacter baumannii* infections: an update. Expert Opin. Pharmacother. **13:**2319–2336. http://dx.doi.org/10.1517/14656566.2012.729820.
22. **Adams MD, Goglin K, Molyneaux N, Hujer KM, Lavender H, Jamison JJ, MacDonald IJ, Martin KM, Russo T, Campagnari AA, Hujer AM, Bonomo RA, Gill SR.** 2008. Comparative genome sequence analysis of multidrug-resistant *Acinetobacter baumannii*. J. Bacteriol. **190:**8053–8064. http://dx.doi.org/10.1128/JB.00834-08.
23. **van Belkum A, Tassios PT, Dijkshoorn L, Haeggman S, Cookson B, Fry**

NK, Fussing V, Green J, Feil E, Gerner-Smidt P, Brisse S, Struelens M, European Society of Clinical Microbiology and Infectious Diseases (ESCMID) Study Group on Epidemiological Markers (ESGEM). 2007. Guidelines for the validation and application of typing methods for use in bacterial epidemiology. Clin. Microbiol. Infect. **13**(Suppl 3):1–46. http://dx.doi.org/10.1111/j.1469-0691.2007.01786.x.

24. **Turton JF, Gabriel SN, Valderrey C, Kaufmann ME, Pitt TL.** 2007. Use of sequence-based typing and multiplex PCR to identify clonal lineages of outbreak strains of *Acinetobacter baumannii*. Clin. Microbiol. Infect. **13:** 807–815. http://dx.doi.org/10.1111/j.1469-0691.2007.01759.x.
25. **Zurawski DV, Thompson MG, McQueary CN, Matalka MN, Sahl JW, Craft DW, Rasko DA.** 2012. Genome sequences of four divergent multidrug-resistant *Acinetobacter baumannii* strains isolated from patients with sepsis or osteomyelitis. J. Bacteriol. **194:**1619–1620. http://dx.doi.org/10.1128/JB.06749-11.
26. **Rasko DA, Myers GS, Ravel J.** 2005. Visualization of comparative genomic analyses by BLAST score ratio. BMC Bioinformatics **6:**2. http://dx.doi.org/10.1186/1471-2105-6-S2-S2.
27. **Desbois AP, Coote PJ.** 2012. Utility of greater wax moth larva (*Galleria mellonella*) for evaluating the toxicity and efficacy of new antimicrobial agents. Adv. Appl. Microbiol. **78:**25–53. http://dx.doi.org/10.1016/B978-0-12-394805-2.00002-6.
28. **Peleg AY, Jara S, Monga D, Eliopoulos GM, Moellering RC, Jr, Mylonakis E.** 2009. *Galleria mellonella* as a model system to study *Acinetobacter baumannii* pathogenesis and therapeutics. Antimicrob. Agents Chemother. **53:**2605–2609. http://dx.doi.org/10.1128/AAC.01533-08.
29. **Manepalli S, Gandhi JA, Ekhar VV, Asplund MB, Coelho C, Martinez LR.** 2013. Characterization of a cyclophosphamide-induced murine model of immunosuppression to study *Acinetobacter baumannii* pathogenesis. J. Med. Microbiol. **62:**1747–1754.
30. **Dorsey CW, Tomaras AP, Actis LA.** 2002. Genetic and phenotypic analysis of *Acinetobacter baumannii* insertion derivatives generated with a transposome system. Appl. Environ. Microbiol. **68:**6353–6360. http://dx.doi.org/10.1128/AEM.68.12.6353-6360.2002.
31. **Kalivoda EJ, Horzempa J, Stella NA, Sadaf A, Kowalski RP, Nau GJ, Shanks RM.** 2011. New vector tools with a hygromycin resistance marker for use with opportunistic pathogens. Mol. Biotechnol. **48:**7–14. http://dx.doi.org/10.1007/s12033-010-9342-x.
32. **Gallagher LA, Ramage E, Patrapuvich R, Weiss E, Brittnacher M, Manoil C.** 2013. Sequence-defined transposon mutant library of *Burkholderia thailandensis*. mBio **4:**e00604-13.
33. **Antunes LC, Imperi F, Carattoli A, Visca P.** 2011. Deciphering the multifactorial nature of *Acinetobacter baumannii* pathogenicity. PLoS One **6:**e22674. http://dx.doi.org/10.1371/journal.pone.0022674.
34. **Gaddy JA, Arivett BA, McConnell MJ, López-Rojas R, Pachón J, Actis LA.** 2012. Role of acinetobactin-mediated iron acquisition functions in the interaction of *Acinetobacter baumannii* strain ATCC 19606T with human lung epithelial cells, *Galleria mellonella* caterpillars, and mice. Infect. Immun. **80:**1015–1024. http://dx.doi.org/10.1128/IAI.06279-11.
35. **Collinet-Adler S, Castro CA, Ledonio CG, Bechtold JE, Tsukayama DT.** 2011. *Acinetobacter baumannii* is not associated with osteomyelitis in a rat model: a pilot study. Clin. Orthop. Relat. Res. **469:**274–282. http://dx.doi.org/10.1007/s11999-010-1488-0.
36. **Thompson MG, Black CC, Pavlicek RL, Honnold CL, Wise MC, Alamneh YA, Moon JK, Kessler JL, Si Y, Williams R, Yildirim S, Kirkup BC, Jr, Green RK, Hall ER, Palys TJ, Zurawski DV.** 2014. Validation of a novel murine wound model of *Acinetobacter baumannii* Infection. Antimicrob. Agents Chemother. **58:**1332–1342. http://dx.doi.org/10.1128/AAC.01944-13.
37. **Buchan BW, McLendon MK, Jones BD.** 2008. Identification of differentially regulated *Francisella tularensis* genes by use of a newly developed Tn5-based transposon delivery system. Appl. Environ. Microbiol. **74:** 2637–2645. http://dx.doi.org/10.1128/AEM.02882-07.
38. **Jacobs MA, Alwood A, Thaipisuttikul I, Spencer D, Haugen E, Ernst S, Will O, Kaul R, Raymond C, Levy R, Chun-Rong L, Guenthner D, Bovee D, Olson MV, Manoil C.** 2003. Comprehensive transposon mutant library of *Pseudomonas aeruginosa*. Proc. Natl. Acad. Sci. U. S. A. **100:**14339–14344. http://dx.doi.org/10.1073/pnas.2036282100.
39. **National Research Council.** 2011. Guide for the care and use of laboratory animals, 8th ed. National Academies Press, Washington, DC.
40. **Choi KH, Gaynor JB, White KG, Lopez C, Bosio CM, Karkhoff-Schweizer RR, Schweizer HP.** 2005. A Tn7-based broad-range bacterial cloning and expression system. Nat. Methods **2:**443–448. http://dx.doi.org/10.1038/nmeth765.
41. **Kumar A, Dalton C, Cortez-Cordova J, Schweizer HP.** 2010. Mini-Tn7 vectors as genetic tools for single copy gene cloning in *Acinetobacter baumannii*. J. Microbiol. Methods **82:**296–300. http://dx.doi.org/10.1016/j.mimet.2010.07.002.

Appendix 2

AAC Journals.ASM.org

Antimicrobial Activity of Gallium Protoporphyrin IX against *Acinetobacter baumannii* Strains Displaying Different Antibiotic Resistance Phenotypes

Brock A. Arivett,[a] Steven E. Fiester,[a] Emily J. Ohneck,[a] William F. Penwell,[a] Cynthia M. Kaufman,[b] Ryan F. Relich,[c] Luis A. Actis[a]

Department of Microbiology, Miami University, Oxford, Ohio, USA[a]; Division of Clinical Microbiology, Indiana University Health Pathology Laboratory, Indianapolis, Indiana, USA[b]; Department of Pathology and Laboratory Medicine, Indiana University School of Medicine, Indianapolis, Indiana, USA[c]

A paucity of effective, currently available antibiotics and a lull in antibiotic development pose significant challenges for treatment of patients with multidrug-resistant (MDR) *Acinetobacter baumannii* infections. Thus, novel therapeutic strategies must be evaluated to meet the demands of treatment of these often life-threatening infections. Accordingly, we examined the antibiotic activity of gallium protoporphyrin IX (Ga-PPIX) against a collection of *A. baumannii* strains, including nonmilitary and military strains and strains representing different clonal lineages and isolates classified as susceptible or MDR. Susceptibility testing demonstrated that Ga-PPIX inhibits the growth of all tested strains when cultured in cation-adjusted Mueller-Hinton broth, with a MIC of 20 μg/ml. This concentration significantly reduced bacterial viability, while 40 μg/ml killed all cells of the *A. baumannii* ATCC 19606^T and ACICU MDR isolate after 24-h incubation. Recovery of ATCC 19606^T and ACICU strains from infected A549 human alveolar epithelial monolayers was also decreased when the medium was supplemented with Ga-PPIX, particularly at a 40-μg/ml concentration. Similarly, the coinjection of bacteria with Ga-PPIX increased the survival of *Galleria mellonella* larvae infected with ATCC 19606^T or ACICU. Ga-PPIX was cytotoxic only when monolayers or larvae were exposed to concentrations 16-fold and 1,250-fold higher than those showing antibacterial activity, respectively. These results indicate that Ga-PPIX could be a viable therapeutic option for treatment of recalcitrant *A. baumannii* infections regardless of the resistance phenotype, clone lineage, time and site of isolation of strains causing these infections and their iron uptake phenotypes or the iron content of the media.

Immediately following the advent of antibiotics as therapeutic agents, resistance to these drugs emerged among pathogenic bacteria. Drug-resistant bacterial strains are selected for immediately after initiation of antibiotic regimens, and as a consequence of continued selective pressure, very few treatment options now exist for infections caused by resistant strains of some pathogens (1, 2). The continuing battle with resistance has led to the initial emergence of pathogens displaying multidrug-resistant (MDR) phenotypes, which has since been followed by the emergence of extremely drug-resistant (XDR) or totally drug-resistant (TDR) strains, an outcome that has recreated the preantibiotic era (3, 4). This crisis has involved major Gram-positive and Gram-negative pathogens, including *Enterococcus* spp., *Staphylococcus aureus*, members of the family *Enterobacteriaceae*, *Neisseria gonorrhoeae*, *Pseudomonas aeruginosa*, and *Acinetobacter* spp. (4). The emergence of MDR strains of each of these microorganisms has contributed to increased morbidity and mortality among patients, leading to extended lengths of hospital stay and exorbitant health care financial burdens that often go unremitted. Compounding this continuum of resistance evolution and treatment failures is the stagnation in the development of new antimicrobial agents used to treat infectious diseases caused by multidrug-resistant organisms (MDROs) (3, 4). All of the aforementioned factors have resulted in a call to action from the Infectious Diseases Society of America (5) and highlight the critical need for alternative therapeutic options that could be used alone or in combination with standard antimicrobials for the treatment of infections caused by MDROs.

Iron acquisition has been considered an alternate target of antimicrobial agents, largely because of the critical role that iron plays in the physiology of bacteria, including pathogens that cause severe human infections (6, 7). Thus, siderophore-mediated iron acquisition processes have been targeted for the development of sideromycins, derivatives in which siderophores have been covalently linked to antibiotics, such as albomycin, salmycin, ferrymicins, the siderophore monosulfactam BAL30072, and a biscatecholate-monohydroxamate-carbacephalosporin conjugate (8–10). This "Trojan Horse" strategy has also included the use of gallium(III) as an anti-infective agent. Gallium binds to virtually all biological complexes that normally contain Fe(III), but it is not reduced to Ga(II) under physiological conditions and thus disrupts essential redox-driven biological processes (11). Accordingly, Ga has been used as simple inorganic and organic salts or complexed with organic compounds, including bacterial siderophores and porphyrins, such as protoporphyrin IX (12, 13). For example, gallium nitrate and gallium desfer-

Received 23 June 2015 **Returned for modification** 25 July 2015
Accepted 24 September 2015

Accepted manuscript posted online 28 September 2015

Citation Arivett BA, Fiester SE, Ohneck EJ, Penwell WF, Kaufman CM, Relich RF, Actis LA. 2015. Antimicrobial activity of gallium protoporphyrin IX against *Acinetobacter baumannii* strains displaying different antibiotic resistance phenotypes. Antimicrob Agents Chemother 59:7657–7665. doi:10.1128/AAC.01472-15.

Address correspondence to Luis A. Actis, actisla@miamioh.edu.

Supplemental material for this article may be found at http://dx.doi.org/10.1128/AAC.01472-15.

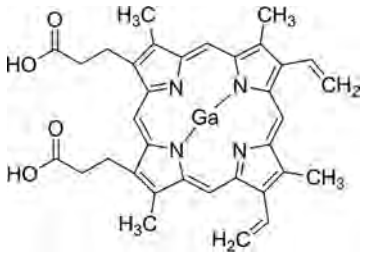

FIG 1 Molecular structure of gallium protoporphyrin IX (Ga-PPIX).

rioxamine showed antimicrobial activity against relevant human pathogens such as *P. aeruginosa* by killing free-living bacteria, blocking biofilm formation, and targeting iron metabolism (14, 15). Noniron metalloporphyrins have also been tested as antibacterials with Ga-protoporphyrin IX (Ga-PPIX) effecting the most potent action against Gram-positive and Gram-negative bacteria. The biological activity of this derivative (Fig. 1) seems to involve high-affinity uptake pathways, which depend on the expression of hemin/hemoglobin receptors, or low-affinity transport processes, whose mechanism of action are unknown (16). Furthermore, Ga-PPIX showed antimicrobial activity against *N. gonorrhoeae* when used topically in a murine vaginal infection model (17).

The Gram-negative obligate aerobe *Acinetobacter baumannii* is an opportunistic pathogen capable of causing a wide range of infections in humans, particularly in those with impaired immune systems (18, 19). The inherent and acquired resistance of clinical isolates of this pathogen complicates the severity of *A. baumannii* infections and their treatment because of the emergence of isolates that are resistant to all commercial antibiotics during the course of treatment (20, 21). This necessitates the investigation into novel chemotherapeutics needed for the treatment of infections, particularly those caused by MDR *A. baumannii* isolates obtained from patients with nosocomial infections and wounded patients. In spite of the increased occurrence of these infections, little is known about the pathobiology of this relevant pathogen. One of the best-understood interactions of this pathogen with the human host is its ability to acquire essential iron during the infection process. The results of genetic and functional analyses of the *A. baumannii* ATCC 19606 type strain showed that it acquires iron via the acinetobactin-mediated siderophore system, which proved to be critical for the infection of human alveolar epithelial cells, *Galleria mellonella* caterpillars, and mice (22). Furthermore, preliminary experimental data (23) and *in silico* genomic studies (24) indicate that *A. baumannii* expresses hemin acquisition systems that remain to be characterized experimentally. These observations suggest that Ga-containing derivatives could be effective microbiocides against *A. baumannii* MDR strains. Accordingly, gallium maltolate and gallium nitrate showed antibacterial activity in mice and *G. mellonella* larvae experimentally infected with different *A. baumannii* clinical strains, including MDR isolates, although the *in vitro* activity of these derivatives depended on the free-iron content of the media (25–27). Furthermore, the analysis of *A. baumannii* LAC-4, which is considered a hypervirulent clinical isolate, showed that it is resistant to gallium nitrate except when it is in the presence of hemin, which it can use as an alternative iron source. Interestingly, the hemin utilization phenotype of the LAC-4 strain is abrogated when Ga-PPIX is added to medium containing serum (28). In addition, the formation of Ga-siderophore complexes, such as those formed with staphyloferrin, could not result in effective antimicrobial activity (13). On the basis of these observations, we studied the effect of Ga-PPIX as an antimicrobial agent against a collection of *A. baumannii* clinical isolates that include strains obtained from military personnel with wound infections. Our results show that Ga-PPIX is an effective antimicrobial agent when tested under *in vitro*, *ex vivo*, and *in vivo* conditions independently of the antimicrobial resistance phenotype of the tested strains.

MATERIALS AND METHODS

Bacterial strains and growth conditions. All strains used in this work, which are listed in Table S1 in the supplemental material, were stored at −80°C as Luria-Bertani (LB) glycerol stocks. All strains were routinely cultured in LB agar or broth at 37°C. For antimicrobial susceptibility determinations, strains were passaged on 5% sheep blood agar prior to growth in cation-adjusted Mueller-Hinton broth (CAMHB; Oxoid, Basingstoke, Hampshire, England) as previously described (29). Iron-rich and iron-chelated conditions were achieved by adding 100 μM $FeCl_3$ and the synthetic iron chelator 2,2′-dipyridyl (DIP), respectively, to the culture media. The identities of the *A. baumannii* isolates listed in Table 1 were confirmed by matrix-assisted laser desorption ionization–time of flight mass spectrometry (MALDI-TOF MS) using a Bruker microflex analyzer. The MALDI Biotyper v3.1 software package (Bruker Daltonic, Billerica, MA) was used to characterize MS fingerprints comprised of the means of 240 mass spectra profiles for each isolate analyzed. Score values greater than 2.000 were considered acceptable for species-level identification. All *A. baumannii* strains provided by D. Zurawski (Walter Reed Army Institute of Research [WRAIR]) were described previously (30). A 10-mg/ml stock solution of Ga-PPIX (Frontier Scientific, Logan, UT), for use whenever Ga-PPIX was required, was prepared using cell culture-grade dimethyl sulfoxide (DMSO) (Sigma-Aldrich, St. Louis, MO) and then sterilized using 0.2-μm nylon membrane filters (Pall Corp., Port Washington, NY).

AST. Strains were subjected to automated and manual antimicrobial susceptibility testing (AST) of standard antimicrobials and the experimental Ga-PPIX. MIC breakpoints and categorical interpretations for conventional antibiotics were mainly based on Clinical and Laboratory Standards Institute (CLSI) breakpoints (31). However, the European Committee on Antimicrobial Susceptibility Testing (EUCAST) breakpoints (http://www.eucast.org/fileadmin/src/media/PDFs/EUCAST_files/Breakpoint_tables/Breakpoint_table_v_3.1.pdf) were used to interpret the MIC of gentamicin for *A. baumannii* 19606^T. Currently, there are no breakpoints for tigecycline or Ga-PPIX.

Epsilometer (Etest)-based MIC tests (bioMérieux, Durham, NC) were performed and interpreted according to the manufacturer's instructions. Briefly, suspensions of the strains equivalent to a 0.5 McFarland standard were used to inoculate Mueller-Hinton agar plates (Remel, Lenexa, KS) prior to strip placement. The plates were incubated for 22 h in ambient air at 35°C prior to MIC interpretation. The MIC was interpreted by observing the concentration of the drug on the strip where the growth of the organism intersected the strip.

Isolate AST of Ga-PPIX and doxycycline was carried out by the Kirby-Bauer disk diffusion method according to standard procedures (32). Ga-PPIX stock solution was added to sterile 6-mm paper disks to deliver 50 μg or 100 μg of Ga-PPIX per disk and allowed to dry. Ga-PPIX paper disks and HardyDisk (Hardy Diagnostics, Franklin, OH) containing 30 μg doxycycline were applied to the surfaces of Mueller-Hinton agar plates inoculated with bacteria. Zones of inhibition (ZOI) were measured after incubation in ambient atmosphere at 37°C for 24 h. ZOI of doxycycline were classified as resistant, intermediate, or susceptible based on CLSI standards.

For automated AST determinations, the Vitek 2 XL (bioMérieux) microbial identification system and the BD Phoenix (BD Diagnostic Sys-

tems, Sparks, MD) automated microbiology system were used according to the manufacturer's instructions. The bioMérieux susceptibility card AST-GN73 and Phoenix NMIC/ID-130 panels were used for each platform, respectively. Interpretive criteria were based on CLSI breakpoints (31).

Broth microdilution MICs. The MIC of Ga-PPIX was determined using the antimicrobial broth microdilution technique in the absence or presence of 10% heat-inactivated normal serum according to standard procedures (29). Briefly, broth microdilution plates were inoculated with 10^5 CFU/ml of each test organism in CAMHB and incubated for 24 h at 37°C in ambient air. Twofold dilutions of Ga-PPIX were performed; the concentrations ranged from 5 μg/ml to 166 μg/ml. A sample with no added antibiotic was included as a growth control on each plate. A more defined Ga-PPIX MIC was determined with 1-μg/ml resolution covering a range of 10 μg/ml to 20 μg/ml for selected strains. The wells on the plates were read for turbidity at an optical density at 595 nm (OD_{595}) with a FilterMax F5 instrument using the multimode analysis software version 3.4.0.25 (Molecular Devices, Sunnyvale, CA). The MIC was determined as the microtiter plate's well with the lowest drug concentration at which there was no detectable growth. The MICs were determined at least three times in triplicate ($n = 9$) using fresh biological samples each time.

Ga-PPIX resistance frequency. CAMH broth samples were inoculated with a 1:100 dilution of 24-h cultures of ATCC 19606^T or ACICU strain and then incubated for 6 h at 37°C. Bacteria were plated onto CAMH agar plates containing 2× (40 μg/ml) and 4× (80 μg/ml) the MIC of Ga-PPIX. The population of bacteria treated with Ga-PPIX was quantified by plate count. Colonies were observed after 24 h and used to determine mutation frequency. The assay was performed twice in triplicate.

Time-kill assays. Time-kill kinetics assays were performed to determine the rapidity of bactericidal activity of Ga-PPIX. The time-kill kinetic assays were performed basically as described previously (33). Briefly, after routine growth, 10^6 CFU/ml of *A. baumannii* ATCC 19606^T or ACICU were inoculated into CAMHB. Cultures were then treated with 0, 10, 20, or 40 μg/ml Ga-PPIX, concentrations that corresponded to 0, 0.5, 1, or 2 times the MIC, respectively. The numbers of CFU were determined at 0, 2, 4, 6, and 24 h postinoculation by plate count. Assays were performed twice in triplicate ($n = 6$) using fresh biological samples each time.

A549 *ex vivo* assays. To test the cytotoxicity of Ga-PPIX, an opaque white 96-well plate was seeded with 10^4 A549 human pulmonary adenocarcinoma cells and incubated for 24 h in Dulbecco's modified Eagle's medium (DMEM) (Mediatech, Inc., Manassas, VA) supplemented with 10% heat-inactivated fetal bovine serum (HyClone, Logan, UT), penicillin, and streptomycin at 37°C in a 5% CO_2 atmosphere as previously described (22). Following incubation, the medium was exchanged for DMEM containing 10% heat-inactivated fetal bovine serum without antibiotics and supplemented with twofold dilutions ranging from 10 μg/ml to 640 μg/ml Ga-PPIX. The samples were incubated for 24 h, and cell viability was assayed using the CellTiter-Glo luminescent cell viability assay (Promega, Madison, WI). Luminescence was measured for 10 ms with a FilterMax F5 instrument. Experiments were performed twice in octuplet ($n = 16$). Groups were compared by analysis of variance (ANOVA) with Tukey's multiple-comparison test.

To test the antimicrobial effect of Ga-PPIX on the infection of submerged A549 cell monolayers, 24-well tissue culture plates were seeded with approximately 10^4 cells per well and then incubated for 16 h as described before (22). Bacteria were cultured for 24 h in CAMHB at 37°C with shaking at 200 rpm, collected by centrifugation at 21,000 × *g* for 10 min, washed, resuspended, and diluted in DMEM with 10% heat-inactivated fetal bovine serum without antibiotics or supplemented with 20 or 40 μg/ml Ga-PPIX. The A549 cell monolayers were infected with 10^4 CFU of the *A. baumannii* ATCC 19606^T or ACICU strain. Inocula were estimated spectrophotometrically at OD_{600} and then confirmed by plate count. Infected-cell monolayers were incubated for 24 h at 37°C in 5% CO_2. The tissue culture supernatants were collected, the A549 monolayers were lysed with sterile distilled H_2O, and the lysates were added to the

TABLE 1 Antibiotic susceptibility profile of nonmilitary *A. baumannii* strains[a]

	Penicillins						Cephalosporins										Carbapenems				Fluoroquinolones				Aminoglycosides						Tetracyclines				Miscellaneous					
	AMP		SAM		TZP		CFZ		FEP		FOX		CAZ		CRO		IMP		MEM		CIP		LVX		AMK		GEN		TOB		TGC		DOX		CST		SXT		Ga-PPIX	
Strain	MIC[b,d]	CI[c]	MIC[d]	CI	MIC[d]	CI	MIC[d]	CI	MIC[e]	CI	MIC[d]	CI	MIC[e]	CI	MIC[d]	CI	MIC[f]	CI	MIC[e]	CI	MIC[e]	CI	MIC[e]	CI	MIC[f]	CI	MIC[e]	CI	MIC[e]	CI	MIC[e]	CI	MIC[h]	CI	MIC[e]	CI	MIC[e]	CI	MIC[i]	CI
ATCC 19606^T	≥32	R	≤2	S	≤4	S	≥64	R	24	*[g]	≥64	R	12	*	16	I	≤1	S	1.5	S	0.8	S	0.5	S	16	S	12	R	3	S	2	*	27	S	0.13	S	>640	R	15	*
ATCC 17978	≥32	R	≤2	S	≤4	S	≥64	R	3	S	≥64	R	6	S	16	I	1	S	0.8	S	0.3	S	0.2	S	≤4	S	1.5	S	0.5	S	0.38	*	26	S	0.38	S	>640	R	17	*
LUH07672	≥32	R	≤2	S	≤4	S	≥64	R	32	R	≥64	R	>256	R	≥64	R	≤1	S	1.5	S	>32	R	24	R	>32	R	>256	R	64	R	6	*	12	I	0.13	S	>640	R	18	*
LUH08809	≥32	R	4	S	≥128	R	≥64	R	96	R	≥64	R	192	R	≥64	R	≤1	S	8	I	>32	R	>32	R	>32	R	>256	R	>256	R	8	*	12	I	0.13	S	>640	R	20	*
LUH05875	≥32	R	4	S	≥128	R	≥64	R	>256	R	≥64	R	64	R	≥64	R	≤1	S	8	I	>32	R	>32	R	>32	R	>256	R	96	R	12	*	14	S	0.13	S	>640	R	19	*
LUH13000	≥32	R	4	S	≥128	R	≥64	R	16	I	≥64	R	≥256	R	≥64	R	2	S	1	S	>32	R	>32	R	>32	R	>256	R	96	R	4	*	6	R	0.3	S	>640	R	20	*
RUH00134	≥32	R	≥32	R	8	S	≥64	R	12	I	≥64	R	6	S	16	I	≤1	S	0.8	S	0.4	S	0.3	S	8	S	≥256	R	1.5	S	3	*	6	R	0.3	S	≥32	R	20	*
RUH00875	≥32	R	≥32	R	16	S	≥64	R	24	I	≥64	R	16	I	16	I	≤1	S	2	S	0.8	S	0.4	S	16	S	>256	R	>256	R	3	*	10	I	0.19	S	>640	R	19	*
AYE	≥32	R	8	S	>128	R	≥64	R	>256	R	≥64	R	>256	R	≥64	R	≤1	S	2	S	>32	R	>32	R	>32	R	>256	R	48	R	3	*	15	S	0.38	S	>640	R	14	*
SDF	ND	-	ND	-	ND	-	ND	-	2	S	ND	-	4	S	ND	-	≤1	S	1	S	0.3	S	0.3	S	<4	S	0.5	S	0.2	S	0.5	*	26	S	0.09	S	5	S	11	*
A118	16	R	≤2	S	8	S	≥64	R	3	S	4	S	6	S	16	I	≤1	S	0.8	S	0.2	S	0.1	S	≤4	S	1.5	S	0.8	S	0.38	*	27	S	0.13	S	0.8	S	18	*
ACICU	≥32	R	≥32	R	≥128	R	≥64	R	≥256	R	≥64	R	≥256	R	≥64	R	>8	R	≥32	R	≥32	R	≥32	R	≥32	R	16	R	16	R	4	*	15	S	0.13	S	≥32	R	18	*

[a] Antibiotic abbreviations: AMK, amikacin; AMP, ampicillin; CAZ, ceftazidime; CFZ, cefazolin; CIP, ciprofloxacin; COX, ceftriaxone; CST, colistin; FEP, cefepime; FOX, cefoxitin; Ga-PPIX, gallium protoporphyrin IX; GEN, gentamicin; IPM, imipenem; LVX, levofloxacin; MEM, meropenem; SAM, ampicillin-sulbactam; SXT, trimethoprim-sulfamethoxazole; TGC, tigecycline; TOB, tobramycin; TZP, piperacillin-tazobactam.

[b] The MIC values are shown in micrograms per milliliter.

[c] The categorical interpretations (CIs) are as follows: R, resistant; S, susceptible; I, intermediate; ND, not determined. Asterisks indicate the absence of interpretive standards.

[d] MIC determined by Vitek-2 AST-GN73 card.

[e] MIC determined by Etest.

[f] MIC determined by BD Phoenix NMIC/ID-130 panel.

[g] *, no interpretive standards available.

[h] Susceptibility determined by Kirby-Bauer disk diffusion.

[i] MIC determined by microdilution.

cognate tissue culture supernatants. Combined lysate samples were serially diluted and then plated on nutrient agar. After overnight incubation at 37°C, the numbers of CFU were counted, and the viable-cell plate count for each sample was calculated and recorded. Experiments were performed twice in octuplet ($n = 16$) using fresh biological samples each time and compared by ANOVA with Tukey's multiple-comparison test.

***Galleria mellonella in vivo* assays.** Ga-PPIX's toxicity and efficacy to treat experimental infections were tested using final instar larvae of the greater wax moth, *G. mellonella* (Grubco Inc., Fairfield, OH) as described before (22). Briefly, larvae weighing between 0.25 g and 0.35 g were randomly assigned to groups of 10 for each trial and then injected into the last left proleg using a syringe pump (New Era Pump Systems Inc., Farmingdale, NY) and 26.5-gauge needles. Larvae were inspected for survival every 24 h for 5 days. Dead larvae were removed at the time of inspection. If more than two larvae died in any control group, the results of the cognate trial were excluded from analysis, and the trial was repeated. Trials were performed in triplicate ($n = 30$).

Ga-PPIX *in vivo* toxicity was tested by using mass-matched *G. mellonella* larvae (i.e., mean mass of each group was statistically indistinguishable by ANOVA from any other group). Larvae were injected with 5 μl of twofold dilutions ranging from 0.2 mM to 25 mM (15.7 mg/ml to 126 μg/ml) Ga-PPIX solubilized in 0.5 N NaOH and 1.5% DMSO. Control groups were either injected or not injected with carrier solution. Probit analysis was performed using R 3.0 (www.r-project.org). To test antimicrobial activity, larvae were injected with a 5-μl bolus of 10^5 CFU of *A. baumannii* ATCC 19606^T or *A. baumannii* ACICU suspended in a phosphate-buffered saline (PBS) solution containing 2% DMSO (carrier) or carrier supplemented with either 20 μg/ml or 40 μg/ml Ga-PPIX. Uninjected larvae and larvae injected with the same volume of sterile carrier were used as controls. Kaplan-Meier survival analysis and odds ratios were determined using Prism 6.0 (GraphPad Software, Inc., La Jolla, CA).

RESULTS

Source and antibiotic susceptibility profiles of *A. baumannii* strains used in this study. Ga-PPIX proved to be an effective antimicrobial when tested against Gram-negative bacteria (*Yersinia enterocolitica*), Gram-positive bacteria (*Staphylococcus aureus*), and acid-fast bacilli (*Mycobacterium smegmatis*) (16). In spite of initial promising results, the application of Ga-PPIX to other pathogens has not been systematically tested. Thus, we used an approach similar to that described in the aforementioned publication (16) to test the Ga-PPIX susceptibility of an *A. baumannii* strain collection that included 30 *A. baumannii* strains isolated from U.S. wounded military personnel (strains 3132 to 3160 and 3284 in Table S1 in the supplemental material) and 12 nonmilitary isolates representing type strains, different international clonal lineages, strains whose genomes were fully sequenced and annotated, and strains that were classified as antimicrobial susceptible or MDR (strains 406 to 3022 and 3161 in Table S1). We initially tested the antibiotic susceptibility of all non-WRAIR strains, the identities of which were confirmed using a combination of standard bacteriological methods and modern technology, such as MALDI-TOF MS. This analysis showed that this set of strains includes isolates, such as SDF, that are susceptible to all tested antibiotics, which included more than six different classes of antimicrobials; isolates that display resistance to some antibiotics, such as ATCC 19606^T and ATCC 17978; MDR isolates, such as LUH07672, LUH08809, LUH05875, LUH13000, RUH00134, and RUH00875; and isolates that are resistant to practically all drugs, such as AYE and ACICU, with ACICU being the most resistant isolate used in this work (Table 1). The U.S. military strain collection of clinical isolates includes 30 strains, each of which are resistant to most of the 11 antibiotics tested (30).

Growth inhibitory effects of Ga-PPIX. All 42 tested strains displayed apparent growth when cultured in CAMHB at 37°C for 18 h using 96-well microtiter plates, although there was some growth variability among the strains (see Table S2 in the supplemental material). The addition of Ga-PPIX produced a dose-dependent growth response with several strains growing to higher optical densities in the presence of 5 μg/ml to 20 μg/ml of this nonferric metalloporphyrin when assayed using an automated twofold microdilution method. However, bacterial growth was significantly reduced when the CAMHB contained more than 20 μg/ml Ga-PPIX, making 40 μg/ml the MIC for all 42 strains when tested using this automated approach, which resulted in inocula containing 10^6 bacteria per sample. A more detailed manual analysis of the nonmilitary isolates following the CLSI standards (using inocula of 10^5 bacteria and CAMHB) using a twofold Ga-PPIX serial dilution scheme resulted in a MIC value of 20 μg/ml for all of these isolates. Furthermore, a 1-μg/ml resolution scheme performed under the latter experimental conditions resulted in Ga-PPIX MIC values ranging between 11 μg/ml and 20 μg/ml (Table 1). The median and mean MIC of these nonmilitary isolates was 19 μg/ml and 17.4 μg/ml, respectively. The presence of 10% heat-inactivated normal human serum increased the MIC for the ATCC 19606^T and ACICU strains to 62.5 μg/ml, a threefold increase compared with the values obtained in the absence of proteins, without causing the complete inactivation or sequestration of Ga-PPIX. The Ga-PPIX susceptibility of these isolates was also tested using disk diffusion assays. All strains tested produced detectable ZOI ranging between 13 mm and 23 mm in diameter when the seeded plates were exposed to sterile filter disks impregnated with 50 μg or 100 μg Ga-PPIX, respectively (Fig. 2), and there were no heteroresistant colonies noted in the ZOI, which is represented in the insets of Fig. 2A and B. This observation is in agreement with the failure to isolate Ga-PPIX-resistant colonies of ATCC 19606^T and ACICU when a population of greater than 9.8×10^9 bacteria were challenged to 2× (40 μg/ml) or 4× (80 μg/ml) the MIC of Ga-PPIX (data not shown).

Comparable results were obtained when the disk assays were conducted using LB agar plates that were supplemented with $FeCl_3$ or DIP to generate iron-rich or iron-chelated conditions, respectively (data not shown). Furthermore, comparable Ga-PPIX susceptibility responses were detected with the ATCC 19606^T strain and the isogenic derivatives ATCC 19606^T t6 (strain 1653 in Table S1 in the supplemental material) and ATCC 19606^T *entA* (strain 3069 in Table S1), which are affected in the uptake and biosynthesis of acinetobactin because of mutations in the genes coding for the BauA acinetobactin receptor protein and the EntA biosynthetic protein, respectively (34, 35). Additionally, the detailed analysis of *A. baumannii* AB5075 (strain 3156 in Table S1), a MDR isolate recently cultured from an infected wound that has been proposed as a model strain to study the pathobiology of this pathogen (30), showed a Ga-PPIX MIC of 20 μg/ml when cultured in CAMHB under standard laboratory conditions following CLSI guidelines (Fig. S1A and S1B in the supplemental material).

These experimental data collected using two different methods show that the susceptibility of different *A. baumannii* clinical strains to Ga-PPIX, with a standard MIC of 20 μg/ml, is independent of their time and site of isolation and their overall antimicrobial resistance phenotypes and clonal lineages. The data also indicate that the susceptibility to Ga-PPIX is independent of the

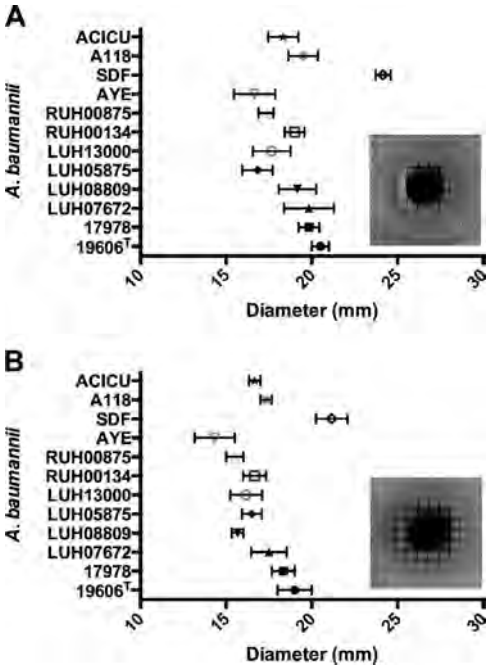

FIG 2 Ga-PPIX disk diffusion assays. *A. baumannii* bacteria were first seeded onto CAMH agar and then disks impregnated with 50 μg (A) or 100 μg (B) of Ga-PPIX were deposited on the surfaces of the plates. Growth inhibition halos were measured after incubation for 24 h at 37°C. Data are expressed as means ± standard errors of the means (SEM) (error bars) from experiments done twice in triplicate. The insets show the growth inhibition halos observed when the CAMH agar plates were seeded with *A. baumannii* ATCC 19606^T and incubated for 24 h at 37°C.

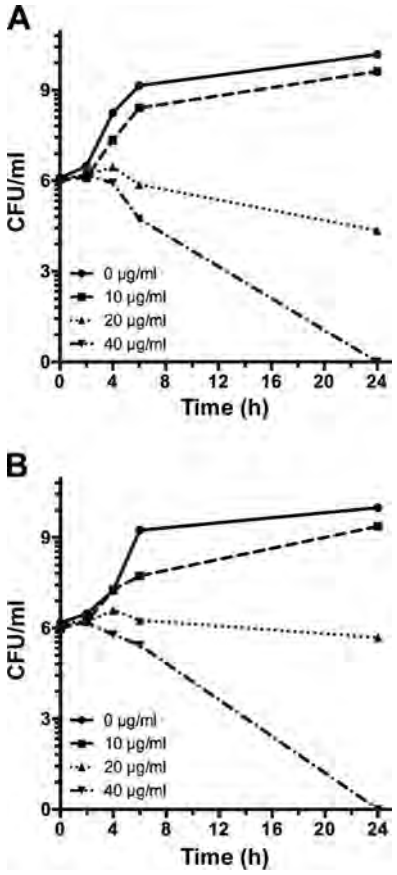

FIG 3 Ga-PPIX time-kill assays. Ga-PPIX time-kill kinetics for *A. baumannii* ATCC 19606^T (A) and ACICU (B) was determined after 0, 2, 4, 6, and 24 h of incubation by CFU count after exposure to 0 μg/ml (0× MIC), 10 μg/ml (0.5× MIC), 20 μg/ml (1× MIC), or 40 μg/ml (2× MIC) Ga-PPIX.

free-iron content of the medium and the capacity of bacteria to produce or use acinetobactin, which seems to be the most common siderophore-mediated iron uptake system found in the genome of different *A. baumannii* clinical isolates (36).

Ga-PPIX time-kill kinetics. The antibacterial activity of Ga-PPIX was tested by determining its time-kill kinetics using the ATCC 19606^T and ACICU nonmilitary isolates, which are considered non-MDR and MDR strains, respectively, at a concentration of 0.5, 1, and 2 times the MIC as determined by the microdilution method. Both *A. baumannii* strains showed similar responses, with the addition of 10 μg/ml Ga-PPIX (0.5× MIC) causing only a small reduction in bacterial viability (Fig. 3). In contrast, the addition of 20 μg/ml (1× MIC) or 40 μg/ml (2× MIC) was effective in reducing the viable cells by >3 log units after 6 h of incubation. Furthermore, 1 × MIC did lead to a statistically significant reduction of 8×10^5- and 2.6×10^3-fold in viable cells after 24 h compared with the cognate untreated samples of ATCC 19606^T and ACICU, respectively. Interestingly, 40 μg/ml of Ga-PPIX caused complete bacterial cell death for both the ATCC 19606^T strain and ACICU MDR isolate. These results indicate that Ga-PPIX is both fast and effective in eliminating viable *A. baumannii* under *in vitro* conditions normally used to test the effectiveness of antimicrobial agents.

Ga-PPIX toxicity to eukaryotic cells and *G. mellonella* larvae. The toxicity of Ga-PPIX was tested using A549 alveolar epithelial tissue culture cells and *G. mellonella* caterpillars. Ga-PPIX exhibited no statistically significant toxicity for A549 cells at concentrations up to 160 μg/ml, 8 times the MIC, when tested using the CellTiter-Glo luminescent cell viability assay. This assay also showed that there was a statistically significant reduction in A549 viability when the culture medium contained 640 μg/ml ($P \leq 0.0001$) or 320 μg/ml ($P = 0.004$) Ga-PPIX (Fig. 4A), concentrations that are far higher than the MIC values reported in the previous section. The *ex vivo* toxicity is corroborated by *in vivo* experiments using *G. mellonella* larvae (Fig. 4B) with comparable body mass (Fig. 4B, inset). After injection with Ga-PPIX over a 3-log-unit range (200 μM to 25 mM), the survival of larvae injected with 25 mM was significantly reduced than survival in the control group ($P = 0.0363$) (data not shown). The 50% lethal concentration (LC_{50}) for Ga-PPIX in *G. mellonella* was extrapolated by probit analysis from the log dose-response curve to be 157 mg/ml (Fig. 4B). It was also observed that the injection of high concentrations of Ga-PPIX resulted in immediate coloration of the larvae, and subsequently excreted feces were noticeably pink (data not shown).

These results demonstrate the ability of eukaryotic cells and organisms to tolerate Ga-PPIX at concentrations much higher than the MIC values determined using standard methods.

Ga-PPIX treatment of *ex vivo* and *in vivo* experimental infections. The antibacterial effectiveness of Ga-PPIX was determined by infecting A549 tissue cultures and *G. mellonella* larvae with the *A. baumannii* ATCC 19606^T strain or the ACICU MDR

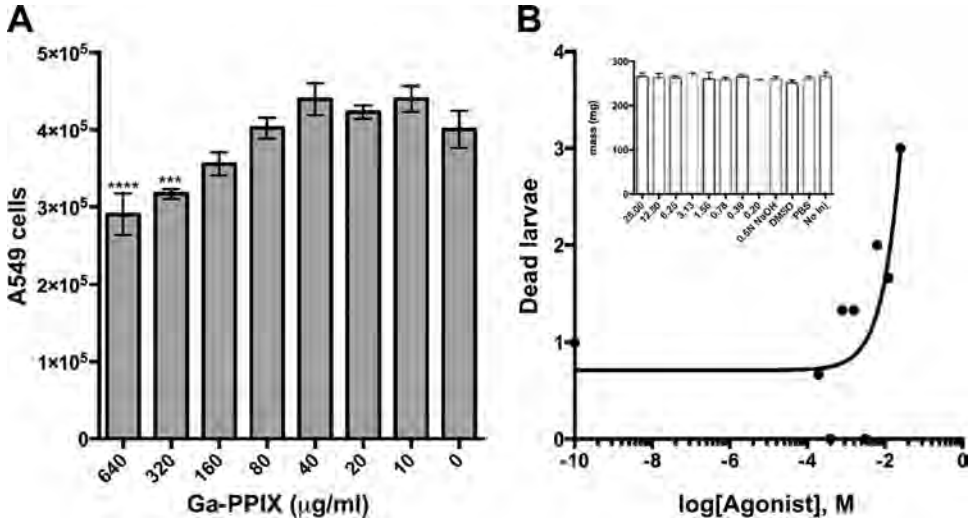

FIG 4 Ga-PPIX toxicity toward A549 human cells and *G. mellonella* larvae. (A) Submerged A549 cell monolayers containing 4×10^5 cells were incubated with increasing concentrations of Ga-PPIX dissolved in DMSO and added to DMEM containing 10% heat-inactivated fetal bovine serum without antibiotics. Cell viability was determined after 24 h of incubation at 37°C in the presence of 5% CO_2. Responses to the presence of Ga-PPIX were compared to those detected with cells cultured in the absence of this metalloporphyrin derivative. Values that are significantly different from the value for the control (0 μg/ml Ga-PPIX) are indicated by asterisks as follows: ***, $P = 0.0004$; ****, $P < 0.0001$. (B) Mass-matched *G. mellonella* larvae were injected with 5 μl of twofold dilutions ranging from 0.2 mM to 25 mM Ga-PPIX solubilized in 0.5 N NaOH and 1.5% DMSO. Larvae injected with 0.5 N NaOH, 1.5% DMSO, or PBS or not injected (No Inj) served as controls. The inset shows the mean masses of all animal groups with error bars showing standard errors.

strain in the presence or absence of this nonferric metalloporphyrin derivative. The presence of 20 μg/ml or 40 μg/ml of Ga-PPIX leads to a statistically significant reduction in CFU for ATCC 19606^T ($P = 0.037$ or $P = 0.014$, respectively) and ACICU ($P = 0.0005$ or $P = 0.0005$, respectively) compared with the samples incubated in the absence of this nonferric metalloporphyrin derivative (Fig. 5A and B). Overall, the addition of 40 μg/ml of Ga-PPIX led to 701-fold and 145-fold reductions of ATCC 19606^T and ACICU CFU recovered from the infected monolayers, respectively.

The *G. mellonella in vivo* infection model also showed the antibacterial activity of Ga-PPIX (Fig. 5C and D). Infection of larvae with an ATCC 19606^T inoculum containing 20 μg/ml and 40 μg/ml Ga-PPIX significantly increased animal survival with *P* values of 0.03 and 0.0003, respectively, and log rank hazard ratios of 2.5 and 8.4, respectively, for each Ga-PPIX concentration tested compared with animals infected in the absence of this metalloporphyrin derivative (Fig. 5C). Similar results were obtained with the MDR ACICU strain (Fig. 5D), where injection with 20 μg/ml and 40 μg/ml of Ga-PPIX resulted in significant increases in survival with $P = 0.008$ and 0.001, respectively, and log rank hazard ratios of 3.4 and 5.0, respectively. Unfortunately, numerous attempts to test the antibacterial effect of Ga-PPIX by injecting it after infection failed to produce valid experimental data, since the death rates of caterpillars injected twice with 5 μl of sterile PBS, which were used as negative controls, were higher than those we consider acceptable—no more than two deaths per sample/per trial. This is one limitation of this otherwise convenient experimental virulence model we expect to address in the future by using vertebrate hosts where the volume of the inoculum is not as critical as is the case of *G. mellonella*.

Taken together, these observations indicate that Ga-PPIX has antibacterial activity when tested using experimental infection models previously used to show the role of iron acquisition functions in the virulence of *A. baumannii* (22).

DISCUSSION

Our previous work has shown that iron acquisition is a critical *A. baumannii* virulence trait when tested using *ex vivo* and *in vivo* experimental infection models (22). Furthermore, we observed that the presence of hemin promoted the growth of *A. baumannii* ATCC 19606^T when cultured in the presence of the synthetic iron chelator 2,2′-dipyridyl. This response is independent of the expression of the acinetobactin-mediated system (23), which is the only complete siderophore-mediated system that allows this strain to prosper under iron-limiting conditions when tested using *in vitro*, *ex vivo*, and *in vivo* experimental conditions (22). All these observations strongly indicate that this strain expresses siderophore and hemin transport and utilization functions that could be targeted to treat *A. baumannii* infections, particularly those caused by MDR isolates. Our initial work (23) and unpublished preliminary observations indicate that the antibacterial activity of Ga nitrate is variable among all strains tested and depends on the free-iron content of the medium as has been reported before (26). These findings and the recent report that hypervirulent strains tolerate high concentrations of Ga nitrate (28) prompted us to study the antibacterial activity of Ga-PPIX against an *A. baumannii* strain collection that includes isolates obtained from different sources at different times, representing different clonal lineages and expressing different antibiotic resistance phenotypes. Our work demonstrated that all tested *A. baumannii* strains, including the *A. baumannii* AB5075 MDR military isolate recently proposed as a working model strain (30), displayed similar MIC values, which ranged between 11 and 20 μg/ml, when tested under standard laboratory conditions following CLSI guidelines. Furthermore, our data show that Ga-PPIX susceptibility is indepen-

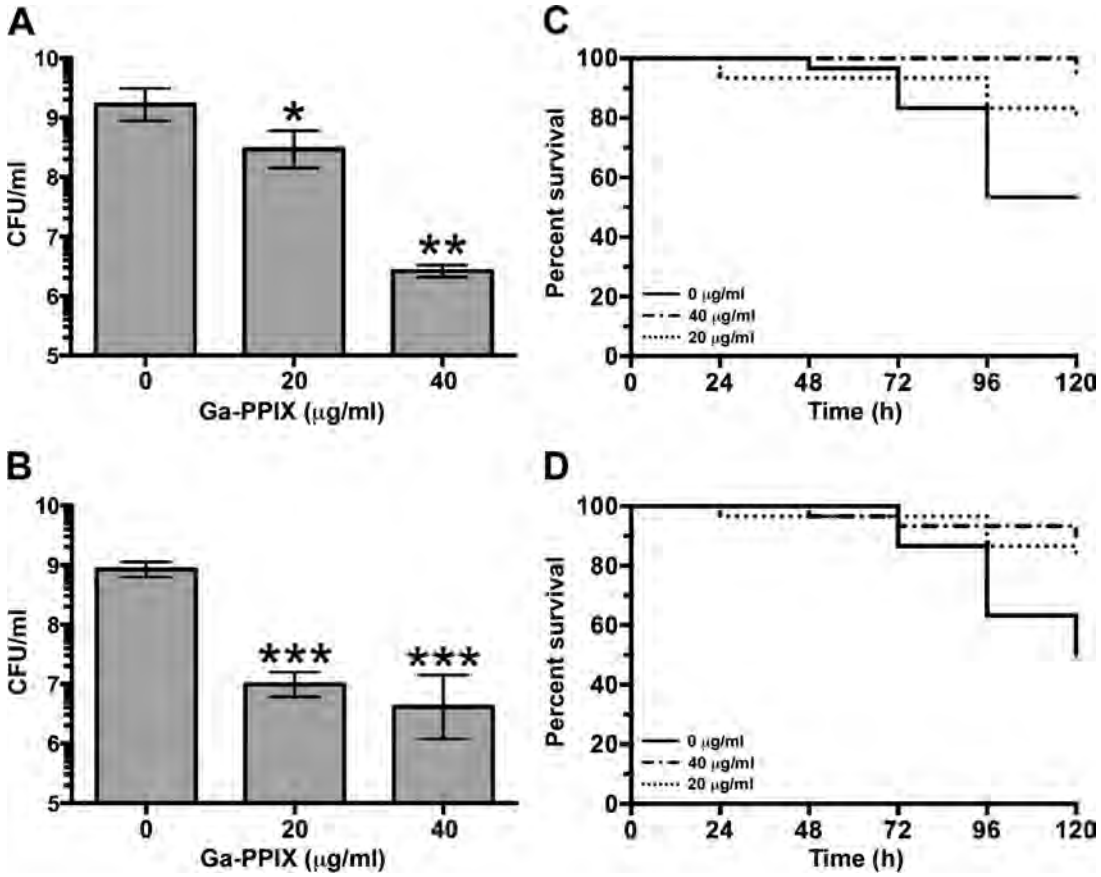

FIG 5 Antibacterial activity of Ga-PPIX against experimental infections. Monolayers of A549 human alveolar epithelial cells (A and B) and *G. mellonella* larvae (C and D) were infected with *A. baumannii* ATCC 19606^T strain (A and C) or ACICU strain (B and D) in the absence or the presence of either 20 μg/ml or 40 μg/ml of Ga-PPIX. Data shown in panels A and B represent the means (± SEM) of experiments performed twice in octuplet ($n = 16$) using fresh biological samples each time. Responses to the presence of Ga-PPIX were compared to those detected with bacteria cultured in the absence of this metalloporphyrin derivative. Values that are significantly different from the value for the control (0 μg/ml Ga-PPIX) are indicated by asterisks as follows: *, $P = 0.037$; **, $P = 0.014$; ***, $P = 0.0005$.

dent of the free-iron content of the media and the active expression of siderophore-mediated iron acquisition functions, while the presence of proteins in the *in vitro*, *ex vivo*, and *in vivo* susceptibility assays showed that they do not drastically affect the antibacterial activity of Ga-PPIX. Our data also showed that Ga-PPIX displays bactericidal activity relatively quickly, particularly when used at twice the MIC (40 μg/ml) under standard laboratory conditions, without causing any detectable cytotoxic effects on human cells and *G. mellonella* caterpillars. These findings are relevant since patients suffering from severe wound and soft tissue infections require immediate and effective antimicrobial chemotherapy. Equally concerning is the emergence of *A. baumannii* isolates with increased and/or altered virulence, such as the LAC-4 strain and isolates obtained from deadly cases of necrotizing fasciitis, respectively (37, 38). These infections require immediate and effective antimicrobial treatment not only because of the devastating nature of these infections but also because of the alarming MDR phenotype of the bacterial agents responsible for these diseases.

Our recent observation that the Ga-PPIX-susceptible strain AYE produces the hydroxamate siderophore baumannoferrin (39), but not acinetobactin or any catechol-derived siderophore due to a natural *entA* natural mutation (35), shows that the antibacterial activity of this nonferric metalloporphyrin extends beyond those strains that produce and use acinetobactin to acquire iron. More recently, it was reported that the *A. baumannii* ATCC 17978 strain, which could rely on the production and use of acinetobactin and fimsbactins to grow under free-iron limiting conditions (40), is also susceptible to Ga-PPIX. These observations further demonstrate that the antibacterial activity of Ga-PPIX is independent of the type or number of high-affinity iron chelators produced by a particular isolate. Whether these conditions also apply to the LAC-4 hypervirulent strain, which proved to be susceptible to Ga-PPIX (28), is currently unknown, since the siderophore-mediated iron acquisition system or systems expressed by this isolate is/are unknown.

The fact that Ga-PPIX displays bactericidal activity even in a medium such as LB agar, which has enough free iron to inhibit the expression of the acinetobactin system in the ATCC 19606^T strain (41), demonstrates the antibacterial effectiveness of this noniron metalloporphyrin derivative even under conditions that inhibit the expression of critical iron-regulated bacterial functions, including those required for iron acquisition via siderophore or hemin uptake processes. However, the mechanisms by which Ga-PPIX is transported into the bacterial cytoplasm and affects iron metabolism are not fully understood. Pioneering work done by

Stoljiljkovic et al. showed that Gram-negative bacteria, such as *Yersinia enterocolitica*, are susceptible to Ga-PPIX when expressing hemin acquisition functions under low-iron conditions (16). Similarly, work done by Moriwaki et al. showed that the *Staphylococcus aureus* IsdH-NEAT3 hemin receptor interacts with Ga-PPIX in a fashion similar to that of the natural hemin ligand (42). However, these results contradict our observations showing that Ga-PPIX displays antibacterial activity against bacteria cultured in iron-rich media such as LB agar or broth, which should significantly inhibit the expression of hemin transport functions according to data collected with *Y. enterocolitica* and *Escherichia coli* (16). Taken together, these results argue in favor of the hypothesis that Ga-PPIX could reach the periplasmic and cytoplasmic spaces either by using unknown low-affinity or TonB-independent hemin receptors or passive diffusion through bacterial membranes (16). Those hypotheses are supported by our data showing that the *A. baumannii* strains AYE and ATCC 17978, which lack the eight-gene cluster coding for putative hemin oxygenase and hemin utilization proteins recently described by de Léséleuc et al. (28), and ATCC 19606^T strain, which does not have an identifiable *hemO* ortholog and therefore lacks this cluster, were as susceptible as the ACICU, SDF, and AB0057 strains, all of which harbor the aforementioned eight-gene cluster. The Ga-PPIX susceptibility of AYE, ATCC 17978, and ATCC 19606^T could be also explained by the presence of a 12-gene cluster (iron uptake gene cluster 2), which codes for predicted hemin uptake functions but lacks a canonical *hemO* ortholog, that is also present in the genomes of the ACICU, SDF, and AB0057 strains (24). Together, these observations indicate that the widespread susceptibility of *A. baumannii* to Ga-PPIX is mediated by more than one cellular process, a property that will most likely not favor the emergence of resistant derivatives at least in the short term as could be predicted from our work, which failed to detect a resistance phenotype using disk diffusion assays, broth MIC, or mutation rate studies.

In summary, our work shows that *A. baumannii* strains are susceptible to Ga-PPIX regardless of their clonal lineages, site and time of isolation, antimicrobial resistance phenotypes, expression of iron acquisition systems, iron content of the media, or presence of proteins in *in vitro* and *ex vivo* tissue culture susceptibility assays. All these properties make this nonferric metalloporphyrin derivative a potentially valuable and convenient antimicrobial agent that affects the viability of bacterial cells not only by interfering with critical physiological processes that depend on the redox properties of iron but also making bacterial cells more susceptible to oxidative stresses due to the presence of reactive oxygen species produced by bacteria growing under aerobic conditions as well as by the host in response to infection (16). However, the relatively low solubility of Ga-PPIX in aqueous solutions is one obstacle that must be overcome before this compound is introduced as a viable therapeutic option, either alone or in combination with current antibiotics, for the treatment of *A. baumannii* infections, particularly those caused by isolates that are highly resistant to current antimicrobial agents.

ACKNOWLEDGMENTS

This work was supported by funds from Public Health AI070174 and Department of Defense W81XWH-12-2-0035 grants and Miami University research funds.

We are grateful to Daniel V. Zurawski from Walter Reed Army Institute of Research for providing the *A. baumannii* strains listed in Table S1 in the supplemental material.

The findings and opinions expressed herein belong to the authors and do not necessarily reflect the official views of the WRAIR, U.S. Army, or Department of Defense.

REFERENCES

1. **Costelloe C, Metcalfe C, Lovering A, Mant D, Hay AD.** 2010. Effect of antibiotic prescribing in primary care on antimicrobial resistance in individual patients: systematic review and meta-analysis. BMJ **340:**c2096. http://dx.doi.org/10.1136/bmj.c2096.
2. **Hawser SP, Bouchillon SK, Hoban DJ, Badal RE, Hsueh PR, Paterson DL.** 2009. Emergence of high levels of extended-spectrum-beta-lactamase-producing gram-negative bacilli in the Asia-Pacific region: data from the Study for Monitoring Antimicrobial Resistance Trends (SMART) program, 2007. Antimicrob Agents Chemother **53:**3280–3284. http://dx.doi.org/10.1128/AAC.00426-09.
3. **Magiorakos AP, Srinivasan A, Carey RB, Carmeli Y, Falagas ME, Giske CG, Harbarth S, Hindler JF, Kahlmeter G, Olsson-Liljequist B, Paterson DL, Rice LB, Stelling J, Struelens MJ, Vatopoulos A, Weber JT, Monnet DL.** 2012. Multidrug-resistant, extensively drug-resistant and pandrug-resistant bacteria: an international expert proposal for interim standard definitions for acquired resistance. Clin Microbiol Infect **18:**268–281. http://dx.doi.org/10.1111/j.1469-0691.2011.03570.x.
4. **Rossolini GM, Arena F, Pecile P, Pollini S.** 2014. Update on the antibiotic resistance crisis. Curr Opin Pharmacol **18:**56–60. http://dx.doi.org/10.1016/j.coph.2014.09.006.
5. **Spellberg B, Guidos R, Gilbert D, Bradley J, Boucher HW, Scheld WM, Bartlett JG, Edwards J, Jr, Infectious Diseases Society of America.** 2008. The epidemic of antibiotic-resistant infections: a call to action for the medical community from the Infectious Diseases Society of America. Clin Infect Dis **46:**155–164. http://dx.doi.org/10.1086/524891.
6. **Bullen JJ, Rogers HJ, Spalding PB, Ward CG.** 2005. Iron and infection: the heart of the matter. FEMS Immunol Med Microbiol **43:**325–330. http://dx.doi.org/10.1016/j.femsim.2004.11.010.
7. **Crosa JH, Mey AR, Payne SM.** 2004. Iron transport in bacteria. ASM Press, Washington, DC.
8. **Braun V, Pramanik A, Gwinner T, Koberle M, Bohn E.** 2009. Sideromycins: tools and antibiotics. Biometals **22:**3–13. http://dx.doi.org/10.1007/s10534-008-9199-7.
9. **de Carvalho CC, Fernandes P.** 2014. Siderophores as "Trojan Horses": tackling multidrug resistance? Front Microbiol **5:**290. http://dx.doi.org/10.3389/fmicb.2014.00290.
10. **Mollmann U, Heinisch L, Bauernfeind A, Kohler T, Ankel-Fuchs D.** 2009. Siderophores as drug delivery agents: application of the "Trojan Horse" strategy. Biometals **22:**615–624. http://dx.doi.org/10.1007/s10534-009-9219-2.
11. **Bernstein LR.** 1998. Mechanisms of therapeutic activity for gallium. Pharmacol Rev **50:**665–682.
12. **Bonchi C, Imperi F, Minandri F, Visca P, Frangipani E.** 2014. Repurposing of gallium-based drugs for antibacterial therapy. Biofactors **40:**303–312. http://dx.doi.org/10.1002/biof.1159.
13. **Kelson AB, Carnevali M, Truong-Le V.** 2013. Gallium-based anti-infectives: targeting microbial iron-uptake mechanisms. Curr Opin Pharmacol **13:**707–716. http://dx.doi.org/10.1016/j.coph.2013.07.001.
14. **Banin E, Lozinski A, Brady KM, Berenshtein E, Butterfield PW, Moshe M, Chevion M, Greenberg EP, Banin E.** 2008. The potential of desferrioxamine-gallium as an anti-Pseudomonas therapeutic agent. Proc Natl Acad Sci U S A **105:**16761–16766. http://dx.doi.org/10.1073/pnas.0808608105.
15. **Kaneko Y, Thoendel M, Olakanmi O, Britigan BE, Singh PK.** 2007. The transition metal gallium disrupts *Pseudomonas aeruginosa* iron metabolism and has antimicrobial and antibiofilm activity. J Clin Invest **117:**877–888. http://dx.doi.org/10.1172/JCI30783.
16. **Stojiljkovic I, Kumar V, Srinivasan N.** 1999. Non-iron metalloporphyrins: potent antibacterial compounds that exploit haem/Hb uptake systems of pathogenic bacteria. Mol Microbiol **31:**429–442. http://dx.doi.org/10.1046/j.1365-2958.1999.01175.x.
17. **Bozja J, Yi K, Shafer WM, Stojiljkovic I.** 2004. Porphyrin-based compounds exert antibacterial action against the sexually transmitted pathogens *Neisseria gonorrhoeae* and *Haemophilus ducreyi*. Int J Antimicrob Agents **24:**578–584. http://dx.doi.org/10.1016/j.ijantimicag.2004.06.008.
18. **Dijkshoorn L, Nemec A, Seifert H.** 2007. An increasing threat in hospi-

tals: multidrug-resistant *Acinetobacter baumannii*. Nat Rev Microbiol **5:**939–951. http://dx.doi.org/10.1038/nrmicro1789.
19. **Peleg AY, Seifert H, Paterson DL.** 2008. *Acinetobacter baumannii*: emergence of a successful pathogen. Clin Microbiol Rev **21:**538–582. http://dx.doi.org/10.1128/CMR.00058-07.
20. **Doi Y, Husain S, Potoski BA, McCurry KR, Paterson DL.** 2009. Extensively drug-resistant *Acinetobacter baumannii*. Emerg Infect Dis **15:**980-982. http://dx.doi.org/10.3201/eid1506.081006.
21. **Fishbain J, Peleg AY.** 2010. Treatment of Acinetobacter infections. Clin Infect Dis **51:**79–84. http://dx.doi.org/10.1086/653120.
22. **Gaddy JA, Arivett BA, McConnell MJ, Lopez-Rojas R, Pachon J, Actis LA.** 2012. Role of acinetobactin-mediated iron acquisition functions in the interaction of *Acinetobacter baumannii* ATCC 19606^T with human lung epithelial cells, *Galleria mellonella* caterpillars, and mice. Infect Immun **80:**1015–1024. http://dx.doi.org/10.1128/IAI.06279-11.
23. **Zimbler DL, Penwell WF, Gaddy JA, Menke SM, Tomaras AP, Connerly PL, Actis LA.** 2009. Iron acquisition functions expressed by the human pathogen *Acinetobacter baumannii*. Biometals **22:**23–32. http://dx.doi.org/10.1007/s10534-008-9202-3.
24. **Antunes LC, Imperi F, Towner KJ, Visca P.** 2011. Genome-assisted identification of putative iron-utilization genes in *Acinetobacter baumannii* and their distribution among a genotypically diverse collection of clinical isolates. Res Microbiol **162:**279–284. http://dx.doi.org/10.1016/j.resmic.2010.10.010.
25. **Antunes LC, Imperi F, Minandri F, Visca P.** 2012. *In vitro* and *in vivo* antimicrobial activities of gallium nitrate against multidrug-resistant *Acinetobacter baumannii*. Antimicrob Agents Chemother **56:**5961–5970. http://dx.doi.org/10.1128/AAC.01519-12.
26. **de Léséleuc L, Harris G, KuoLee R, Chen W.** 2012. *In vitro* and *in vivo* biological activities of iron chelators and gallium nitrate against *Acinetobacter baumannii*. Antimicrob Agents Chemother **56:**5397–5400. http://dx.doi.org/10.1128/AAC.00778-12.
27. **DeLeon K, Balldin F, Watters C, Hamood A, Griswold J, Sreedharan S, Rumbaugh KP.** 2009. Gallium maltolate treatment eradicates *Pseudomonas aeruginosa* infection in thermally injured mice. Antimicrob Agents Chemother **53:**1331–1337. http://dx.doi.org/10.1128/AAC.01330-08.
28. **de Léséleuc L, Harris G, KuoLee R, Xu HH, Chen W.** 2014. Serum resistance, gallium nitrate tolerance and extrapulmonary dissemination are linked to heme consumption in a bacteremic strain of *Acinetobacter baumannii*. Int J Med Microbiol **304:**360–369. http://dx.doi.org/10.1016/j.ijmm.2013.12.002.
29. **Clinical and Laboratory Standards Institute.** 2006. Methods for dilution antimicrobial susceptibility tests for bacteria that grow aerobically - 7th ed. Approved standard. CLSI document M7-A7. Clinical and Laboratory Standards Institute, Wayne, PA.
30. **Jacobs AC, Thompson MG, Black CC, Kessler JL, Clark LP, McQueary CN, Gancz HY, Corey BW, Moon JK, Si Y, Owen MT, Hallock JD, Kwak YI, Summers A, Li CZ, Rasko DA, Penwell WF, Honnold CL, Wise MC, Waterman PE, Lesho EP, Stewart RL, Actis LA, Palys TJ, Craft DW, Zurawski DV.** 2014. AB5075, a highly virulent isolate of *Acinetobacter baumannii*, as a model strain for the evaluation of pathogenesis and antimicrobial treatments. mBio **5:**e01076–14. http://dx.doi.org/10.1128/mBio.01076-14.
31. **Clinical and Laboratory Standards Institute.** 2014. Performance standards for antimicrobial susceptibility testing; twenty-third informational supplement M100-23. Clinical and Laboratory Standards Institute, Wayne, PA.
32. **Bauer AW.** 1966. Current status of antibiotic susceptibility testing with single high potency discs. Am J Med Technol **32:**97–102.
33. **Petersen PJ, Jones CH, Bradford PA.** 2007. *In vitro* antibacterial activities of tigecycline and comparative agents by time-kill kinetic studies in fresh Mueller-Hinton broth. Diagn Microbiol Infect Dis **59:**347–349. http://dx.doi.org/10.1016/j.diagmicrobio.2007.05.013.
34. **Dorsey CW, Tomaras AP, Connerly PL, Tolmasky ME, Crosa JH, Actis LA.** 2004. The siderophore-mediated iron acquisition systems of *Acinetobacter baumannii* ATCC 19606 and *Vibrio anguillarum* 775 are structurally and functionally related. Microbiology **150:**3657–3667. http://dx.doi.org/10.1099/mic.0.27371-0.
35. **Penwell WF, Arivett BA, Actis LA.** 2012. The *Acinetobacter baumannii entA* gene located outside the acinetobactin cluster is critical for siderophore production, iron acquisition and virulence. PLoS One **7:**e36493. http://dx.doi.org/10.1371/journal.pone.0036493.
36. **Sahl JW, Gillece JD, Schupp JM, Waddell VG, Driebe EM, Engelthaler DM, Keim P.** 2013. Evolution of a pathogen: a comparative genomics analysis identifies a genetic pathway to pathogenesis in *Acinetobacter*. PLoS One **8:**e54287. http://dx.doi.org/10.1371/journal.pone.0054287.
37. **Charnot-Katsikas A, Dorafshar AH, Aycock JK, David MZ, Weber SG, Frank KM.** 2009. Two cases of necrotizing fasciitis due to *Acinetobacter baumannii*. J Clin Microbiol **47:**258–263. http://dx.doi.org/10.1128/JCM.01250-08.
38. **Harris G, Kuo Lee R, Lam CK, Kanzaki G, Patel GB, Xu HH, Chen W.** 2013. A mouse model of *Acinetobacter baumannii*-associated pneumonia using a clinically isolated hypervirulent strain. Antimicrob Agents Chemother **57:**3601–3613. http://dx.doi.org/10.1128/AAC.00944-13.
39. **Penwell WF, DeGrace N, Tentarelli S, Gauthier L, Gilbert CM, Arivett BA, Miller AA, Durand-Reville TF, Joubran C, Actis LA.** 2015. Discovery and characterization of new hydroxamate siderophores, baumannoferrin A and B, produced by *Acinetobacter baumannii*. Chembiochem **16:**1896–1904. http://dx.doi.org/10.1002/cbic.201500147.
40. **Proschak A, Lubuta P, Grun P, Lohr F, Wilharm G, De Berardinis V, Bode HB.** 2013. Structure and biosynthesis of fimsbactins A-F, siderophores from *Acinetobacter baumannii* and *Acinetobacter baylyi*. Chembiochem **14:**633–638. http://dx.doi.org/10.1002/cbic.201200764.
41. **Nwugo CC, Gaddy JA, Zimbler DL, Actis LA.** 2011. Deciphering the iron response in *Acinetobacter baumannii*: a proteomics approach. J Proteomics **74:**44–58. http://dx.doi.org/10.1016/j.jprot.2010.07.010.
42. **Moriwaki Y, Caaveiro JM, Tanaka Y, Tsutsumi H, Hamachi I, Tsumoto K.** 2011. Molecular basis of recognition of antibacterial porphyrins by heme-transporter IsdH-NEAT3 of *Staphylococcus aureus*. Biochemistry **50:**7311–7320. http://dx.doi.org/10.1021/bi200493h.

Appendix 3

Iron-regulated phospholipase C activity contributes to the cytolytic activity and virulence of *Acinetobacter baumannii*

Steven E. Fiester*, Brock A. Arivett, Robert E. Schmidt, Amber C. Beckett[†], Tomislav Ticak[§], Mary V. Carrier, Emily J. Ohneck, Maeva L. Metz, Marlo K. Sellin Jeffries[‡] and Luis A. Actis[#]

Department of Microbiology, Miami University, Oxford, Ohio

[#]Corresponding author:
Department of Microbiology, Miami University
97 Pearson Hall, Oxford, Ohio 45056
Telephone number: (513) 529-5424
Fax number: (513) 529-2431
E-mail address: actisla@MiamiOH.edu

*Current address: Miami University Middletown, Middletown, OH
[†]Current address: Vanderbilt University, Nashville, TN
[‡]Current address: Texas Christian University, Fort Worth, TX
[§]Current address: University of Idaho, Moscow, ID

Running Title: Phospholipase C in *A. baumannii*

ABSTRACT

Acinetobacter baumannii is an opportunistic Gram-negative coccobacillus pathogen that causes a wide range of infections including urinary tract infections, pneumonia, septicemia, necrotizing fasciitis and severe wound infections. Analysis of *A. baumannii* representative strains grown in Chelex 100-treated medium for hemolytic activity demonstrated that this pathogen is increasingly hemolytic to sheep, human and horse erythrocytes, which interestingly contain increasing amounts of phosphatidylcholine in their membranes. Bioinformatic, genetic and functional analyses of 19 *A. baumannii* isolates showed that the genomes of each strain contained two phosphatidylcholine-specific phospholipase C (PC-PLC) genes, which were named *plc1* and *plc2*, and their culture supernatants tested positive for PC-PLC activity. Further analyses showed that the transcriptional expression of *plc1* and *plc2* and the production of phospholipase activity increased when bacteria were cultured under iron-chelated conditions, which also affected the expression of the acinetobactin-mediated iron acquisition system. Testing of the *A. baumannii* ATCC 19606^{T} *plc1*::*aph-FRT*, *plc2*::*aph* and *plc1*::*ermAM/plc2*::*aph* isogenic insertion derivatives demonstrated that the double PC-PLC mutant expressed significantly reduced cytolytic and hemolytic activity. However, only *plc1* was shown to contribute significantly to *A. baumannii* virulence using the *Galleria mellonella* infection model. Taken together, our data demonstrate that both PLC1 and PLC2, which have diverged from a common ancestor, play a concerted role in hemolytic and cytolytic activities; although PLC1 seems to play a more critical role in the virulence of *A. baumannii* when tested in an animal model. These activities would provide access to intracellular iron stores this pathogen could use during growth in the infected host.

INTRODUCTION

Acinetobacter baumannii is a Gram-negative coccobacillus pathogen linked to severe nosocomial infections including pneumonia, bacteremia, urinary tract infections and necrotizing fasciitis (1, 2). *A. baumannii* infections have been commonly associated with immunocompromised patients; however, cases of community-acquired *A. baumannii* infections in healthy individuals have also been reported (3). Reports have also associated *A. baumannii* with wound infections acquired by combatants deployed to Iraq earning it the popularized name 'Iraqibacter' (4).

Treatment of *A. baumannii* infections is exceedingly difficult due to increasing multi-drug resistance and the limited understanding of its virulence factors, conditions that have a paramount impact on human health worldwide. While the mechanisms of antibiotic resistance associated with this emerging pathogen have been extensively studied, there is a troublesome paucity of literature reporting the molecular mechanisms of virulence associated with *A. baumannii* pathogenicity (5). Among the more understood properties that make *A. baumannii* a successful pathogen is its versatility in acquiring iron (6).

The majority of iron in a host is intracellular; thus the availability of intracellular iron-containing molecules such as hemin, hemoglobin and ferritin is dependent on the lysis of host cells and their subsequent release due to cell and tissue damage found in wounds (7, 8). The liberation of intracellular nutrients may be accomplished by bacterial-mediated cell damage such as that described in *V. cholerae* infections, in which hemolysin-based cytotoxicity lyses intestinal epithelial cells and erythrocytes releasing intracellular iron compounds into the extracellular environment for bacterial utilization (9). One avenue by which bacterial pathogens can lyse host cells is by producing phospholipases, which act on phospholipids in host membranes resulting in

70 membrane destabilizing products thereby leading to cytolysis and the release of host intracellular
71 contents (10).

72 The *A. baumannii* ATCC 19606^{T} strain genome contains genes encoding proteins
73 harboring phospholipase domains including four with a patatin-like protein (PLP) phospholipase
74 domain, one outer membrane protein with a phospholipase A1 domain and two with a
75 phospholipase C domain (http://www.broadinstitute.org/). A more recent report showed that the
76 genome of this strain also includes three genes the products of which are proteins that harbor
77 PLD domains (11). These phospholipases differ in the types of reactions they catalyze; PLP
78 phospholipases are non-specific acyl lipid hydrolases that cleave the acyl ester bond of a
79 phospholipid (12), phospholipase A1 specifically cleaves phospholipids through the hydrolysis
80 of the fatty acyl ester bond at the *sn*-1 position of the glycerol moiety (13), and phospholipase C
81 and phospholipase D cleave before and after the phosphate, respectively.

82 Patatins are plant storage glycoproteins with lipid acyl hydrolase activity that account for
83 30-40% of the total soluble proteins in potatoes (14). The first, and one of the few, PLPs to be
84 characterized in bacteria was the ExoU protein from *Pseudomonas aeruginosa*, which was
85 shown to have phospholipase activity (15, 16). While bacterial PLPs have not been linked to
86 cytolysis, their presence in the genomes of animal and plant pathogens/symbionts is significantly
87 higher than in the genomes of non-pathogens (15). The bacterial phospholipase A1 (PhlA) from
88 *Serratia marcescens* has been implicated in hemolysis of human erythrocytes and cytotoxicity to
89 cervical cancer HeLa and 5637 human bladder epithelial cells (17). The phospholipase C of
90 *Clostridium perfringens*, which is also known as the α toxin, causes cytolysis, tissue destruction
91 and necrosis (10). The phospholipase C produced by *P. aeruginosa* has been linked to
92 hemolysis, tissue destruction and pathologies reminiscent of burn infections (10). Purified

93 phospholipase D, such as that produced by *Corynebacterium pseudotuberculosis*, is
94 dermonecrotic and fatal when injected into animals (18). While many of the phospholipases
95 encoded within the *A. baumannii* ATCC 19606^T genome have possible implications in cytolysis
96 and the ultimate release of iron-rich intracellular contents, the roles of only a few of these
97 phospholipases have been elucidated in this pathogen. Specifically, the role of a phospholipase
98 C and a phospholipase D has been associated with cytolytic activity to the FaDu hypopharyngeal
99 carcinoma epithelial cell line (19) and serum survival and invasion into both human bronchial
100 epithelial BEAS-2B cells and HeLa cells, respectively (20). A recent report showed that three
101 phospholipase D proteins play a critical role in the pathobiology of ATCC 19606^T strain (11).
102 Taken together, these observations indicate that bacterial pathogens can gain access to
103 additional intracellular iron pools and other nutrients present in erythrocytes and tissues through
104 the expression of hemolytic/cytolytic activities. Supernatants of *A. baumannii* cultures grown
105 under iron-chelation are hemolytic to horse erythrocytes and possess phospholipase C activity
106 (21, 22). Our report extends this knowledge by focusing on the characterization of *plc1* and *plc2*
107 and the involvement of the protein products of these two genes in the hemolytic, cytolytic and
108 virulence phenotypes displayed by the *A. baumannii* ATCC 19606^T strain and isogenic
109 derivatives affected in the expression of these two genes.

MATERIALS AND METHODS

Bacterial strains, plasmids, media and culture conditions. The bacterial strains and plasmids used in this work are listed in Table 1. All bacterial strains were routinely stored as Luria-Bertani (LB) broth/glycerol stocks at -80°C (23). *Escherichia coli* DH5α recombinant clones were cultured in LB broth or on LB agar (LBA) (23) supplemented with appropriate antibiotics and incubated overnight (12-14 h) at 37°C. *A. baumannii* strains as well as the *E. coli* MG1655 strain were subcultured from LBA into Chelex 100-treated trypticase soy broth dialysate (TSBD) (24) and grown for 24 h at 37°C with shaking at 200 rpm. These cultures were then used to inoculate fresh TSBD or TSBD containing 10% erythrocytes at a 1/100 ratio and grown for 24 h at 37°C with shaking at 200 rpm unless otherwise indicated. Bacterial cells were enumerated after 24 h using flow cytometry. Culture medium supplemented with erythrocytes was prepared by centrifuging whole blood at 1,000 *x g*, resuspending and washing the erythrocyte pellet three times in erythrocyte wash buffer (20 mM KH_2PO_4, 60 mM Na_2HPO_4 and 120 mM NaCl, pH 8.0) (9) and then resuspending the pellet to a final erythrocyte concentration of 10% in TSBD. Iron-repleted culture conditions were accomplished through the addition of 50 μM $FeCl_3$ dissolved in 0.01 N HCl, while iron-chelated conditions were generated by treating TSB with Chelex 100 (Bio-Rad Laboratories). Bacterial growth curves were determined in octuplet using 96-well microtiter plates containing TSBD under the aforementioned culturing conditions over a 24-h time period. OD_{600} values of these cultures were recorded hourly.

Defibrinated sheep and horse erythrocytes were obtained from Cleveland Scientific, Ltd., and sodium citrate-treated whole human blood was purchased from Bioreclamation, LLC. A549 human alveolar epithelial cells were passaged three times in Dulbecco's modified Eagle's medium (DMEM) supplemented with 10% heat-inactivated fetal bovine serum, 100 IU

penicillin, and 100 μg/ml streptomycin at 37°C in the presence of 5% CO_2. Approximately $1x10^5$ A549 cells, as enumerated using a hemocytometer, were seeded into each well of a 96-well, white, opaque tissue culture plate for a fourth passage that was incubated at 37°C in the presence of 5% CO_2 for 24 h without antibiotics. A549 cell monolayers were infected with 10^6 bacteria suspended in DMEM and incubated at 37°C in the presence of 5% CO_2 for 24 h. The cell monolayers were washed three times with DMEM prior to performing cytolysis assays.

General DNA procedures. Total genomic DNA was isolated using an adapted mini-scale procedure from a previously published method (25), and plasmid DNA was isolated using commercial kits (Qiagen). Restriction digests were performed as suggested by the supplier (New England Biolabs) and size-fractionated by agarose gel electrophoresis (23). PCR primer pairs 3824/3826 and 3822/3827 (Table S1), which hybridize internally of *plc1* and *plc2*, respectively (Fig. 2), were used to confirm the presence of these two genes in 19 *A. baumannii* clinical isolates.

Sequence acquisition and phylogenetic analyses. Nucleotide sequences were analyzed with DNASTAR (DNASTAR, Inc.), BLAST (26) and data available from the Broad Institute. *In silico* identification of potential ferric uptake repressor (Fur)-binding sites upstream of *plc1* and *plc2* was performed using a small training set of predicted Fur-binding sites (27), which were analyzed using MEME Suite 4.10.0 (28). GLAM2 PSSM was used to generate a WebLogo representing the *A. baumannii* Fur-binding motif, and MAST was used to search nucleotide sequences upstream of *plc1* and *plc2* (29-32).

155 The PLC1 and PLC2 amino acid sequences from *A. baumannii* ATCC 19606^T were used
156 as queries for BLASTp (26) to obtain similar sequences, excluding additional amino acid
157 sequences from *A. baumannii*. A total of 101 amino acid sequences were retrieved by setting an
158 arbitrary cutoff of approximately 40% amino acid identity for phylogenetic comparisons to
159 PLC1, PLC2, and the hemolytic (PLCH) and non-hemolytic (PLCN) *P. aeruginosa*
160 phospholipase C proteins (GI 489205171 and GI 489204069), which were added manually.
161 These sequences, which were aligned with MUCSLE using default settings, were analyzed with
162 the multiple sequence alignment (MSA) MEGA6 software package (33, 34). The MSA analysis
163 was done using an apparent-maximum-likelihood method encompassing the WAG (Whelan
164 Goldman) model (35) with a discrete Gamma distribution and rate calculations among invariable
165 sites with FastTree (36). The phylogenetic tree, which was drawn to scale with the highest log
166 likelihood (-714043.274), represents 109 residues analyzed with 1,099 positions in the final
167 dataset.
168
169 **Site-directed insertional mutagenesis of *plc* genes.** The 2.2-kb *plc1* gene (A1S_0043
170 following the *A. baumannii* ATCC 17978 genome annotation) was amplified from ATCC
171 19606^T genomic DNA with *Taq* DNA polymerase and primers 3824 and 3825 (Table S1 and Fig.
172 2). The *plc1* amplicon was cloned into pCR8/GW/TOPO generating pMU1042 (Table 1).
173 Inverse PCR was performed using pMU1042 as a template, Phusion DNA polymerase (New
174 England Biolabs) and primers 4017 and 4018 (Table S1), which hybridize within the *plc1* gene
175 (Fig. 2). The *aph-FRT* cassette, which codes for kanamycin resistance (Km^R), was amplified
176 from pKD13 with Phusion DNA polymerase and primers 4003 and 4004 (Table S1) and ligated
177 within *plc1* using the inverse PCR amplicon described above to generate pMU1089 (Table 1).

178 The *ermAM* cassette, which codes for erythromycin resistance (Em^R), was amplified from
179 pIL252 (Table 1) with Phusion DNA polymerase and primers 4046 and 4047 (Table S1) and
180 ligated within the *plc1* coding region using the inverse PCR amplicon described above to
181 generate pMU1101 (Table 1). Phusion DNA polymerase and primers 3824 and 3825 (Table S1)
182 were used to amplify *plc1*::*aph-FRT* and *plc1*:: *ermAM*, which were each subcloned into the
183 *Sma*I site of pEX100T to generate pMU1091 and pMU1108, respectively (Table 1).

184 The 2.2-kb *plc2* gene (A1S_2055 following the *A. baumannii* ATCC 17978 genome
185 annotation) was PCR amplified from ATCC 19606^T genomic DNA using *Taq* DNA polymerase
186 and primers 3822 and 3823 (Table S1 and Fig. 2), and the resulting amplicon was ligated into
187 pCR8/GW/TOPO to generate pMU1039 (Table 1). Phusion DNA polymerase and primers 3171
188 and 3172 (Table S1) were used to amplify the *aph* cassette from pUC4K (Table 1), which was
189 inserted into the unique *Nsi*I site of the *plc2* gene (Fig. 2) after end repair of *Nsi*I-digested
190 pMU1039 (Table 1) with the End-It Kit (Epicentre) resulting in pMU1040 (Table 1). Phusion
191 DNA polymerase and primers 3822 and 3823 (Table S1) were used to amplify *plc2*::*aph*, which
192 was subsequently cloned into the *Sma*I site of pEX100T to generate pMU1076 (Table 1).

193 Electrocompetent ATCC 19606^T cells were electroporated with pMU1091 and pMU1076
194 as described before (37) to generate the 3452 *plc1*::*aph-FRT* and 3430 *plc2*::*aph* isogenic
195 derivatives, respectively (Table 1). For the generation of the 3494 *plc1*::*ermAM/plc2*::*aph*
196 double insertion isogenic derivative, electrocompetent 3430 cells were electroporated with
197 pMU1108 (Table 1). The ATCC 19606^T 3430 and 3452 isogenic derivatives were selected on
198 LBA plates containing 40 μg/ml kanamycin, while the 3494 derivative was selected on LBA
199 supplemented with 40 μg/ml erythromycin. All isogenic derivatives were plated on LBA plates
200 supplemented with 10% sucrose to ensure loss of pMU1076, pMU1091 and pMU1108. Proper

allelic exchanges were confirmed with PCR using external primers 3905 and 3906 (*plc1*) and 3815 and 3918 (*plc2*) (Table S1).

Transcriptional analyses. Bacterial strains were each grown as five independent 1-ml cultures for 24 h in TSBD or TSBD supplemented with 50 μM $FeCl_3$ at 37°C with shaking at 200 rpm. RNA isolation, cDNA synthesis and qRT-PCR analyses were performed as previously described (38). Briefly, bacterial cells were lysed in lysis buffer [0.3 M sodium acetate (pH 4.0), 30 mM EDTA and 3% SDS] previous to RNA purification following the manufacturer's protocol included with the Maxwell 16 LEV simplyRNA Tissue Kit (Promega). Total RNA concentrations and the 260/280 nm ratios of each RNA sample were assessed using a NanoDrop 2000 UV-Vis spectrophotometer (Thermo Fisher Scientific). RNA integrity was assessed using a RNA 6000 NanoKit for the Bioanalyzer 2100 (Agilent Technologies) and the manufacturers' protocols. Only RNA samples with 260/280 ratios > 1.7 and RNA integrity numbers (RINs) > 5 were further processed for qRT-PCR analysis. The iScript cDNA synthesis kit (Bio-Rad Laboratories) was utilized for cDNA synthesis from 100 ng of total RNA template following the manufacturer's protocol, and iQ SYBR Green (Bio-Rad Laboratories) was used to examine gene transcription following the manufacturer's recommendations. The 10-μl reaction mix included 0.4 μl cDNA, 5 μl iQ SYBR-Green supermix and 300 nM of forward and reverse primers.

Primers 3966 and 3967 (Table S1) were used to amplify a 179-bp internal fragment of the 16S ribosomal RNA gene, which served as an internal control of gene expression, while primers 3970 and 3971 (Table S1) were used to amplify a 156-bp internal fragment of *bauA*, which served as a positive control for gene expression under iron chelation. Primers 3972 and 3973 or 3974 and 3975 (Table S1 and Fig. 2) were used to amplify a 197-bp internal fragment of *plc1*

and a 181-bp internal fragment of *plc2*, respectively. The cycling conditions for qRT-PCR assays, which were performed on a Bio-Rad CFX Connect real-time PCR detection system, were as follows: 95°C for 3 min followed by 40 cycles of 95°C for 10 s and 60°C for 45 s. Relative expression of *plc1* and *plc2* between iron-chelated and iron-repleted conditions was quantified by the standard curve method in which serial dilutions of cDNA samples served as standards. The expression of *plc1* and *plc2* was normalized to that of the 16S ribosomal RNA gene. Samples containing no cDNA template were used as negative controls. qPCR efficiencies were as follow: 16S, 82.4%; *bauA*, 100.9 %; *plc1*, 106.7%; and *plc2*, 97.7%. All samples were analyzed in triplicate and melting curve data were included in the analysis to confirm primers specificity. Data analysis also showed that there were no significant differences in 16S expression between iron-chelated and iron-repleted conditions.

Phospholipase C and cytolysis assays. The presence of phosphatidylcholine-specific phospholipase C activity in *A. baumannii* culture supernatants obtained after centrifugation at 15,000 *x g* for 30 min was tested with the Amplex Red Phosphatidylcholine-Specific Phospholipase C Assay Kit (Molecular Probes) using lecithin as a substrate and following the conditions suggested by the manufacturer's protocol. Erythrocytes incubated in the presence of bacteria were diluted 1:1000 into filter-sterilized FACSFlow sheath fluid (BD Biosciences) for differential interference microscopy (DIC) and enumeration using flow cytometry. Erythrocyte morphological changes were observed in these samples using DIC microscopy on a Zeiss 710 Laser Scanning Confocal System (Carl Zeiss Microscopy GmbH). The number of erythrocytes present in each analyzed sample was quantified using a FACScan flow cytometer (BD Biosciences). Flow Cytometry Absolute Count Standard beads (Bangs Laboratories, Inc.) were

247 added 1:40 to diluted samples to standardize volumes amongst 5-second samplings. Erythrocyte
248 populations were gated using the forward and side scatter channels.

249 The relative number of A549 cells remaining in cell culture following incubation with the
250 parental ATCC 19606^T strain or the 3430, 3452 or 3494 isogenic derivatives was assessed using
251 the CellTiter-Glo luminescent cell viability assay (Promega) following the manufacturer's
252 instructions. Briefly, the number of A549 cells remaining after incubation with bacteria was
253 assessed by measuring the luminescence resulting from the reaction of the provided Ultra-Glo
254 recombinant luciferase with ATP released from metabolically-active A549 cells. The relative
255 luminescence units (RLUs) produced, and thus the relative number of viable A549 cells
256 remaining following infection, was quantified using a FilterMax F5 microplate reader (Beckman
257 Coulter) and reported as a ratio of RLUs produced following lysis of infected A549 cells versus
258 the RLUs produced following lysis of uninfected A549 cells.

259

260 ***Galleria mellonella* virulence assays.** Virulence assays were conducted using the *G. mellonella*
261 model as previously described (39). Briefly, assays were performed by injecting in triplicate 10
262 randomly selected healthy final-instar *G. mellonella* larvae (n=30) injected with 10^5 CFUs/larva
263 (± 0.5 log) of the ATCC 19606^T or its isogenic derivatives suspended in sterile phosphate-
264 buffered saline (PBS). Non-injected larvae or larvae injected with five microliters of sterile PBS
265 were included as controls. After injection, larvae were incubated in darkness at 37°C, and the
266 numbers of dead larvae were assessed at 24-hour intervals over 5 days with removal of dead
267 larvae at times of inspection. Trials were repeated if more than two deaths were observed in any
268 of the control groups.

269

Statistical analyses. The Student's *t*-test or one-way analysis of variance (ANOVA), both provided as part of the GraphPad InStat software package (GraphPad Software, Inc.), were used to analyze the statistical significance of data, as appropriate for the data set. Means of experimental data were compared to the means of the respective control groups using the Tukey-Kramer multiple comparisons post-hoc test. Survival curves were plotted using the Kaplan-Meier method (40) and analyzed for statistical significance using the log-rank test of survival curves (SAS Institute Inc.). Significances for all data analyses were set *a priori* at $P \leq 0.05$.

RESULTS

Membrane lipid preference of the *A. baumannii* hemolytic activity. DIC microscopy of horse erythrocytes incubated in the presence of ATCC 19606^T cells shows that the presence of this strain significantly decreases the number of intact red blood cells remaining in TSBD culture after incubation at 37°C for 24 h (Fig. 1, panels A and B). In addition, the horse erythrocytes showed morphological changes characteristic of cell membrane damage following incubation with ATCC 19606^T (Fig. 1B). In contrast, the number and morphology of sheep erythrocytes did not change after co-incubation under the same conditions (data not shown). These data prompted us to quantitatively determine the number of sheep, horse or human erythrocytes remaining as well as the number of bacterial cells present after 24-h co-incubations in TSBD medium. Flow cytometry analyses of samples obtained from *A. baumannii* ATCC 19606^T, LUH 13000 or AYE cultures containing sheep erythrocytes showed that AYE was the only strain, of the three tested *A. baumannii* strains, to be significantly hemolytic ($P < 0.05$) to sheep erythrocytes, as compared to *E. coli* MG1655, which was used as a hemolysis-negative control (Fig. 1C). A comparison of the mean amounts of sheep erythrocytes remaining after 24-h incubations with ATCC 19606^T, LUH 13000 or AYE under iron-chelation demonstrated a 5%, 3% and 17% reduction in sheep erythrocytes, as compared to the *E. coli* MG1655 hemolysis-negative control, respectively. In contrast, all three *A. baumannii* strains were significantly hemolytic to horse erythrocytes ($P < 0.001$) with the percentage reduction of intact horse erythrocytes ranging from 95% after incubation with ATCC 19606^T or LUH 13000 to 98% after incubation with AYE. Flow cytometry analyses also showed that ATCC 19606^T, LUH 13000 and AYE were hemolytic to human erythrocytes as demonstrated by 41%, 23% and 41% reductions in the numbers of intact human erythrocytes, respectively, with only the hemolysis

caused by ATCC 19606^T and AYE being statistically different from the hemolysis-negative *E. coli* control ($P < 0.001$) (Fig. 1C). Together, flow cytometry analyses of the hemolytic activity of the three tested strains indicate that *A. baumannii* is poorly hemolytic to sheep erythrocytes, intermediately hemolytic to human erythrocytes and almost completely hemolytic to horse erythrocytes (Fig. 1C). Interestingly, we observed that this hemolytic trend correlates with the amount of phosphatidylcholine present in the outer leaflet of the sheep, human or horse erythrocyte membrane when these erythrocytes were incubated in the presence of *A. baumannii* strains grown under chelation to a cell density of approximately 10^8 (41, 42).

***A. baumannii* harbors two phospholipase C genes and produces phosphatidylcholine-specific phospholipase activity.** The direct correlation between the amount of phosphatidylcholine in the erythrocyte membrane and the extent of hemolysis after incubation with *A. baumannii* suggests the potential role of a phosphatidylcholine-specific phospholipase C as the hemolytic effector. Analysis of the ATCC 19606^T genome available through the Broad Institute website (http://www.broadinstitute.org/) showed that this strain has two genes predicted to code for phosphocholine-specific phospholipase C enzymes. One of them (annotated as HMPREF0010_03297 and referred to as *plc1*) has a 2169-nt open reading frame (ORF) coding for a potential 722-amino acid protein (Fig. 2A), which is located downstream of a gene transcribed in the same direction and predicted to code for an RNase PH. A gene coding for a putative nicotinate-nucleotide diphosphorylase is located downstream of *plc1* and transcribed in the opposite direction. The *plc1* gene corresponds to the *plc* ortholog reported as A1S_0043 in ATCC 17978, the expression of which is enhanced by 2.5-fold when bacteria are cultured in the presence of ethanol (19). The other ATCC 19606^T phosphocholine-specific phospholipase C

gene (annotated as HMPREF0010_00294 and referred to as *plc2*) encompasses a predicted 2229-nt ORF coding for a 742- amino acid protein (Fig. 2B). This gene corresponds to the ATCC 17978 A1S_2055 gene identified by Camarena *et al*. (19). A 48-nt intergenic region containing an inverted repeat resembling a Rho-independent transcription termination sequence follows *plc2* and separates this coding region from a potential bicistronic operon, containing a thioesterase and a lactaldehyde reductase coding region, which is transcribed in the opposite direction of *plc2*. Based on ATCC 17978 genomic data (43), a 480-nt intergenic region separates *plc2* from a predicted gene transcribed in the same direction and coding for the DNA polymerase III tau and gamma subunits. These observations indicate that the ATCC 19606^{T} *plc1* and *plc2* are coded for by monocystronic operons as it was reported for ATCC 17978 (19). Other *A. baumannii* genomes including AB0057 (44), ACICU (45), ATCC 17978 (43) and AYE (22) show similar gene arrangements for the chromosomal regions harboring *plc1* and *plc2*, an observation that suggests the conservation of this genomic region across different *A. baumannii* isolates.

Currently, it is unknown if other nosocomial *A. baumannii* strains that have yet to be sequenced possess *plc1* and *plc2*; therefore, the presence of these genes in additional *A. baumannii* strains that had not yet been sequenced was tested by PCR using total genomic DNA and primers which hybridize within the respective coding regions of both phospholipase C genes (Fig. 2). Amplicons of the predicted sizes, 993 bp for *plc1* and 1,167 bp for *plc2*, were obtained for all 19 tested isolates (Fig. S1) confirming the presence of these genes in a variety of *A. baumannii* strains. This screening study was further complemented by testing the presence of phosphatidylcholine-specific phospholipase activity in the culture supernatants of the same 19 *A. baumannii* strains using the Amplex Red phosphatidylcholine-specific phospholipase C assay kit. These assays showed that although the phospholipase C activity of all culture supernatants

347 was significantly higher than the negative control (Fig. 3, $P < 0.001$), there were significant
348 variations among the strains, with the AB3560 and AB3806 wound isolates obtained from
349 injured soldiers being the strains that produced the lowest and highest activities, respectively.
350 However, the phospholipase activity of this particular set of isolates is comparable with the
351 enzymatic activity detected in non-military isolates tested in this study.

352 Preliminary assays showed that phospholipase activity was detected only when ATCC
353 19606^T bacteria were cultured in TSBD, a liquid medium that was dialyzed against Chelex 100,
354 an insoluble polymer that binds several metals, including iron. This observation suggested that
355 the expression of the genes responsible for the production of phospholipase activity could be
356 iron-regulated. Quantitative RT-PCR analyses using total RNA extracted from ATCC 19606^T
357 cells grown in iron-chelated or iron-repleted TSBD showed that transcription of *plc1* and *plc2* is
358 indeed significantly higher ($P < 0.01$ and $P < 0.05$, respectively) in bacteria cultured under iron-
359 depleted conditions when compared with TSBD supplemented with inorganic iron (Fig. 4A).
360 These analyses also showed that the iron-regulated expression of *plc1* and *plc2* is similar to that
361 of *bauA*, which codes for the iron-regulated production of the ATCC 19606^T BauA acinetobactin
362 outer membrane receptor protein (46). It appears likely that the iron-regulated expression of *plc1*
363 and *plc2* is due to the presence of putative Fur-binding sites (Fig. 5), which were located
364 approximately 100 nt and 200 nt upstream of *plc1* and *plc2*, respectively, and found to be
365 significantly related (e-value > 0.05) to the *A. baumannii* Fur motif recently reported (27). This
366 possibility is strongly supported by the observation that hemolysin and siderophore production in
367 *V. cholerae* is co-regulated by iron through a Fur-dependent transcriptional regulatory process
368 (9).

The possibility of compensatory expression between *plc1* and *plc2* was examined using ATCC 19606^T isogenic derivatives harboring the appropriate *plc* mutation. Quantitative RT-PCR analyses of *plc1* transcription in 3430 *plc2*::*aph* cells or *plc2* transcription in 3452 *plc1*::*aph-FRT* cells, all grown in TSBD, showed that there is not a regulatory mechanism by which *plc1* transcription compensates for the lack of *plc2* transcription and *vice versa* (Fig. 4B).

Taken together, these results show that the genomes of multiple *A. baumannii* strains contain two phosphatidylcholine-specific phospholipase C genes, the presence of which could correlate with their capacity to express hemolytic activity, preferentially toward human and horse erythrocytes. Furthermore, the production of this activity depends on the effect of free iron on the differential transcription of *plc1* and *plc2*, which are expressed independently of each other at higher rates under iron limiting conditions.

The *A. baumannii* PLC1 and PLC2 have diverged from a common ancestor protein. Both PLC1 and PLC2 from ATCC 19606^T cluster with phospholipase C proteins from other known pathogens (Fig. 6). PLC1 is located within a clade that includes proteins produced by seven different *Acinetobacter* species with two of them, *oleivorans* and *radioresistens* not being commonly associated with human infections. Interestingly, two of these seven species have been reported as being hemolytic, *A. beijerinckii* sp. nov. (47) and the *A. calcoaceticus* strain 1318/69 that was isolated from the urine of a 70-year old male patient (48, 49). Our preliminary observations also indicate that *A. nosocomialis* M2 expresses hemolytic activity (data not shown). The hemolytic activity of *A. nosocomialis* M2 is not surprising since it is so closely related to *A. baumannii* that it was originally identified as *A. baumannii* M2 (50).

PLC2 groups with a more diverse clade that includes *Achromobacter*, *Cupriavidus* and *Acinetobacter* sequences, with *A. gyllenbergii* being reported to lyse both horse and sheep erythrocytes (47). Interestingly, PLC2 is also in the same clade as phospholipase C produced by bacteria belonging to different genera and species. Although most of these bacteria are non-pathogenic environmental microorganisms that share symbiotic relationships with invertebrates such as *Verminephrobacter aporrectodeae* (51), some of them have been isolated from human patients such as *Massilia timonae* (52), *Bordetella hinzii* (53) and the Melioidosis agent *Burkholderia pseudomallei* (54).

More distant branches from PLC1 and PLC2 contain clusters encompassing phospholipase C proteins from *P. aeruginosa*. The non-hemolytic PLCN of *P. aeruginosa* resides in a group containing *Lysobacter antibioticus* and *Lysobacter capsici*, which play roles in the rhizospheres of rice or peppers, respectively (55, 56). The hemolytic PLCH of *P. aeruginosa* groups outside a cluster of environmental isolates with *Burkholderia* spp. reported to be involved with wound infections, bacteremia and hemolysis (57-60).

Effect of *plc* interruption on cytolysis. The role of the ATCC 19606^T PLC1 and PLC2 proteins in the lysis of erythrocytes and human epithelial cells was tested using the 3452 (*plc1*::*aph-FRT*), 3430 (*plc2*::*aph*) and 3494 (*plc1::ermAM/plc2::aph*) isogenic insertion derivatives. Interruptions in one or both of these genes did not affect the growth of these derivatives; their growth kinetics were not statistically different from that of parental ATCC 19606^T when cultured in TSBD under non-selective conditions (Fig. S2). Flow cytometry analyses showed that the number of intact horse erythrocytes remaining after incubation with the 3430 or 3452 isogenic derivative is not significantly different from the number of erythrocytes remaining after incubation with the

414 ATCC 19606^T parental strain (Fig. 7A). However, the number of erythrocytes remaining
415 following incubation with the 3494 isogenic derivative, which has interruptions in both *plc1* and
416 *plc2*, is more than 3-fold higher ($P < 0.001$) than the number of erythrocytes remaining after
417 incubation with either ATCC 19606^T or the 3430 or 3452 isogenic derivatives (Fig. 7A).

418 The decreased ability of the 3494 isogenic derivative to lyse erythrocytes correlates with
419 that observed when these strains were incubated with A549 human alveolar epithelial cells. In
420 these experiments, the number of A549 cells remaining after 24 h incubation in the presence of
421 ATCC 19606^T, 3430 or 3452 were not significantly different from one another; however, the
422 number of remaining A549 cells following incubation with 3494 was significantly higher ($P <$
423 0.001) than the number remaining after incubation with ATCC 19606^T, 3430 or 3452 (Fig. 7B).
424 Taken together, these observations indicate that the phospholipase C proteins produced by
425 ATCC 19606^T are not host cell specific and have cytolytic activity against different cell types
426 this pathogen could encounter during infection.

427

428 **Role of *plc1* and *plc2* in virulence.** The same strains used to test cytolytic activity were also
429 used to examine the role of *plc1* and *plc2* in the virulence of *A. baumannii* ATCC 19606^T with
430 the *G. mellonella* experimental virulence model we have used previously to determine the
431 virulence role of the acinetobactin-mediated iron acquisition system (39). Figure 8 shows that
432 infection of caterpillars with ATCC 19606^T resulted in a 47% mortality rate, which is
433 significantly higher than the 16% rate scored ($P < 0.05$) with animals that were not injected or
434 injected with sterile PBS as negative controls. There was also a significant difference in percent
435 survival when larvae infected with ATCC 19606^T were compared with larvae infected with
436 either the *plc1*::*aph-FRT* 3452 or the *plc1::ermAM/plc2::aph* 3494 double mutant (13%

437 mortality, $P < 0.01$). Furthermore, the killing rates of these two mutants were not significantly
438 different from each other as well as from the rates scored with animals that were not injected or
439 injected with sterile PBS. In contrast, the death rates of caterpillars infected with the *plc2*::*aph*
440 3430 isogenic derivative, which actively expresses *plc1*, were very similar to those recorded after
441 infection with the ATCC 19606^T parental strain (43% vs. 47%). These observations together
442 with those collected with the cytolytic assays described above indicate that while PLC1 and
443 PLC2 seem to play similar roles in lysing different host cells when tested either under laboratory
444 or *ex vivo* conditions, PLC1 appears to play a more critical role during the infection of a host that
445 mounts an innate immune response that resembles that of vertebrate animals (61).
446

DISCUSSION

Acinetobacter baumannii has been generally considered a non-hemolytic pathogen because, according to our observations, the detection of such an activity depends on two critical factors. One of these factors is the type of erythrocytes used in the detection tests, which are normally conducted using Columbia agar plates containing 5% sheep red blood cells. Our work demonstrates that *A. baumannii* is poorly hemolytic to sheep and increasingly hemolytic to human and horse erythrocytes (Fig. 1C). These observations, which resemble those previously reported for the strains ACICU, AYE, ATCC 17978 and SDF using sheep and horse erythrocytes (21), suggest a direct correlation between the bacterial hemolytic activity and the membrane lipid composition of the different red blood cells used in the hemolytic assays. Accordingly, we observed that the percentage of phosphatidylcholine in the outer leaflet of the sheep, human and horse erythrocyte membrane is 0%, 30% and 42%, respectively (41, 42). Furthermore, the positive correlation between the *A. baumannii* hemolytic activity and the erythrocyte phosphatidylcholine content is reminiscent of a phospholipase C homolog in *P. aeruginosa*, where a hemolytic phospholipase C (PLCH) acts exclusively on phosphatidylcholine and sphingomyelin (62).

The effect of the co-incubation of *A. baumannii* with sensitive erythrocytes, such as those from horse, is apparent not only because of their lysis but also because of the generation of schistocytes due to significant cell membrane damage (Fig. 1B). These fragmented red blood cells have been detected in blood smears obtained from infected neonates during an *A. baumannii* infection outbreak in a Saudi Arabian hospital (63). In this case study of seven neonates, five had a total erythrocyte count lower than controls throughout the course of *A. baumannii* infection, and two of the seven neonates succumbed to *A. baumannii* bacteremia.

These observations clearly underscore the potential role of hemolytic activity in the pathobiology of *A. baumannii*.

The second factor that determines the detection as well as the expression of *A. baumannii* hemolytic activity is the iron content of the culture media. Our data demonstrate that this activity is detectable when bacteria are cultured in an iron-chelated medium but not when the medium is iron rich. Columbia agar, which is used in standard clinical bacteriology methods to detect hemolytic activity, is considered a rich-nutrient medium that would have to be treated with a chelating agent such as Chelex 100 (24) to properly detect hemolytic activity. Accordingly, the differential expression of phospholipase C activity in response to iron chelation correlates well with the iron-regulated transcription of the *plc1* and *plc2* gene orthologs (Fig. 4A), through a regulatory process that is most likely controlled by the interaction of the Fur transcriptional repressor with predicted iron boxes located upstream of these two genes (Fig. 5). The iron-regulated expression of the *plc1* and *plc2* genes and the corresponding phospholipase C activity suggests that *A. baumannii* uses Plc1 and Plc2 for iron acquisition through the lysis of host cells and the subsequent release of iron-rich cytoplasmic contents. This possibility is further supported by the fact that iron co-regulates the expression of *plc1* and *plc2* genes as well as the expression of genes involved in the acinetobactin-mediated iron acquisition system, a response that is similar to that described in *V. cholerae* where the production of hemolysin and vibriobactin are regulated by a Fur-mediated process (9). Whether *A. baumannii* acquires iron from intracellular pools via a siderophore-mediated system or the expression of uncharacterized hemin utilization processes (64) remains to be tested experimentally.

All previous considerations and the observation that *plc1* and *plc2* are present in all sequenced *A. baumannii* genomes as well as the genomes of the clinical strains tested in this

493 study, but absent in the non-pathogenic *A. baylyi* ADP1strain, strongly indicate a role of these
494 phospholipases in bacterial virulence. Until this report, only *plc1* and its role in cytolysis had
495 been tested experimentally where an *A. baumannii* ATCC 17978 *plc1*::*aph* isogenic insertion
496 derivative was less effective in damaging FaDu hypopharyngeal carcinoma epithelial cells as
497 compared to the parental strain (19). Our data not only support the virulence role of *A.*
498 *baumannii* phospholipase C as established by this previous report (19), but also indicate that the
499 modest cytotoxic effect reported is most likely due to the fact that only the inactivation of both
500 *plc1* and *plc2* results in a significant reduction of host cell damage (Fig. 7). Our work also shows
501 that the product of these two genes target different types of host cells *A. baumannii* could
502 encounter during the pathogenesis of systemic infections, as well as the infection of the digestive
503 and respiratory systems as revealed by the damage this pathogen causes to erythrocytes, and the
504 FaDu and A549 epithelial cell lines, respectively. Our data collected using laboratory and *ex-*
505 *vivo* experimental conditions (Fig. 7) suggest that the *plc1* and *plc2* genes code for potentially
506 redundant cytotoxic functions. Only a double *plc1/plc2* mutant showed a significant reduction in
507 cytolytic activity when tested using horse red blood cells and A549 human alveolar epithelial
508 cells. However, the *G. mellonella* experimental infection model showed that this is not the case
509 in an *in vivo* infection model. This model showed that PLC1 but not PLC2 is critical for the
510 virulence of the ATCC 19606^{T} strain (Fig. 8). Interestingly, *plc1* but not *plc2* proved to be
511 transcribed at higher rates when ATCC 17978 bacteria were cultured in the presence of ethanol
512 (19), a condition that also increases the virulence and the expression of virulence-associated
513 traits including biofilm biogenesis and bacterial surface motility (65). Based on all these
514 observations, it is possible to speculate that PLC1 and PLC2 play different roles during the
515 pathogenesis of *A. baumannii* infections, with PLC1 being coded for by a gene the expression of

516 which appears to be regulated at least by iron and stress signals, which are critical for the
517 virulence of this pathogen (39, 65), in an invertebrate host that mounts a complex defense
518 response that mimics that of the human host (61). It is also possible that the biological role of
519 these two enzymes depends on the nature of potential targets, which may reflect significant
520 differences in phospholipid and fatty acid composition between insect and mammalian cells (66).
521 Interestingly, the phylogenetic analysis of PLC2 shows that this protein clusters with a
522 phospholipase C protein from the invertebrate endosymbiote *Verminephrobacter aporrectodeae*
523 (51) (Fig. 6). This finding could explain the lackluster role of PLC2 in virulence using the
524 invertebrate *G. mellonella* virulence model due to a host adaptation process. The phylogenetic
525 analysis also showed that although many of the amino acid sequences used to construct the
526 phylogenetic tree shown in Fig. 6 are from environmental microorganisms isolated from soil,
527 aquatic environments, or industrial sites, it is apparent that there is also a strong correlation of the
528 bacteria producing these enzymes with plants in either antagonistic or synergistic ways (*e.g.*,
529 pathogenesis of blight disease in some plants or nitrogen-fixing bacteria present in the
530 rhizosphere).

531 Taking into account our experimental data together with the observations published by
532 other investigators using different clinical isolates (11, 19-21), it is apparent that *A. baumannii*
533 produces two PLC and three PLD phospholipases. In the particular case of the ATCC 19606^T
534 strain, the three PLD phospholipases are not essential for the utilization of phosphatidylcholine
535 as a carbon and energy source. This finding may indicate that the two PLC produced by this
536 strain could be responsible for the utilization of phosphatidylcholine as a nutrient source by the
537 triple PLD deficient derivative (11). It is also apparent that the ATCC 19606^T PLC and PLD
538 enzymes play a virulence role; although they may function differently during the infection

539 process. The report by Stahl et *al*. (11) shows that all single and double PLD mutants display a
540 virulence phenotype indistinguishable from the parental ATCC 19606^T strain and only the triple
541 Δ*pld1-3* mutant showed a significant reduction in the killing rates throughout the course of the
542 experiment when compared to the parental strain. However, the killing rate of this triple PLD
543 mutant (74% for day 4 after infection) seems to be high if one considers data published by other
544 investigators who have used the same experimental model and included in their Kaplan-Meier
545 plots the control data collected with non-injected animals or animals injected with the same
546 volume of sterile PBS, which unfortunately were not shown in this report (11). Furthermore, the
547 lack of information regarding the CFUs injected per larva rather than OD_{600} also impairs the
548 proper comparison of our results with those recently reported using the same strain and
549 comparable experimental conditions. Nevertheless, it is possible to speculate that there is a
550 residual virulence activity in the triple Δ*pld1-3* ATCC 19606^T mutant that could account for the
551 activity of the PLC1 but not PLC2 as we describe in this report. This critical issue as well as the
552 question of whether the *A. baumannii* PLD enzymes are differentially produced in response to
553 extracellular signals and display selective cytolytic activity in response to differences in
554 membrane lipid composition are critical topics that remain to be tested experimentally using the
555 proper ATCC 19606^T isogenic derivatives. Such knowledge will not only further our
556 understanding of the role(s) of phospholipases in the pathobiology of *A. baumannii*, but also
557 provide critical information needed to determine whether these enzymes could be used as
558 alternative targets to treat the severe infections caused by this pathogen, particularly by emerging
559 multi-drug resistant isolates.

ACKNOWLEDGEMENTS

This work was supported by funding from Public Health AI070174 and Department of Defense W81XWH-12-2-0035 awards, and Miami University research funds. We thank Drs. D. Zurawski (Walter Reed Army Institute of Research, Silver Spring, Maryland, USA) and L. Dijkshoorn (Leiden University Medical Center, Department of Infectious Diseases, Leiden, The Netherlands) for providing the wound clinical isolates and the LUH and RUH strains, respectively, which are listed in Table 1. We are also grateful to Dr. E. Lafontaine (College of Veterinary Medicine, University of Georgia, USA) for providing the A549 cell line. The findings and opinions expressed herein belong to the authors and do not necessarily reflect the official views of the WRAIR, the U.S. Army, or the Department of Defense.

REFERENCES

1. **Charnot-Katsikas A, Dorafshar AH, Aycock JK, David MZ, Weber SG, Frank KM.** 2009. Two cases of necrotizing fasciitis due to *Acinetobacter baumannii*. J. Clin. Microbiol. **47:**258-263.
2. **Peleg AY, Seifert H, Paterson DL.** 2008. *Acinetobacter baumannii*: emergence of a successful pathogen. Clin. Microbiol. Rev. **21:**538-582.
3. **Ozaki T, Nishimura N, Arakawa Y, Suzuki M, Narita A, Yamamoto Y, Koyama N, Nakane K, Yasuda N, Funahashi K.** 2009. Community-acquired *Acinetobacter baumannii* meningitis in a previously healthy 14-month-old boy. J. Infect. Chemother. **15:**322-324.
4. **Davis KA, Moran KA, McAllister CK, Gray PJ.** 2005. Multidrug-resistant *Acinetobacter* extremity infections in soldiers. Emerg. Infect. Dis. **11:**1218-1224.
5. **Actis LA.** 2010. Insight into innovative approaches to battle *Acinetobacter baumannii* infection therapy struggles. Virulence **1:**6-7.
6. **McConnell MJ, Actis L, Pachon J.** 2013. *Acinetobacter baumannii*: human infections, factors contributing to pathogenesis and animal models. FEMS Microbiol. Rev. **37:**130-155.
7. **Fiester SE, Actis LA.** 2013. Stress responses in the opportunistic pathogen *Acinetobacter baumannii*. Future Microbiol. **8:**353-365.
8. **Yeoh-Ellerton S, Stacey MC.** 2003. Iron and 8-isoprostane levels in acute and chronic wounds. J. Invest. Dermatol. **121:**918-925.
9. **Stoebner JA, Payne SM.** 1988. Iron-regulated hemolysin production and utilization of heme and hemoglobin by *Vibrio cholerae*. Infect. Immun. **56:**2891-2895.
10. **Schmiel DH, Miller VL.** 1999. Bacterial phospholipases and pathogenesis. Microbes and infection / Institut Pasteur **1:**1103-1112.

11. **Stahl J, Bergmann H, Gottig S, Ebersberger I, Averhoff B.** 2015. *Acinetobacter baumannii* virulence is mediated by the concerted action of three phospholipases D. PLoS One **10:**e0138360.
12. **Rydel TJ, Williams JM, Krieger E, Moshiri F, Stallings WC, Brown SM, Pershing JC, Purcell JP, Alibhai MF.** 2003. The crystal structure, mutagenesis, and activity studies reveal that patatin is a lipid acyl hydrolase with a Ser-Asp catalytic dyad. Biochemistry **42:**6696-6708.
13. **Istivan TS, Coloe PJ.** 2006. Phospholipase A in Gram-negative bacteria and its role in pathogenesis. Microbiology **152:**1263-1274.
14. **Andrews DL, Beames B, Summers MD, Park WD.** 1988. Characterization of the lipid acyl hydrolase activity of the major potato (*Solanum tuberosum*) tuber protein, patatin, by cloning and abundant expression in a baculovirus vector. Biochem. J. **252:**199-206.
15. **Banerji S, Flieger A.** 2004. Patatin-like proteins: a new family of lipolytic enzymes present in bacteria? Microbiology **150:**522-525.
16. **Phillips RM, Six DA, Dennis EA, Ghosh P.** 2003. *In vivo* phospholipase activity of the *Pseudomonas aeruginosa* cytotoxin ExoU and protection of mammalian cells with phospholipase A2 inhibitors. J. Biol. Chem. **278:**41326-41332.
17. **Shimuta K, Ohnishi M, Iyoda S, Gotoh N, Koizumi N, Watanabe H.** 2009. The hemolytic and cytolytic activities of *Serratia marcescens* phospholipase A (PhlA) depend on lysophospholipid production by PhlA. BMC Microbiol. **9:**261.
18. **Muckle CA, Gyles CL.** 1983. Relation of lipid content and exotoxin production to virulence of *Corynebacterium pseudotuberculosis* in mice. Am. J. Vet. Res. **44:**1149-1153.

19. **Camarena L, Bruno V, Euskirchen G, Poggio S, Snyder M.** 2010. Molecular mechanisms of ethanol-induced pathogenesis revealed by RNA-sequencing. PLoS Pathog. **6:**e1000834.
20. **Jacobs AC, Hood I, Boyd KL, Olson PD, Morrison JM, Carson S, Sayood K, Iwen PC, Skaar EP, Dunman PM.** 2010. Inactivation of phospholipase D diminishes *Acinetobacter baumannii* pathogenesis. Infect. Immun. **78:**1952-1962.
21. **Antunes LC, Imperi F, Carattoli A, Visca P.** 2011. Deciphering the multifactorial nature of *Acinetobacter baumannii* pathogenicity. PLoS One **6:**e22674.
22. **Vallenet D, Nordmann P, Barbe V, Poirel L, Mangenot S, Bataille E, Dossat C, Gas S, Kreimeyer A, Lenoble P, Oztas S, Poulain J, Segurens B, Robert C, Abergel C, Claverie JM, Raoult D, Medigue C, Weissenbach J, Cruveiller S.** 2008. Comparative analysis of Acinetobacters: three genomes for three lifestyles. PLoS One **3:**e1805.
23. **Sambrook J, Russell DW.** 2001. Molecular Cloning. A Laboratory Manual, 3rd ed. Cold Spring Harbor Laboratory Press, Cold Spring Harbor, N. Y.
24. **Ohman DE, Sadoff JC, Iglewski BH.** 1980. Toxin A-deficient mutants of *Pseudomonas aeruginosa* PA103: isolation and characterization. Infect. Immun. **28:**899-908.
25. **Barcak JG, Chandler MS, Redfield RJ, Tomb JF.** 1991. Genetic systems in *Haemophilus influenzae*. Methods Emzymol. **204:**321-432.
26. **Altschul SF, Gish W, Miller W, Myers EW, Lipman DJ.** 1990. Basic local alignment search tool. J. Mol. Biol. **215:**403-410.
27. **Eijkelkamp BA, Hassan KA, Paulsen IT, Brown MH.** 2011. Investigation of the human pathogen *Acinetobacter baumannii* under iron limiting conditions. BMC Genomics **12:**126.

28. **Bailey TL, Boden M, Buske FA, Frith M, Grant CE, Clementi L, Ren J, Li WW, Noble WS.** 2009. MEME SUITE: tools for motif discovery and searching. Nucleic Acids Res. **37:**W202-208.

29. **Bailey TL, Gribskov M.** 1998. Combining evidence using p-values: application to sequence homology searches. Bioinformatics **14:**48-54.

30. **Crooks GE, Hon G, Chandonia JM, Brenner SE.** 2004. WebLogo: a sequence logo generator. Genome Res. **14:**1188-1190.

31. **Frith MC, Saunders NF, Kobe B, Bailey TL.** 2008. Discovering sequence motifs with arbitrary insertions and deletions. PLoS Comput. Biol. **4:**e1000071.

32. **Schneider TD, Stephens RM.** 1990. Sequence logos: a new way to display consensus sequences. Nucleic Acids Res. **18:**6097-6100.

33. **Edgar RC.** 2004. MUSCLE: multiple sequence alignment with high accuracy and high throughput. Nucleic Acids Res. **32:**1792-1797.

34. **Tamura K, Stecher G, Peterson D, Filipski A, Kumar S.** 2013. MEGA6: Molecular Evolutionary Genetics Analysis version 6.0. Mol. Biol. Evol. **30:**2725-2729.

35. **Whelan S, Goldman N.** 2001. A general empirical model of protein evolution derived from multiple protein families using a maximum-likelihood approach. Mol. Biol. Evol. **18:**691-699.

36. **Price MN, Dehal PS, Arkin AP.** 2010. FastTree 2 – approximately maximum-likelihood trees for large alignments. PLoS One **5:**e9490.

37. **Dorsey CW, Tomaras AP, Actis LA.** 2002. Genetic and phenotypic analysis of *Acinetobacter baumannii* insertion derivatives generated with a Transposome system. Appl. Environ. Microbiol. **68:**6353-6360.

38. **Fiester SE, Nwugo CC, Penwell WF, Neary JM, Beckett AC, Arivett BA, Schmidt RE, Geiger SC, Connerly PL, Menke SM, Tomaras AP, Actis LA.** 2015. Role of the carboxy terminus of SecA in iron acquisition, protein translocation, and virulence of the bacterial pathogen *Acinetobacter baumannii*. Infect. Immun. **83:**1354-1365.

39. **Gaddy JA, Arivett BA, McConnell MJ, Lopez-Rojas R, Pachon J, Actis LA.** 2012. Role of acinetobactin-mediated iron acquisition functions in the interaction of *Acinetobacter baumannii* ATCC 19606^{T} with human lung epithelial cells, *Galleria mellonella* caterpillars and mice. Infect. Immun. **80:**1015-1024.

40. **Kaplan EL, Meier P.** 1958. Nonparametric estimation from incomplete data. J. Amer. Statist. Assn. **53:**457-481.

41. **Engelmann B, Streich S, Schonthier UM, Richter WO, Duhm J.** 1992. Changes of membrane phospholipid composition of human erythrocytes in hyperlipidemias. I. Increased phosphatidylcholine and reduced sphingomyelin in patients with elevated levels of triacylglycerol-rich lipoproteins. Biochim. Biophys. Acta **1165:**32-37.

42. **Nelson GJ.** 1967. Lipid composition of erythrocytes in various mammalian species. Biochim. Biophys. Acta **144:**221-232.

43. **Smith MG, Gianoulis TA, Pukatzki S, Mekalanos JJ, Ornston LN, Gerstein M, Snyder M.** 2007. New insights into *Acinetobacter baumannii* pathogenesis revealed by high-density pyrosequencing and transposon mutagenesis. Genes Dev. **21:**601-614.

44. **Adams MD, Goglin K, Molyneaux N, Hujer KM, Lavender H, Jamison JJ, MacDonald IJ, Martin KM, Russo T, Campagnari AA, Hujer AM, Bonomo RA, Gill SR.** 2008. Comparative genome sequence analysis of multidrug-resistant *Acinetobacter baumannii*. J. Bacteriol. **190:**8053-8064.

45. **Iacono M, Villa L, Fortini D, Bordoni R, Imperi F, Bonnal RJ, Sicheritz-Ponten T, De Bellis G, Visca P, Cassone A, Carattoli A.** 2008. Whole-genome pyrosequencing of an epidemic multidrug-resistant *Acinetobacter baumannii* strain belonging to the European clone II group. Antimicrob. Agents Chemother. **52:**2616-2625.

46. **Dorsey CW, Tomaras AP, Connerly PL, Tolmasky ME, Crosa JH, Actis LA.** 2004. The siderophore-mediated iron acquisition systems of *Acinetobacter baumannii* ATCC 19606 and *Vibrio anguillarum* 775 are structurally and functionally related. Microbiology **150:**3657-3667.

47. **Nemec A, Musilek M, Maixnerova M, De Baere T, van der Reijden TJ, Vaneechoutte M, Dijkshoorn L.** 2009. *Acinetobacter beijerinckii* sp. nov. and *Acinetobacter gyllenbergii* sp. nov., haemolytic organisms isolated from humans. Int. J. Syst. Evol. Microbiol. **59:**118-124.

48. **Lehmann V.** 1971. Haemolytic activity of *Acinetobacter calcoaceticus*. Acta Pathol. Microbiol. Scand. B Microbiol. Immunol. **79:**61-66.

49. **Lehmann V.** 1973. Haemolytic activity of various strains of *Acinetobacter*. Acta Pathol. Microbiol. Scand. B Microbiol. Immunol. **81:**427-432.

50. **Carruthers MD, Harding CM, Baker BD, Bonomo RA, Hujer KM, Rather PN, Munson RS, Jr.** 2013. Draft Genome Sequence of the Clinical Isolate *Acinetobacter nosocomialis* Strain M2. Genome. Announc. **1:**e00906-00913.

51. **Lund MB, Schatzle S, Schramm A, Kjeldsen KU.** 2012. *Verminephrobacter aporrectodeae* sp. nov. subsp. *tuberculatae* and subsp. *caliginosae*, the specific nephridial symbionts of the earthworms *Aporrectodea tuberculata* and *A. caliginosa*. Antonie Van Leeuwenhoek **101:**507-514.

52. **Lindquist D, Murrill D, Burran WP, Winans G, Janda JM, Probert W.** 2003. Characteristics of *Massilia timonae* and *Massilia timonae*-like isolates from human patients, with an emended description of the species. J. Clin. Microbiol. **41:**192-196.

53. **Fry NK, Duncan J, Edwards MT, Tilley RE, Chitnavis D, Harman R, Hammerton H, Dainton L.** 2007. A UK clinical isolate of *Bordetella hinzii* from a patient with myelodysplastic syndrome. J. Med. Microbiol. **56:**1700-1703.

54. **Limmathurotsakul D, Peacock SJ.** 2011. Melioidosis: a clinical overview. Br. Med. Bull. **99:**125-139.

55. **Ji GH, Wei LF, He YQ, Wu YP, Bai XH.** 2008. Biological control of rice bacterial blight by *Lysobacter antibioticus* strain 13-1. Biol. Control **45:**288-296.

56. **Park JH, Kim R, Aslam Z, Jeon CO, Chung YR.** 2008. *Lysobacter capsici* sp nov., with antimicrobial activity, isolated from the rhizosphere of pepper, and emended description of the genus *Lysobacter*. Int. J. Syst. Evol. Microbiol. **58:**387-392.

57. **Bevivino A, Dalmastri C, Tabacchioni S, Chiarini L, Belli ML, Piana S, Materazzo A, Vandamme P, Manno G.** 2002. *Burkholderia cepacia* complex bacteria from clinical and environmental sources in Italy: genomovar status and distribution of traits related to virulence and transmissibility. J. Clin. Microbiol. **40:**846-851.

58. **Gerrits GP, Klaassen C, Coenye T, Vandamme P, Meis JF.** 2005. *Burkholderia fungorum* septicemia. Emerg. Infect. Dis. **11:**1115-1117.

59. **Glass MB, Steigerwalt AG, Jordan JG, Wilkins PP, Gee JE.** 2006. *Burkholderia oklahomensis* sp. nov., a *Burkholderia pseudomallei*-like species formerly known as the Oklahoma strain of *Pseudomonas pseudomallei*. Int. J. Syst. Evol. Microbiol. **56:**2171-2176.

60. **McCormick JB, Weaver RE, Hayes PS, Boyce JM, Feldman RA.** 1977. Wound infection by an indigenous *Pseudomonas pseudomallei*-like organism isolated from the soil: case report and epidemiologic study. J. Infect. Dis. **135:**103-107.

61. **Kavanagh K, Reeves EP.** 2004. Exploiting the potential of insects for *in vivo* pathogenicity testing of microbial pathogens. FEMS Microbiol. Rev. **28:**101-112.

62. **Ostroff RM, Vasil AI, Vasil ML.** 1990. Molecular comparison of a nonhemolytic and a hemolytic phospholipase C from *Pseudomonas aeruginosa*. J. Bacteriol. **172:**5915-5923.

63. **El-Feky EAM, Aref SH.** 2011. A Study of hematological profile during the outbreak of *Acinetobacter baumannii* bacteremia in neonatal ward in Pediatrics Hospital in Saudi Arabia. Aust. J. Basic and Appl. Sci. **5:**747-754.

64. **Zimbler DL, Penwell WF, Gaddy JA, Menke SM, Tomaras AP, Connerly PL, Actis LA.** 2009. Iron acquisition functions expressed by the human pathogen *Acinetobacter baumannii*. Biometals **22:**23-32.

65. **Nwugo CC, Arivett BA, Zimbler DL, Gaddy JA, Richards AM, Actis LA.** 2012. Effect of ethanol on differential protein production and expression of potential virulence functions in the opportunistic pathogen *Acinetobacter baumannii*. PLoS One **7:**e51936.

66. **Marheineke K, Grunewald S, Christie W, Reilander H.** 1998. Lipid composition of *Spodoptera frugiperda* (Sf9) and *Trichoplusia ni* (Tn) insect cells used for baculovirus infection. FEBS Lett. **441:**49-52.

67. **van Dessel H, Dijkshoorn L, van der Reijden T, Bakker N, Paauw A, van den Broek P, Verhoef J, Brisse S.** 2004. Identification of a new geographically widespread multiresistant *Acinetobacter baumannii* clone from European hospitals. Res. Microbiol. **155:**105-112.

68. **van den Broek PJ, Arends J, Bernards AT, De Brauwer E, Mascini EM, van der Reijden TJ, Spanjaard L, Thewessen EA, van der Zee A, van Zeijl JH, Dijkshoorn L.** 2006. Epidemiology of multiple *Acinetobacter* outbreaks in The Netherlands during the period 1999-2001. Clin. Microbiol. Infect. **12:**837-843.

69. **van den Broek PJ, van der Reijden TJ, van Strijen E, Helmig-Schurter AV, Bernards AT, Dijkshoorn L.** 2009. Endemic and epidemic *Acinetobacter* species in a university hospital: an 8-year survey. J. Clin. Microbiol. **47:**3593-3599.

70. **Dijkshoorn L, Aucken H, Gerner-Smidt P, Janssen P, Kaufmann ME, Garaizar J, Ursing J, Pitt TL.** 1996. Comparison of outbreak and nonoutbreak *Acinetobacter baumannii* strains by genotypic and phenotypic methods. J. Clin. Microbiol. **34:**1519-1525.

TABLE 1 Strains and plasmids used in this study

Strain/plasmid	Relevant characteristic(s)[a]	Source/reference
Strains		
A. baumannii		
17978	Clinical isolate	ATCC
19606^T	Clinical isolate, type strain	ATCC
19606^T 3452	*plc1*::*aph-FRT* derivative of 19606^T; Km^R	This work
19606^T 3430	*plc2*::*aph* derivative of 19606^T; Km^R	This work
19606^T 3494	*plc1*::*ermAM/plc2*::*aph* derivative of 19606^T; Em^R, Km^R	This work
AB3340	Wound isolate	Zurawski, D.
AB3560	Wound isolate	Zurawski, D.
AB3638	Wound isolate	Zurawski, D.
AB3806	Wound isolate	Zurawski, D.
AB4026	Wound isolate	Zurawski, D.
AB4052	Wound isolate	Zurawski, D.
AB4456	Wound isolate	Zurawski, D.
AB4498	Wound isolate	Zurawski, D.
AB5075	Wound isolate	Zurawski, D.
AB5197	Wound isolate	Zurawski, D.
AYE	Wound isolate	ATCC
LUH 5875	Clinical isolate, reference strain, EU clone III	(67)
LUH 07672	Clinical isolate, EU clone III	(68)
LUH 8809	Clinical isolate, EU clone I	(69)
LUH 13000	Clinical isolate, EU clone II	Dijkshoorn, L.
RUH 134	Clinical isolate, reference strain, EU clone II	(70)
RUH 875	Clinical isolate, reference strain, EU clone I	(70)
E. coli		
DH5α	Used for recombinant DNA methods	Gibco-BRL
MG1655	Displays γ-hemolysis	Blattner, F. R.
Plasmids		
pCR8/GW/TOPO	PCR cloning vector; Sp^R	Life Technologies
pKD13	Source of *aph-FRT* cassette; Ap^R, Km^R	Crosa, J. H.
pUC4K	Source of *aph* cassette; Ap^R, Km^R	Life Technologies
pIL252	Source of *ermAM* cassette; Em^R	Kruse, T.
pEX100T	Mobilizable suicide plasmid in 19606^T; Ap^R	ATCC
pMU1039	pCR8/GW/TOPO harboring *plc2*; Sp^R	This work
pMU1040	Insertion of *aph* into pMU1039; Sp^R, Km^R	This work
pMU1042	pCR8/GW/TOPO harboring *plc1*; Sp^R	This work
pMU1076	Insertion of pMU1040 into pEX100T; Ap^R, Km^R	This work
pMU1089	Insertion of *aph-FRT* into pMU1042; Sp^R, Km^R	This work
pMU1091	Insertion of pMU1089 into pEX100T; Ap^R, Km^R	This work
pMU1101	Insertion of *ermAM* into pMU1042; Sp^R, Em^R	This work
pMU1108	Insertion of pMU1101 into pEX100T; Ap^R, Em^R	This work

[a]Ap^R, ampicillin resistance; Em^R, erythromycin resistance; Km^R, kanamycin resistance; Sp^R, spectinomycin resistance.

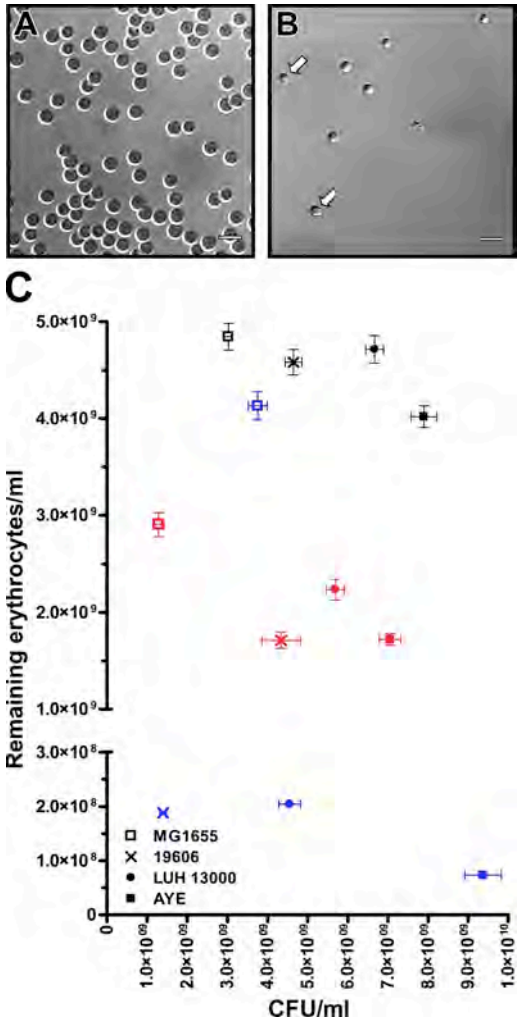

FIG 1 Hemolytic activity of *E. coli* and *A. baumannii*. DIC image of horse erythrocytes incubated in TSBD alone (A) or TSBD inoculated with ATCC 19606^{T} (B). White arrows identify damaged erythrocytes. White bars represent 10 μm. (C) Quantification of intact sheep (black), human (red) or horse (blue) erythrocytes remaining after incubation with *E. coli* MG1655 or each of the three different *A. baumannii* strains. All incubations were conducted for 24 h at 37°C with shaking at 200 rpm. Error bars represent the standard error (SE) of the mean for data collected in triplicate from three individual biological samples.

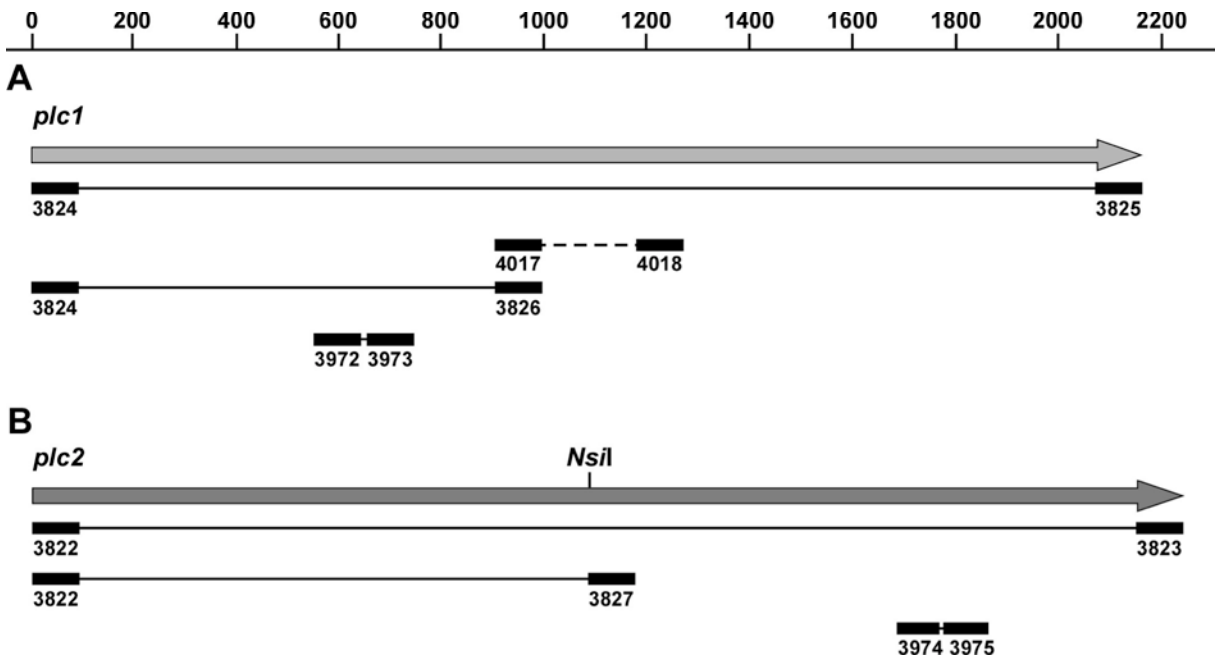

FIG 2 *A. baumannii* ATCC 19606^T genetic loci harboring the *plc1* and *plc2* genes. Genetic map of *plc1* (A) and *plc2* (B). The horizontal arrows represent the direction of transcription of predicted coding regions. Numbers on top of A indicate size in base pairs. The location of the *Nsi*I restriction site used to generate the *plc2::aph* insertion derivative is indicated in panel B. Black rectangles connected with solid black lines identify primers and amplicons used to clone *plc1* and *plc2*, test their presence in different *A. baumannii* strains and examine their transcription by qRT-PCR. Numbers underneath of each black rectangle indicate primer numbers as listed in Table S1. The black rectangles connected with a dashed line in panel A indicate the location of the primers 4017 and 4018 and the deleted fragment replaced with the *aph-FRT* gene used to generate the *plc1* deletion/insertion derivative by inverse PCR.

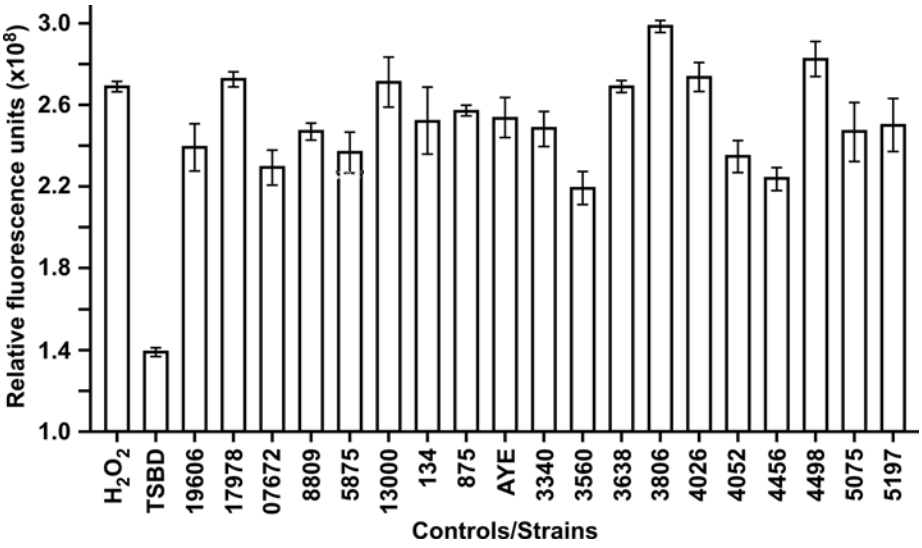

FIG 3 Phosphatidylcholine-specific phospholipase C activity among *A. baumannii* isolates. Culture supernatants from 19 *A. baumannii* strains grown in TSBD were tested for phosphatidylcholine-specific phospholipase C using the Amplex Red phosphatidylcholine-specific phospholipase C assay kit, using hydrogen peroxide or uninoculated TSBD medium as positive and negative controls, respectively. Tested strains are identified as follows: 19606 and 17978 represent ATCC strains, 07672-13000 represent LUH strains, 134 and 875 represent RUH strains, and 3340-5197 represent AB wound isolates as listed in Table 1. Error bars represent the standard error (SE) of the mean.

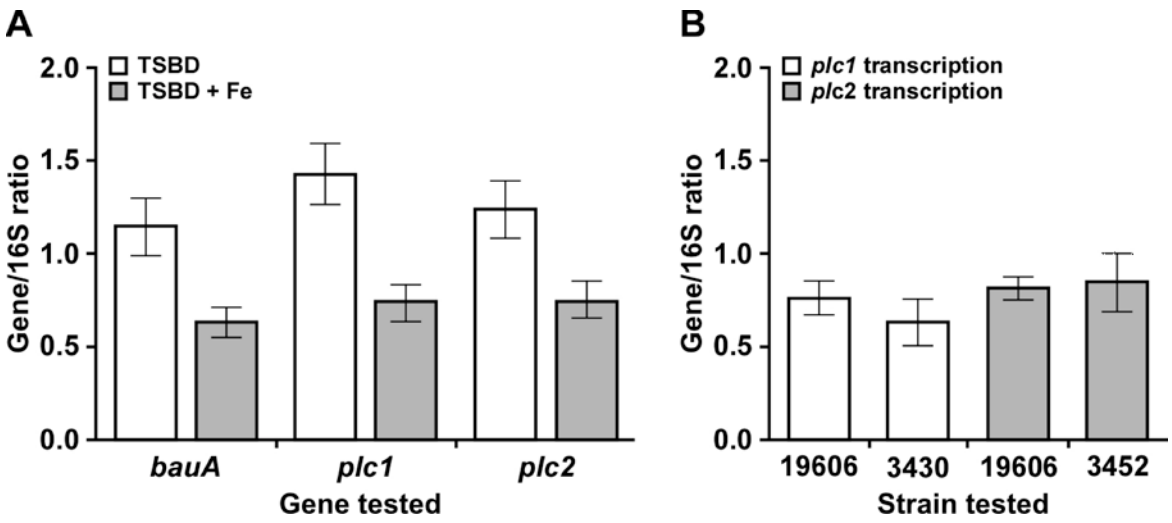

FIG 4 Analyses of *plc1* and *plc2* transcription in ATCC 19606^T and isogenic derivatives. (A) Transcriptional analyses of *plc1* and *plc2* in ATCC 19606^T cells grown in TSBD or TSBD supplemented with 50 μM $FeCl_3$ (TSBD + Fe). Expression of *bauA* was used as a positive control for iron-regulated gene expression. (B) Transcriptional analyses of *plc1* and *plc2* genes in cells of the ATCC 19606^T parental strain or the isogenic derivatives 3430 (*plc2::aph*) or 3452 (*plc1::aph-FRT*) cells grown in TSBD for 24 h at 37°C with shaking at 200 rpm. Expression of *plc* genes was normalized to the expression of the 16S gene. Error bars represent the standard error (SE) of the mean.

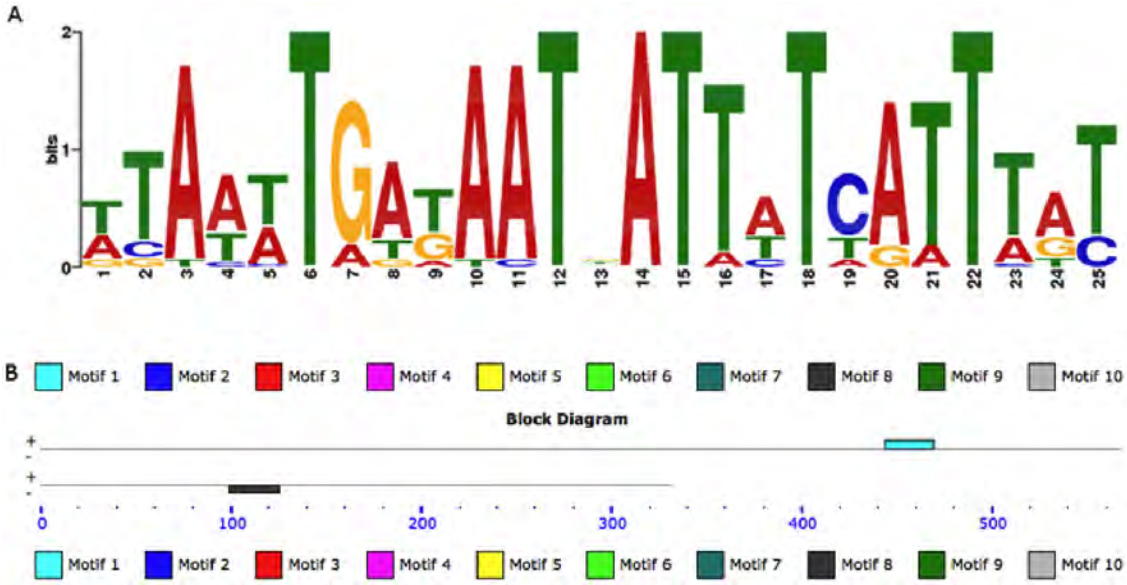

FIG 5 *In silico* ferric uptake repressor (Fur)-binding site prediction. The most significant prediction of the Fur-binding motif (A) and the locations of the motifs in the mRNA leader sequences of *plc1* (top line) and *plc2* (bottom line) from ATCC 19606^T (B). The location of the predicted Fur boxes in *plc1* (top line) and *plc2* are shown as aqua and black rectangles, respectively.

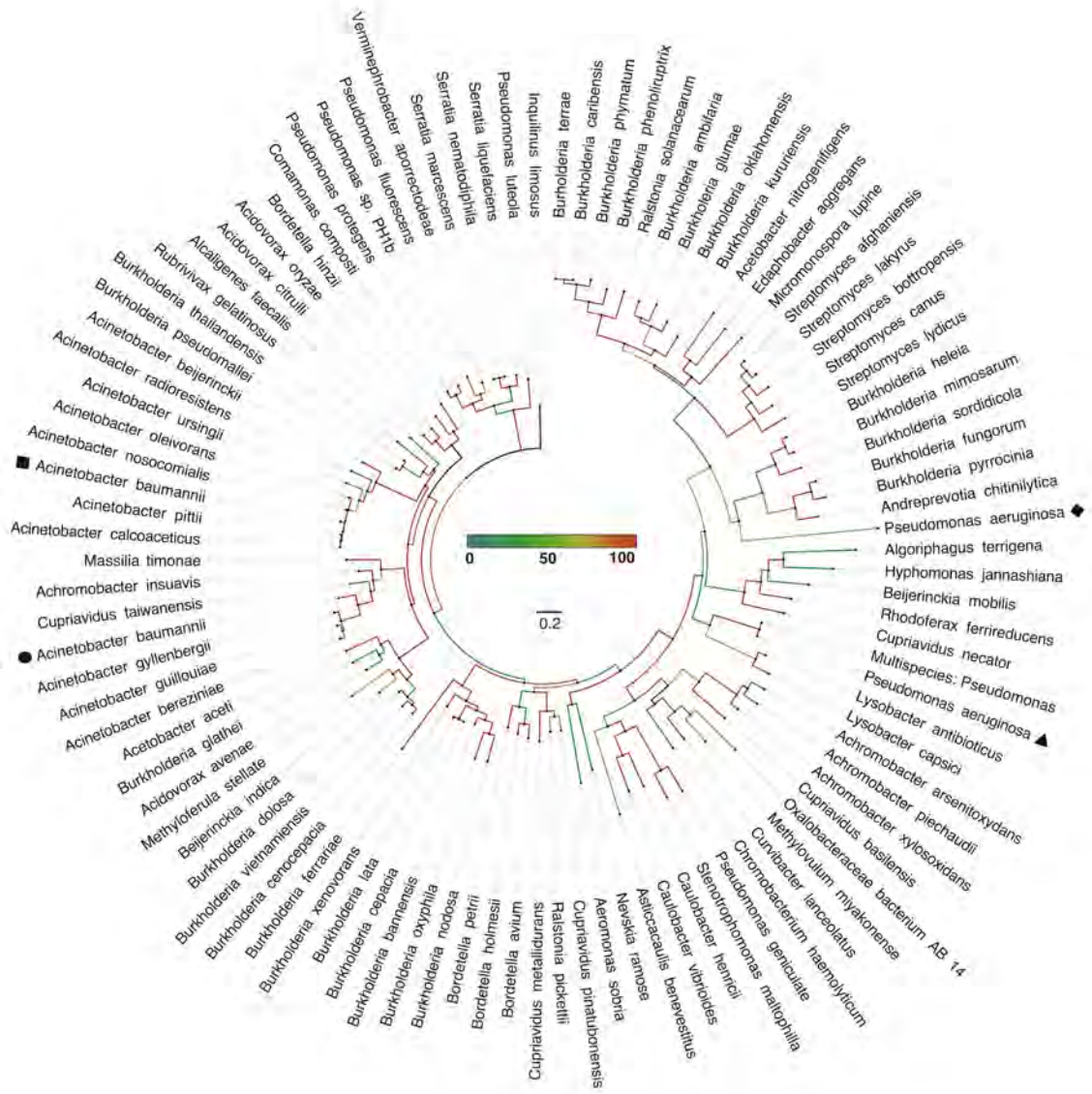

FIG 6 Phylogenetic analysis of phospholipase C protein sequences of *A. baumannii* ATCC 19606^{T}. An unrooted approximate-maximum-likelihood tree inferred in FastTree showing the locations of both *A. baumannii* (Plc1, black square; Plc2, black circle,) and *P. aeruginosa* (non-hemolytic, black triangle; hemolytic, black diamond,) phospholipase C proteins relative to other Plc proteins. Percent confidence through 1,000 iterations is represented in the center of the image as a heat map in addition to a scale bar representing substitutions per site.

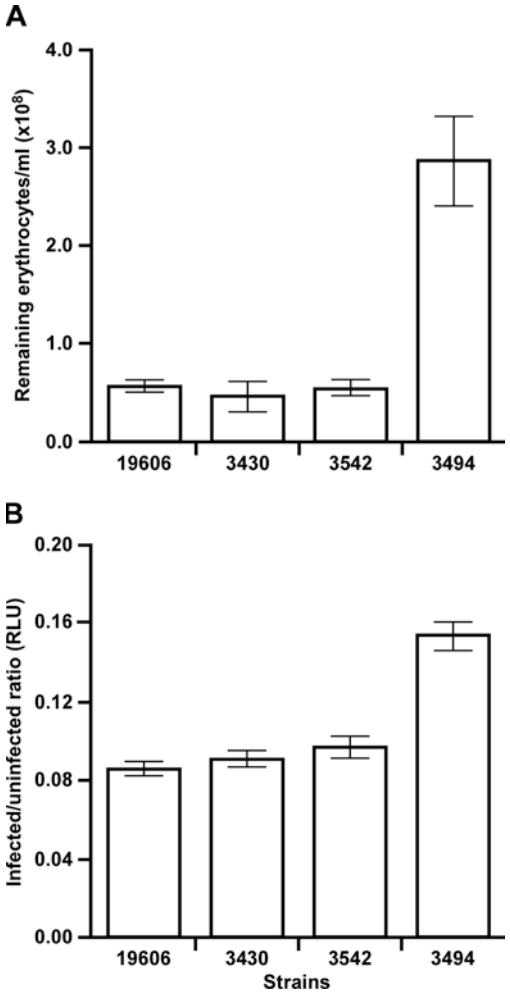

FIG 7 Cytolytic activity of ATCC 19606^T and the 3430, 3452 and 3494 isogenic derivatives. (A) Number of remaining horse erythrocytes after incubation with ATCC 19606^T or the isogenic derivatives 3430 (*plc2*::*aph*), 3452 (*plc1*::*aph-FRT*) or 3494 (*plc1::ermAM/plc2::aph*) in TSBD for 24 h at 37°C with shaking at 200 rpm. (B) Relative number of intact A549 cells remaining after incubation in the presence of ATCC 19606^T or the isogenic derivatives 3430, 3452 or 3494 for 24 h at 37°C in the presence of 5% CO_2. Relative luminescence units (RLU) were determined as the ratio between the number of A549 cells present in uninfected samples and each sample infected with a different bacterial strain. Error bars represent the standard error (SE) of the mean.

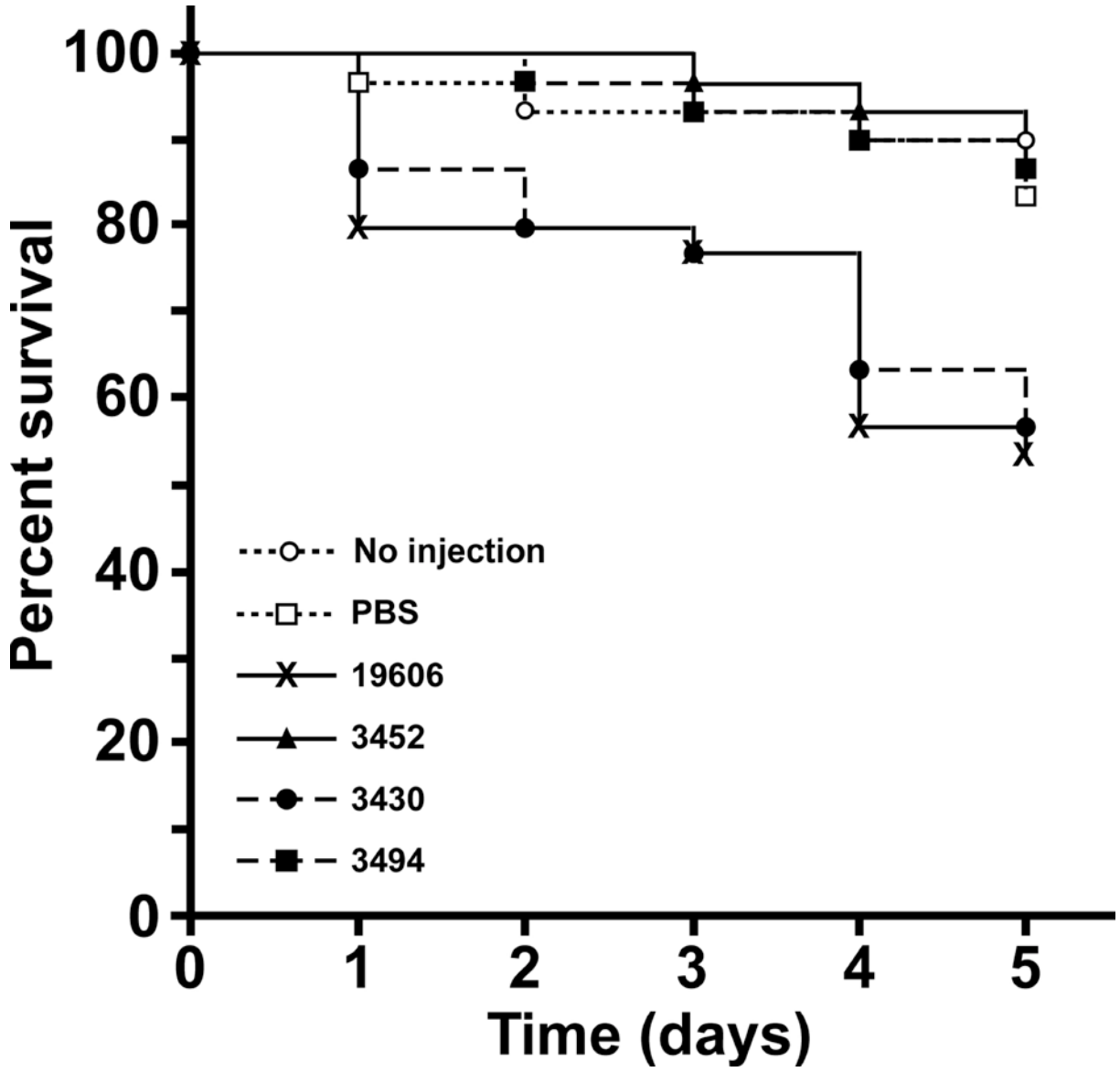

FIG 8 Role of *plc* in the virulence of ATCC 19606^T. *G. mellonella* larva (n = 30) were injected with 1 x 10^5 cells of the ATCC 19606^T parental strain or the isogenic derivatives 3430 (*plc2*::*aph*), 3452 (*plc1*::*aph-FRT*) or 3494 (*plc1::ermAM/plc2::aph*) and incubated at 37°C in darkness. Negative controls included uninjected larva or larva injected with sterile PBS. Larva survival was monitored daily for five days with removal of dead larva at times of inspection.

SUPPLEMENTAL MATERIALS

TABLE S1 Primers used in this work

Number	Nucleotide sequence[a]
3171	5’-GTTGCTGACTCATACCAG-3’
3172	5’-ATTCCAACATGGATGCTG-3’
3815	5’-TTCCGGTACCAGAACAAA-3’
3822	5’-CATGATTACACGTCGTAAATT-3’
3823	5’-CTTAGATCATTGCGGGATCACTA-3’
3824	5’-ATGAATCGTCGCGAATTTCTTTT-3’
3825	5’-TTAAGACTCTAAATATCCCATA-3’
3826	5’-ATACCAAGCGCCTTGTAC-3’
3827	5’-GGCGATGGCATATGGTCA-3’
3905	5’-CGACTCAGATAATTCATCG-3’
3906	5’-GGATGAGCTAAACCAAGC-3’
3918	5’-CGAAACACGCTTTGAAGC-3’
3966	5’-CCTAGAGATAGTGGACGTTACTCG-3’
3967	5’-CCAGTATCGAATGCAATTCCCAAG-3’
3970	5’-GGAATGTATCGAGATGGAGATGC-3’
3971	5’-GTTAACACCACGTGTCACGC-3’
3972	5’-GGAACCAATGGACCTACAGG-3’
3973	5’-CGGCGATATTGCTTGAAACC-3’
3974	5’-CGTTGTAAAGCAGATGGTAAGGTG-3’
3975	5’-GGTCATAACGGCCTAAGTTATCG-3’
4003	5’-GTGTAGGCTGGAGCTGCTTC-3’
4004	5’-CGCCATTAATTCACTGATCA-3’
4017	5’-<u>TTA</u>ATACCAAGCGCCTTGTAC-3’
4018	5’-GAATACTTTAACCATCCAGCAGTAG-3’
4046	5’-GCAAACTTAAGAGTGTGTTG-3’
4047	5’-CCTTTAGTAACGTGTAACTTTC-3’

[a]Underlined sequence indicates the addition of a stop codon

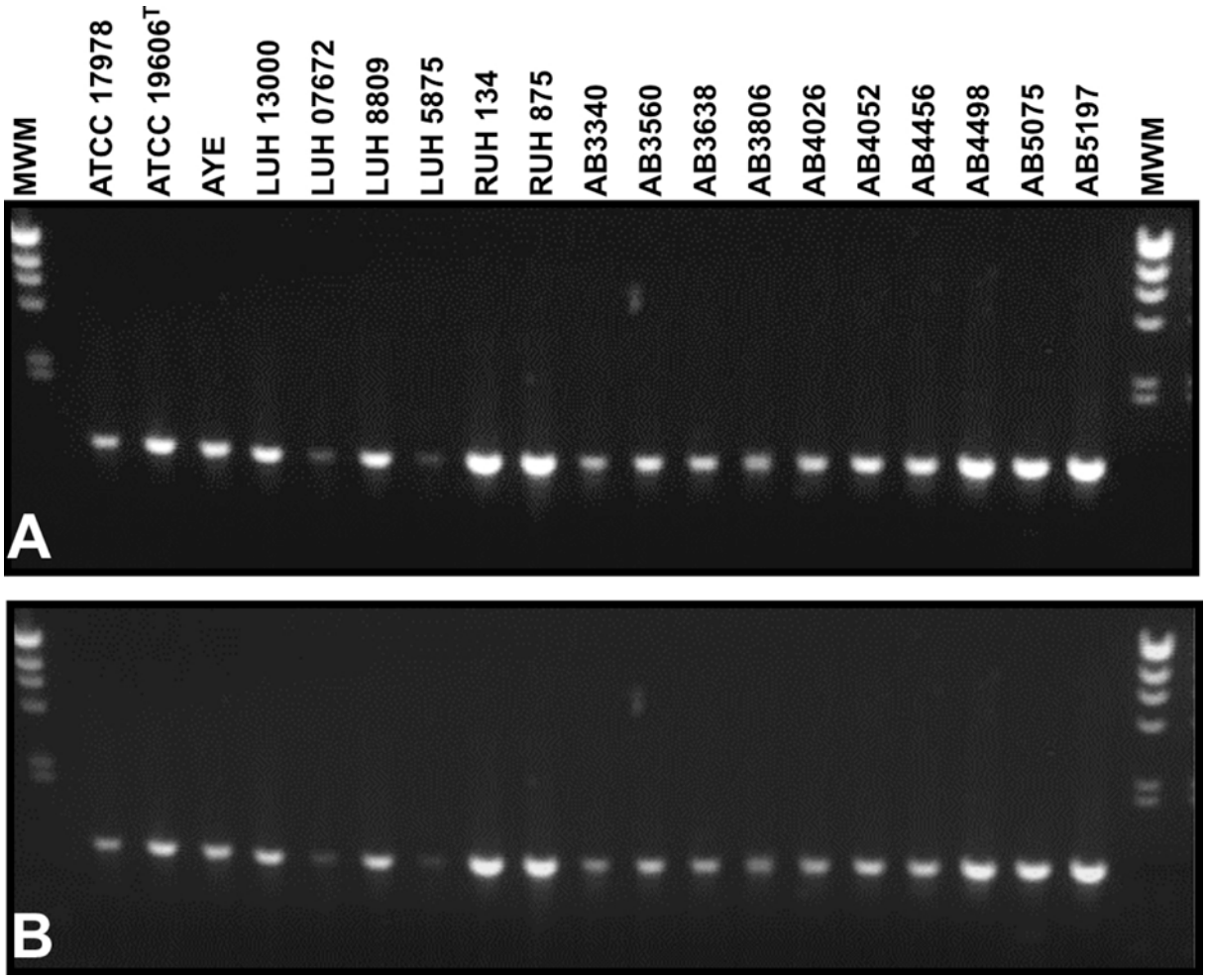

FIG S1 Detection of *plc1* and *plc2* in the genomes of *A. baumannii* strains. Agarose gel electrophoresis of internal amplicons of *plc1* (A) or *plc2* (B) using total genomic DNA isolated from 19 *A. baumannii* strains and primers 3824 and 3826 or 3822 and 3827 (Table 1 and Fig. 2), which hybridize internally to *plc1* or *plc2*, respectively. MWM, *Hin*dIII-digested λ DNA.

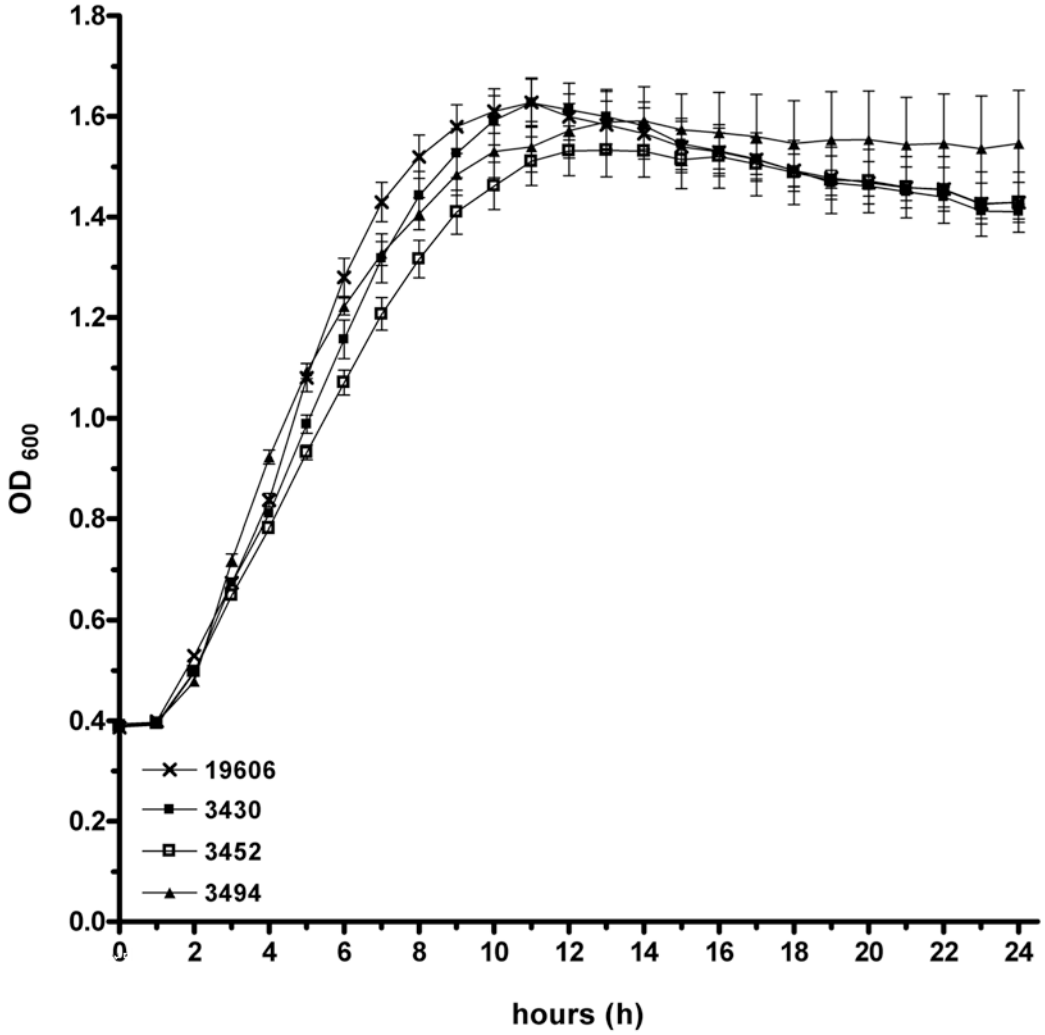

FIG S2 Growth of the ATCC 19606^T parental strain and the 3430, 3452 and 3494 isogenic derivatives. The OD_{600} values of each strain grown in TSBD at 37°C for 24 h with shaking at 200 rpm were determined hourly. Error bars represent the standard error (SE) of the mean.

Appendix 4

genomeA Journals.ASM.org

Draft Genome Sequences of *Klebsiella pneumoniae* Clinical Type Strain ATCC 13883 and Three Multidrug-Resistant Clinical Isolates

Brock A. Arivett,[a] David C. Ream,[a] Steven E. Fiester,[a] Katrin Mende,[b,c] Clinton K. Murray,[b] Mitchell G. Thompson,[d] Shrinidhi Kanduru,[d] Amy M. Summers,[d] Amanda L. Roth,[d] Daniel V. Zurawski,[d] Luis A. Actis[a]

Department of Microbiology, Miami University, Oxford, Ohio, USA[a]; Department of Medicine, San Antonio Military Medical Center, JBSA Fort Sam Houston, San Antonio, Texas, USA[b]; Infectious Disease Clinical Research Program, Uniformed Services University of the Health Sciences, Bethesda, Maryland, USA[c]; Department of Wound Infections, Walter Reed Army Institute of Research (WRAIR), Silver Spring, Maryland, USA[d]

***Klebsiella pneumoniae* is a Gram-negative human pathogen capable of causing hospital-acquired infections with an increasing risk to human health. The total DNA from four clinically relevant strains was sequenced to >100× coverage, providing high-quality genome assemblies for *K. pneumoniae* strains ATCC 13883, KP4640, 101488, and 101712.**

Received 21 November 2014 **Accepted** 4 December 2014 **Published** 15 January 2015

Citation Arivett BA, Ream DC, Fiester SE, Mende K, Murray CK, Thompson MG, Kanduru S, Summers AM, Roth AL, Zurawski DV, Actis LA. 2015. Draft genome sequences of *Klebsiella pneumoniae* clinical type strain ATCC 13883 and three multidrug-resistant clinical isolates. Genome Announc 3(1):e01385-14. doi:10.1128/genomeA.01385-14.

Address correspondence to Luis A. Actis, actisla@MiamiOH.edu.

Klebsiella pneumoniae is the fourth most common cause of Gram-negative-associated hospital-acquired infections, including urinary tract infections, pneumonia, septicemia, and wound infections (1, 2). The nosocomial prevalence of *K. pneumoniae* is exacerbated by the emergence of multidrug-resistant strains, especially those producing carbapenemase (KPC-1). This has made *K. pneumoniae* a threat to human health worldwide. Many reports have explored the multidrug resistance and capsular properties of *K. pneumoniae*; however, there remains a paucity of literature regarding the elucidation of virulence factors and the general physiology of this pathogen. The dearth of information is highlighted by the absence of the genome sequence of the *K. pneumoniae* clinical type strain ATCC 13883 from publicly available databases. To this end, the genome sequence of strain ATCC 13883, as well as those of *K. pneumoniae* strains KP4640, 101712, and 101488, three strains isolated from wounded warriors at the Walter Reed Army Medical Center (WRAMC) and San Antonio Military Medical Center (SAMMC), Fort Sam Houston, TX, were determined using next-generation sequencing methods.

The strains were routinely stored at -80°C in 10% glycerol. DNA was isolated from overnight LB cultures grown with agitation at 37°C using the DNeasy blood and tissue kit (Qiagen, Valencia, CA). The absorption at 260 nm and 280 nm was measured for each sample to determine quantity and quality using the NanoDrop 2000 (Thermo Scientific, Wilmington, DE, USA). The DNA concentrations for library preparation were determined by the SYBR green (Life Technologies, Grand Island, NY) standard curve method in a black 96-well plate (Corning, Tewksbury, MA, USA) using a FilterMax F5 spectrophotometer with Multimode Analysis software version 3.4.0.25 (Molecular Devices, Sunnyvale, CA, USA). The Nextera XT kit (Illumina, San Diego, CA, USA) was used to simultaneously fragment and adapter tag the libraries, as per the manufacturer's instructions. Library production was visualized with a Bioanalyzer 2100 high-sensitivity DNA analysis kit (Agilent Technologies, Santa Clara, CA) using the version B.02.08.SI648 software to analyze the fragmentation of the resultant libraries. Individual libraries were normalized by bead-based affinity, pooled, and then sequenced using the MiSeq v3 600-cycle kit (Illumina, San Diego, CA, USA) to perform 300-bp paired-end sequencing on a MiSeq instrument (Illumina), per the manufacturer's instructions. *De novo* assembly was performed using Genomics Workbench 7.5 with the Bacterial Genome Finishing Module (CLC bio, Boston, MA), run on a workstation with an AMD Opteron 2.10 GHz 16-core processor with 128 GB DDR3 ECC random access memory (RAM). The genomes were annotated with Prokka version 1.10 on a quadcore i7 workstation with 32 GB DDR3 running Ubuntu 14.04 long-term support (LTS) (3).

The *de novo* assembly resulted in a 5,725,870-bp genome containing 68 tRNAs and 5,525 genes with 5,456 proposed coding sequences (CDS) for the clinical type strain ATCC 13883. The remaining three genomes were 5,590,832, 5,570,720, and 5,575,268 bp for strains KP4640, 101488, and 101712, respectively. The strain KP4640 genome contains 71 tRNAs and 5,270 genes with 5,198 CDS. Strains 101488 and 101712 have 75 and 73 tRNAs, 5,375 and 5,208 genes, and 5,299 and 5,134 CDS, respectively.

Nucleotide sequence accession numbers. The whole-genome shotgun projects were deposited into GenBank under Bioproject ID PRJNA261239 with accession numbers JSZI00000000 (ATCC 13883), JSZJ00000000 (101712), JSZK00000000 (101488), and JSZL00000000 (KP4640). The versions described in this paper are versions JSZI01000000 (ATCC 13883), JSZJ01000000 (101712), JSZK01000000 (101488), and JSZL01000000 (KP4640).

ACKNOWLEDGMENTS

This work was supported by funds from Miami University, Department of Defense W81XWH-12-2-0035 award to L.A.A. and a grant-in-aid from Illumina, Inc. (San Diego, CA).

We thank the MRSN for supplying KP4640. We also thank Andor Kiss

and the Miami University Center for Bioinformatics and Functional Genomics for assistance in sequence acquisition.

The findings and opinions expressed herein belong to the authors and do not necessarily reflect the official views of the WRAIR, the U.S. Army, or the Department of Defense.

REFERENCES

1. **Hidron AI, Edwards JR, Patel J, Horan TC, Sievert DM, Pollock DA, Fridkin SK, National Healthcare Safety Network Team, Participating National Healthcare Safety Network Facilities.** 2008. NHSN annual update: antimicrobial-resistant pathogens associated with healthcare-associated infections: annual summary data reported to the National Healthcare Safety Network at the Centers for Disease Control and Prevention, 2006–2007. Infect Control Hosp Epidemiol **29:**996–1011. http://dx.doi.org/10.1086/591861.
2. **Podschun R, Ullmann U.** 1998. *Klebsiella* spp. as nosocomial pathogens: epidemiology, taxonomy, typing methods, and pathogenicity factors. Clin Microbiol Rev **11:**589–603.
3. **Seemann T.** 2014. Prokka: rapid prokaryotic genome annotation. Bioinformatics **30:**2068–2069. http://dx.doi.org/10.1093/bioinformatics/btu153.

Appendix 5

genomeA Journals.ASM.org

Draft Genome of the Multidrug-Resistant *Acinetobacter baumannii* Strain A155 Clinical Isolate

Brock A. Arivett,[a] Steven E. Fiester,[a] David C. Ream,[a] Daniela Centrón,[b] Maria S. Ramírez,[c] Marcelo E. Tolmasky,[c] Luis A. Actis[a]

Department of Microbiology, Miami University, Oxford, Ohio, USA[a]; Instituto de Microbiología y Parasitología Médica, Universidad de Buenos Aires, Consejo Nacional de Investigaciones Científicas y Tecnológicas, Buenos Aires (IMPaM, UBA-CONICET), Ciudad Autónoma de Buenos Aires, Argentina[b]; Department of Biological Science, Center for Applied Biotechnology Studies, California State University Fullerton, Fullerton, California, USA[c]

***Acinetobacter baumannii* is a bacterial pathogen with serious implications on human health, due to increasing reports of multidrug-resistant strains isolated from patients. Total DNA from the multidrug-resistant *A. baumannii* strain A155 clinical isolate was sequenced to greater than 65× coverage, providing high-quality contig assemblies.**

Received 16 February 2015 **Accepted** 18 February 2015 **Published** 26 March 2015

Citation Arivett BA, Fiester SE, Ream DC, Centrón D, Ramírez MS, Tolmasky ME, Actis LA. 2015. Draft genome of the multidrug-resistant *Acinetobacter baumannii* strain A155 clinical isolate. Genome Announc 3(2):e00212-15. doi:10.1128/genomeA.00212-15.

Address correspondence to Luis A. Actis, actisla@miamioh.edu.

Acinetobacter baumannii, a Gram-negative pathogen, causes a variety of nosocomial infections such as bacteremia, meningitis, skin and soft tissue infections such as necrotizing fasciitis, ventilator-associated pneumonia, and urinary tract infections (1, 2). These infections are becoming harder to treat due to the rise in the number of multidrug-resistant *A. baumannii* strains present in clinical settings (1, 3). *A. baumannii* strain A155 is a multidrug-resistant strain originally isolated from a urinary sample at a hospital in Buenos Aires, Argentina, in 1994 (4). At that time, unlike in most of the world where clonal complex 109 (CC109) and CC92 (also known as international clonal lineage 1 and 2, respectively) were predominant, most strains isolated in Argentina belonged to CC113 (5). *A. baumannii* A155 was among the first CC109 isolates in Argentina (4). This strain includes the AbaR-type island inserted within *comM*, and the *aac(6′)-Ib* gene, which confers resistance to numerous aminoglycosides (4, 6, 7).

A. baumannii A155 whole-genome sequencing and annotation were performed as described previously (8). Briefly, the A155 isolate was routinely stored at −80°C in 10% glycerol, passaged to overnight LB cultures grown with agitation at 37°C, and total DNA was isolated using the DNeasy blood and tissue kit (Qiagen, Valencia, CA, USA). DNA quantity and quality were assessed using Nanodrop 2000 (Thermo Scientific, Wilmington, DE, USA). The SYBR Green (Life Technologies, Grand Island, NY, USA) standard curve method was used to estimate DNA concentration for library preparation in a black 96-well plate (Corning, Tewksbury, MA, USA), and fluorescence values were obtained using a FilterMax F5 spectrophotometer with Multi-Mode Analysis software version 3.4.0.25 (Molecular Devices, Sunnyvale, CA, USA). The Nextera XT kit (Illumina, Inc., San Diego, CA, USA) was used to simultaneously fragment and construct adapter-tagged libraries per the manufacturer's instructions. The Bioanalyzer 2100 High Sensitivity DNA analysis kit (Agilent Technologies, Santa Clara, CA, USA) with version B.02.08.SI648 software was used to determine the fragmentation of the resultant libraries. Individual libraries were normalized by bead-based affinity, pooled, and then sequenced using the MiSeq version 3 600-cycle kit (Illumina) to perform 300-bp paired-end sequencing on a MiSeq instrument (Illumina) per the manufacturer's instructions. *De novo* assembly was performed using Genomics Workbench version 7.5 with the Bacterial Genome Finishing module (CLC bio, Boston, MA, USA) on a workstation with an AMD Opteron 2.10-GHz 16-core processor and 128-GB DDR3 ECC RAM. Genomes were annotated with Prokka version 1.10 on a quadcore i7 workstation with 32-GB DDR3 running Ubuntu 14.04 LTS (9).

The *de novo* assembly resulted in a 3,933,455-bp genome encoding 55 tRNAs and 3,760 genes with 3,704 proposed CDSs for the *A. baumannii* A155 clinical strain.

Nucleotide sequence accession numbers. The first version of the *de novo* whole-genome assembly of *A. baumannii* A155 was deposited into GenBank under Bioproject ID PRJNA261239 with the accession number JXSV00000000, version JXSV01000000.

ACKNOWLEDGMENTS

This work was supported by funds from Miami University, Department of Defense W81XWH-12-2-0035 award (to L.A.A.), and a grant-in-aid from Illumina, Inc. (San Diego, CA, USA).

The findings and opinions expressed herein belong to the authors and do not necessarily reflect the official views of the WRAIR, the U.S. Army, or the Department of Defense.

We thank Andor Kiss and the Miami University Center for Bioinformatics and Functional Genomics for assistance in sequence acquisition.

REFERENCES

1. **Roca I, Espinal P, Vila-Farrés X, Vila J.** 2012. The *Acinetobacter baumannii* oxymoron: commensal hospital dweller turned pan-drug-resistant menace. Front Microbiol **3**:148. http://dx.doi.org/10.3389/fmicb.2012.00148.
2. **Hartstein AI, Rashad AL, Liebler JM, Actis LA, Freeman J, Rourke JW, Jr, Stibolt TB, Tolmasky ME, Ellis GR, Crosa JH.** 1988. Multiple intensive care unit outbreak of *Acinetobacter calcoaceticus* subspecies *anitratus* respiratory infection and colonization associated with contaminated, reusable ventilator circuits and resuscitation bags. Am J Med **85**:624–631. http://dx.doi.org/10.1016/S0002-9343(88)80233-X.
3. **Perez F, Hujer AM, Hujer KM, Decker BK, Rather PN, Bonomo RA.**

2007. Global challenge of multidrug-resistant *Acinetobacter baumannii*. Antimicrob Agents Chemother **51:**3471–3484. http://dx.doi.org/10.1128/AAC.01464-06.

4. **Ramírez MS, Vilacoba E, Stietz MS, Merkier AK, Jeric P, Limansky AS, Márquez C, Bello H, Catalano M, Centrón D.** 2013. Spreading of AbaR-type genomic islands in multidrug resistance *Acinetobacter baumannii* strains belonging to different clonal complexes. Curr Microbiol **67:**9–14. http://dx.doi.org/10.1007/s00284-013-0326-5.
5. **Stietz MS, Ramírez MS, Vilacoba E, Merkier AK, Limansky AS, Centrón D, Catalano M.** 2013. *Acinetobacter baumannii* extensively drug resistant lineages in Buenos Aires hospitals differ from the international clones I–III. Infect Genet Evol **14:**294–301. http://dx.doi.org/10.1016/j.meegid.2012.12.020.
6. **Lin DL, Tran T, Alam JY, Herron SR, Ramirez MS, Tolmasky ME.** 2014. Inhibition of aminoglycoside 6′-*N*-acetyltransferase type Ib by zinc: reversal of amikacin resistance in *Acinetobacter baumannii* and *Escherichia coli* by a zinc ionophore. Antimicrob Agents Chemother **58:**4238–4241. http://dx.doi.org/10.1128/AAC.00129-14.
7. **Ramirez MS, Tolmasky ME.** 2010. Aminoglycoside modifying enzymes. Drug Resist Updat **13:**151–171. http://dx.doi.org/10.1016/j.drup.2010.08.003.
8. **Arivett BA, Ream DC, Fiester SE, Mende K, Murray CK, Thompson MG, Kanduru S, Summers AM, Roth AL, Zurawski DV, Actis LA.** 2015. Draft genome sequences of *Klebsiella pneumoniae* clinical type strain ATCC 13883 and three multidrug-resistant clinical isolates. Genome Announc **3**(1):e01385-14. http://dx.doi.org/10.1128/genomeA.01385-14.
9. **Seemann T.** 2014. Prokka: rapid prokaryotic genome annotation. Bioinformatics **30:**2068–2069. http://dx.doi.org/10.1093/bioinformatics/btu153.

Appendix 6

jga00416/jga4273d16z | xppws | S=5 | 7/11/16 | 12:12 | Subject: Prokaryotes | DOI:10.1128/genomeA.00773-16 | NLM: brief-report

AMERICAN SOCIETY FOR MICROBIOLOGY | genomeAnnouncements

Draft Genome Sequences of *Acinetobacter baumannii* Isolates from Wounded Military Personnel

AQ: au Brock A. Arivett,[a,b] Dave C. Ream,[a] Steven E. Fiester,[a] Destaalem Kidane,[b] Luis A. Actis[a]

AQ: aff Department of Microbiology, Miami University, Oxford, Ohio, USA[a]; Biology Department, Middle Tennessee State University, Murfreesboro, Tennessee, USA[b]

***Acinetobacter baumannii* is a Gram-negative bacterium capable of causing hospital-acquired infections that ~~have~~ been grouped ~~as~~ *Enterococcus faecium*, *Staphylococcus aureus*, *Klebsiella pneumoniae*, *Acinetobacter baumannii*, *Pseudomonas aeruginosa*, and *Enterobacter* species ~~(~~ESKAPE~~)~~ pathogens because their extensive drug resistance phenotypes and increasing risk to human health. Twenty-four multidrug-resistant *A. baumannii* strains isolated from wounded military were sequenced and annotated.**

Received 8 June 2016 **Accepted** 6 July 2016 **Published** XXX

Citation Arivett BA, Ream DC, Fiester SE, Kidane D, Actis LA. 2016. Draft genome sequences of *Acinetobacter baumannii* isolates from wounded military personnel. Genome Announc 4(4):e00773-16. doi:10.1128/genomeA.00773-16.

Address correspondence to Luis A. Actis, actisla@miamioh.edu.

The Gram-negative coccobacillus *Acinetobacter baumannii* is an opportunistic human pathogen causing myriad human diseases, including pneumonia, bacteremia, urinary tract infections, meningitis, and wound infections. *A. baumannii* is the fifth most common Gram-negative pathogen associated with nosocomial infections (1, 2). Of concern is the increasing multidrug resistance of *A. baumannii* isolates, which has caused this bacterium to be included as an ESKAPE (*Enterococcus faecium, Staphylococcus aureus, Klebsiella pneumoniae, Acinetobacter baumannii, Pseudomonas aeruginosa*, and *Enterobacter* species) pathogen, underscoring its ability to "escape" antimicrobials (3). In fact, *A. baumannii* strains resistant to all known antibiotics have been encountered, demonstrating the paramount impact of this pathogen on public health (2). The genomes of 24 *A. baumannii* strains isolated from wounded warriors at Walter Reed Army Medical Center (WRAMC) and San Antonio Military Medical Center (SAMMC), Fort Sam, Houston, TX, were sequenced using next-generation sequencing for future analyses to investigate the resistance and virulence mechanisms of this emerging pathogen.

As described previously, strains were routinely stored at -80°C in 10% glycerol (4). DNA was isolated from overnight LB cultures grown with agitation at 37°C using the DNeasy blood and tissue kit (Qiagen, Valencia, CA, USA). Absorption at 260 nm and 280 nm was measured for each sample to determine quantity and quality using the NanoDrop 2000 (Thermo Scientific, Wilmington, DE, USA). DNA concentrations for library preparation were determined by the SYBR green (Life Technologies, Grand Island, NY) standard curve method in a black 96-well plate (Corning, Tewksbury, MA, USA) using a FilterMax F5 spectrophotometer with multimode analysis software version 3.4.0.25 (Molecular Devices, Sunnyvale, CA, USA). Whole DNA was sheared to approximately 500 bp in a microTUBE-50 using an M220 focused ultrasonicator (Covaris, Woburn, MA, USA). Fragmentation of the resultant libraries was examined with a Bioanalyzer 2100 high-sensitivity DNA analysis kit (Agilent Technologies, Santa Clara, CA, USA) using version B.02.08.SI648 software. Individual libraries were normalized, pooled, and then sequenced using the MiSeq version 3 600-cycle kit (Illumina, San Diego, CA, USA) to perform 300-bp paired-end sequencing on a MiSeq instrument (Illumina), as per the manufacturer's instructions. *De novo* assembly was performed using Genomics Workbench 8.0 with the Bacterial Genome Finishing module (CLC bio, Boston, MA) run on a workstation with an AMD Opteron 2.10 GHz 16-core processor with 128 Gb DDR3 ECC random access memory (RAM). Genomes were annotated with Prokka version 1.10 on a quad-core i7 workstation with 32 Gb DDR3 running Ubuntu 14.04 LTS (5). The *de novo* assembly statistics for 24 *A. baumannii* isolates are shown in Table 1. T1

Accession numbers. The whole-genome shotgun projects were deposited into GenBank under BioProject ID PRJNA261239 with accession numbers listed in Table 1.

ACKNOWLEDGMENTS

This work was supported by funds from Miami University and U.S. Department of Defense W81XWH-12-2-0035 award to L.A.A.

We are grateful to Daniel V. Zurawski from Walter Reed Army Institute of Research for providing the *A. baumannii* strains listed in Table 1. We also thank Andor Kiss and the Miami University Center for Bioinformatics and Functional Genomics for assistance in sequence acquisition.

The findings and opinions expressed herein belong to the authors and do not necessarily reflect the official views of the WRAIR, the U.S. Army, or the Department of Defense.

FUNDING INFORMATION

This work, including the efforts of Luis A Actis, was funded by U.S. Department of Defense (DOD) (W81XWH-12-2-0035).

REFERENCES

1. **Hidron AI, Edwards JR, Patel J, Horan TC, Sievert DM, Pollock DA, Fridkin SK, National Healthcare Safety Network Team, Participating National Healthcare Safety Network Facilities.** 2008. NHSN annual update: antimicrobial-resistant pathogens associated with health care-associated infections: annual summary of data reported to the National Healthcare Safety Network at the Centers for Disease Control and Prevention, 2006–2007. Infect Control Hosp Epidemiol **29**:996–1011. http://dx.doi.org/10.1086/591861.

TABLE 1 Assembly metrics and accession numbers of *A. baumannii* genomes

Strain ID	No. of contigs	N_{50} contig size (bp)	Total size (bp)	Coverage (×)	% G+C content	No. of ORFs[a]	No. of RNA	Accession no.
AB2828	107	124,070	4,426,896	30	39.21	4,274	53	LRDT000000000
AB3340	76	132,604	4,010,248	28	38.86	3,864	49	LRDU000000000
AB3560	58	247,914	4,012,126	30	38.92	3,894	59	LRDV000000000
AB967	27	401,652	3,795,032	29	38.84	3,633	62	LRDS000000000
AB3785	70	134,647	3,894,584	29	39.01	3,745	58	LRDX000000000
AB3638	78	108,414	4,294,582	31	38.72	4,113	62	LRDW000000000
AB3806	86	96,852	4,295,294	33	38.75	4,117	59	LRDY000000000
AB3927	45	227,995	4,113,781	30	38.82	3,978	58	LRDZ000000000
AB4026	67	160,728	3,905,198	30	38.99	3,749	50	LREB000000000
AB4027	72	152,887	3,903,961	32	39.00	3,749	54	LREC000000000
AB4025	69	152,887	3,902,672	29	39.00	3,741	55	LREA000000000
AB4456	58	182,799	4,001,807	27	38.92	3,857	47	LREF000000000
AB4052	43	262,160	3,921,338	33	39.00	3,739	51	LRED000000000
AB4448	43	369,360	3,992,257	28	38.92	3,854	58	LREE000000000
AB4490	98	84,980	3,947,403	31	38.99	3,786	60	LREG000000000
AB4498	76	128,212	3,905,177	32	39.00	3,753	57	LREH000000000
AB4795	78	113,293	3,882,341	33	39.03	3,727	62	LREI000000000
AB4878	45	223,470	3,862,567	26	38.98	3,685	50	LREJ000000000
AB4957	50	223,470	3,882,040	33	38.97	3,722	60	LREL000000000
AB4932	39	237,199	3,865,974	33	38.99	3,703	60	LREK000000000
AB5001	33	223,470	3,789,469	30	38.99	3,586	52	LREN000000000
AB4991	52	310,788	3,877,107	28	39.09	3,686	58	LREM000000000
AB5674	34	419,504	3,869,253	29	39.03	3,679	52	LREP000000000
AB5197	58	184,472	3,959,484	33	39.04	3,799	58	LREO000000000

[a] ORFs, open reading frames.

2. **Peleg AY, Seifert H, Paterson DL.** 2008. *Acinetobacter baumannii*: emergence of a successful pathogen. Clin Microbiol Rev **21:**538–582. http://dx.doi.org/10.1128/CMR.00058-07.
3. **Rice L.** 2008. Federal funding for the study of antimicrobial resistance in nosocomial pathogens: no ESKAPE. J Infect Dis **197:**1079–1081. http://dx.doi.org/10.1086/533452.
4. **Arivett BA, Ream DC, Fiester SE, Mende K, Murray CK, Thompson MG, Kanduru S, Summers AM, Roth AL, Zurawski DV, Actis LA.** 2015. Draft genome sequences of *Klebsiella pneumoniae* clinical type strain ATCC 13883 and three multidrug-resistant clinical isolates. Genome Announc **3**(1):e01385-14. http://dx.doi.org/10.1128/genomeA.01385-14.
5. **Seemann T.** 2014. Prokka: rapid prokaryotic genome annotation. Bioinformatics **30:**2068–2069. http://dx.doi.org/10.1093/bioinformatics/btu153.

Appendix 7

jga00416/jga4205d16z | xppws | S=5 | 6/28/16 | 14:34 | Subject: Prokaryotes | DOI:10.1128/genomeA.00828-16 | NLM: brief-report

AMERICAN SOCIETY FOR MICROBIOLOGY | genomeAnnouncements

Draft Genome Sequences of *Escherichia coli* Isolates from Wounded Military Personnel

AQ: au Brock A. Arivett,[a,b] Dave C. Ream,[a] Steven E. Fiester,[a] Destaalem Kidane,[b] Luis A. Actis[a]

AQ: aff Department of Microbiology, Miami University, Oxford, Ohio, USA[a]; Biology Department, Middle Tennessee State University, Murfreesboro, Tennessee, USA[b]

Members of the *Escherichia coli* bacterial family have been grouped as ESKAPE (*Enterococcus faecium*, *Staphylococcus aureus*, *Klebsiella pneumoniae*, *Acinetobacter baumannii*, *Pseudomonas aeruginosa*, and *Enterobacter* species) pathogens because of their extensive drug resistance phenotypes and increasing threat to human health. The genomes of six extended-spectrum β-lactamase (ESBL)-producing *E. coli* strains isolated from wounded military personnel were sequenced and annotated.

Received 17 June 2016 **Accepted** 17 June 2016 **Published** XXX

Citation Arivett BA, Ream DC, Fiester SE, Kidane D, Actis LA. 2016. Draft genome sequences of *Escherichia coli* isolates from wounded military personnel. Genome Announc 4(4):e00828-16. doi:10.1128/genomeA.00828-16.

Address correspondence to Luis A. Actis, actisla@MiamiOH.edu.

Escherichia coli is a Gram-negative bacillus that is a component of the normal bacterial flora of the human colonic tract (1–3). *E. coli* within the intestinal tract is typically nonpathogenic unless the intestinal tract barriers have been violated or the host has been immunocompromised; however, there are also several highly adapted *E. coli* clones that have evolved to cause human diseases including meningitis, diarrhea, sepsis, and urinary tract infections (3). In fact, *E. coli* is the most common Gram-negative pathogen associated with nosocomial infections, and isolates with the ability to produce extended-spectrum β-lactamase (ESBL) continue to increase in frequency and severity (4, 5). The genomes of six ESBL-producing isolates obtained from wounded soldiers at the Walter Reed Army Medical Center (WRAMC) were sequenced using next-generation sequencing methods for future analyses to elucidate their virulence mechanisms.

As described previously, strains were routinely stored at −80°C in 10% glycerol (6). DNA was isolated from overnight LB cultures grown with agitation at 37°C using the DNeasy blood and tissue kit (Qiagen, Valencia, CA, USA). Absorption at 260 nm and 280 nm was measured for each sample to determine DNA quantity and quality using a Nanodrop 2000 (Thermo Scientific, Wilmington, DE, USA). DNA concentrations for library preparation were determined by the SYBR green (Life Technologies, Grand Island, NY, USA) standard curve method in black 96-well plates (Corning, Tewksbury, MA, USA) using a FilterMax F5 spectrophotometer with Multi-Mode Analysis software version 3.4.0.25 (Molecular Devices, Sunnyvale, CA, USA). Whole DNA was sheared to approximately 500 bp in a microTUBE-50 using the M220 Focused-ultrasonicator (Covaris, Woburn, MA, USA). Fragmentation of resultant libraries was examined with a Bioanalyzer 2100 high sensitivity DNA analysis kit (Agilent Technologies, Santa Clara, CA, USA) using version B.02.08.SI648 software. Individual libraries were normalized, pooled, and then sequenced using MiSeq v3 600-cycle kit (Illumina, San Diego, CA, USA) to perform 300-bp paired-end sequencing on a MiSeq instrument (Illumina) per manufacturer's instructions. *De novo* assembly was performed using Genomics Workbench 8.0 with the bacterial genome finishing module (CLC bio, Boston, MA, USA) on a workstation with an AMD Opteron 2.10 GHz 16-core processor with 128 GB DDR3 ECC RAM. Prokka version 1.10 on a quadcore i7 workstation with 32 GB DDR3 running Ubuntu 14.04 LTS (7) was used for genome annotation. The *de novo* assembly statistics for the sequenced *E. coli* isolates are shown in Table 1. T1

Accession number(s). The whole-genome shotgun projects were deposited into GenBank under Bioproject ID PRJNA261239 with the accession numbers listed in Table 1.

ACKNOWLEDGMENTS

This work was supported by funds from Miami University and the United States Department of Defense grant W81XWH-12-2-0035 awarded to L.A.A.

We are grateful to Daniel V. Zurawski from Walter Reed Army Insti-

TABLE 1 Assembly metrics and accession numbers of *Escherichia coli* genomes

Strain ID	No. of contigs	N_{50} contigs (bp)	Total size (bp)	Coverage (×)	% G+C	No. of ORFs[a]	No. of RNAs	Accession no.
105454	101	191,011	5,335,253	16	50.68	5,121	70	LOJL000000000
105547	93	127,705	4,858,207	18	50.68	4,649	74	LOJM000000000
109497	99	222,697	5,221,557	34	50.78	5,050	74	LORD000000000
108191	98	115,521	4,727,016	28	50.81	4,518	73	LORE000000000
105433	89	138,092	4,820,700	33	50.74	4,556	73	LORF000000000
105438	81	204,373	5,226,940	34	50.68	4,996	60	LORC000000000

[a] Open reading frames.

tute of Research for providing the *E. coli* strains listed in Table 1. We would also like to thank Andor Kiss and the Miami University Center for Bioinformatics and Functional Genomics for assistance in sequence acquisition.

The findings and opinions expressed herein belong to the authors and do not necessarily reflect the official views of the WRAIR, the U.S. Army, or Department of Defense.

FUNDING INFORMATION

This work, including the efforts of Luis A Actis, was funded by U.S. Department of Defense (DOD) (W81XWH-12-2-0035).

REFERENCES

1. **Edwards PR, Ewing WH**. 1972. Identification of *Enterobacteriaceae*, 3rd ed. Burgess Publishing Company, Minneapolis, MN.
2. **Bettelheim KA**. 1994. Biochemical characteristics of *Escherichia coli*, p 3–30. In Gyles CL (ed), *Escherichia coli* in domestic animals and humans. CAB International, Wallingford, United Kingdom.
3. **Nataro JP, Kaper JB**. 1998. Diarrheagenic *Escherichia coli*. Clin Microbiol Rev **11:**142–201. PubMed.
4. **Boucher HW, Talbot GH, Bradley JS, Edwards JE, Gilbert D, Rice LB, Scheld M, Spellberg B, Bartlett J**. 2009. Bad bugs, no drugs: no ESKAPE! An update from the Infectious Diseases Society of America. Clin Infect Dis **48:**1–12. http://dx.doi.org/10.1086/595011.
5. **Hidron AI, Edwards JR, Patel J, Horan TC, Sievert DM, Pollock DA, Fridkin SK, National Healthcare Safety Network Team, Participating National Healthcare Safety Network Facilities**. 2008. Antimicrobial-resistant pathogens associated with health care-associated infections: annual summary of data reported to the National Healthcare Safety Network at the Centers for Disease Control and Prevention, 2006–2007. Infect Control Hosp Epidemiol **29:**996–1011. http://dx.doi.org/10.1086/591861.
6. **Arivett BA, Ream DC, Fiester SE, Mende K, Murray CK, Thompson MG, Kanduru S, Summers AM, Roth AL, Zurawski DV, Actis LA**. 2015. Draft genome sequences of *Klebsiella pneumoniae* clinical type strain ATCC 13883 and three multidrug-resistant clinical isolates. Genome Announc **3**(1):e01385-01314. http://dx.doi.org/10.1128/genomeA.01385-14.
7. **Seemann T**. 2014. Prokka: rapid prokaryotic genome annotation. Bioinformatics **30:**2068–2069. http://dx.doi.org/10.1093/bioinformatics/btu153.

Appendix 8

AMERICAN SOCIETY FOR MICROBIOLOGY | genomeAnnouncements

Draft Genome Sequences of *Pseudomonas aeruginosa* Isolates from Wounded Military Personnel

AQ: au Brock A. Arivett,[a,b] Dave C. Ream,[a] Steven E. Fiester,[a] Destaalem Kidane,[b] Luis A. Actis[a]

AQ: aff Department of Microbiology, Miami University, Oxford, Ohio, USA[a]; Biology Department, Middle Tennessee State University, Murfreesboro, Tennessee, USA[b]

***Pseudomonas aeruginosa*, a Gram-negative bacterium that causes severe hospital-acquired infections, is grouped as an ESKAPE (*Enterococcus faecium, Staphylococcus aureus, Klebsiella pneumoniae, Acinetobacter baumannii, Pseudomonas aeruginosa*, and *Enterobacter* species) pathogen because of its extensive drug resistance phenotypes and effects on human health worldwide. Five multidrug resistant *P. aeruginosa* strains isolated from wounded military personnel were sequenced and annotated in this work.**

Received 17 June 2016 **Accepted** 17 June 2016 **Published** XXX

Citation Arivett BA, Ream DC, Fiester SE, Kidane D, Actis LA. 2016. Draft genome sequences of *Pseudomonas aeruginosa* isolates from wounded military personnel. Genome Announc 4(4):e00829-16. doi:10.1128/genomeA.00829-16.

Address correspondence to Luis A. Actis, actisla@MiamiOH.edu.

Pseudomonas aeruginosa is a common environmental Gram-negative bacillus bacterium often associated with nosocomial infections including chronic lung infections in cystic fibrosis patients and bacteremia in burn victims. Human infections with *P. aeruginosa* can likely be traced back to 1862 when Luke observed rod-shaped particles in the blue-green pus of infections allowing this bacterium the opportunity to develop into a formidable human pathogen (1). Nosocomial pathogens, such as *P. aeruginosa*, have developed sophisticated resistance mechanisms since the introduction of antibiotics into the clinical setting (2). *P. aeruginosa* is currently the second most prevalent Gram-negative nosocomial pathogen preceded by *Escherichia coli* with as many as 2% of *P. aeruginosa* isolates specifically presenting with carbapenem-resistance (3). *P. aeruginosa* is referred to as an ESKAPE (*Enterococcus faecium, Staphylococcus aureus, Klebsiella pneumoniae, Acinetobacter baumannii, Pseudomonas aeruginosa*, and *Enterobacter* species) pathogen due to its ability to escape the lethal action of antibiotics (4). In order to develop a broader understanding of the mechanisms by which nosocomial *P. aeruginosa* strains escape death by antibiotics, the genome sequences of five *P. aeruginosa* strains isolated from wounded soldiers at the Walter Reed Army Medical Center (WRAMC) were determined using next-generation sequencing methods for future bioinformatic analyses.

Strains routinely stored at −80°C in 10% glycerol (5) were used to isolate total DNA from overnight LB cultures grown with agitation at 37°C using the DNeasy blood and tissue kit (Qiagen, Valencia, CA, USA). Absorption at 260 nm and 280 nm was measured for each sample to determine quantity and quality using the Nanodrop 2000 (Thermo Scientific, Wilmington, DE, USA). DNA concentrations for library preparation were determined by the SYBR green (Life Technologies, Grand Island, NY, USA) standard curve method in black 96-well plates (Corning, Tewksbury, MA, USA) using a FilterMax F5 spectrophotometer with MultiMode Analysis software version 3.4.0.25 (Molecular Devices, Sunnyvale, CA, USA). Whole DNA was sheared to approximately 500 bp in microTUBE-50 using M220 Focused-ultrasonicator (Covaris, Woburn, MA, USA). Fragmentation of resultant libraries was examined with a Bioanalyzer 2100 High Sensitivity DNA analysis kit (Agilent Technologies, Santa Clara, CA, USA) using version B.02.08.SI648 software. Individual libraries were normalized, pooled and then sequenced using MiSeq v3 600-cycle kit (Illumina, San Diego, CA, USA) to perform 300-bp paired-end sequencing on a MiSeq instrument (Illumina) per manufacturer's instructions. *De novo* assembly was performed using Genomics Workbench 8.0 with the bacterial genome finishing module (CLC bio, Boston, MA, USA) on a workstation with an AMD Opteron 2.10 GHz 16-core processor with 128 GB DDR3 ECC RAM. Genomes were annotated with Prokka version 1.10 on a quadcore i7 workstation with 32 GB DDR3 running Ubuntu 14.04 LTS (6). The *de novo* assembly statistics for the five *P. aeruginosa* sequenced isolates are shown in Table 1. T1

TABLE 1 Assembly metrics and accession numbers of *Pseudomonas aeruginosa* Genomes

Strain ID	No. of contigs	N_{50} contigs (bp)	Total size (bp)	Coverage (×)	% G+C	No. of ORFs[a]	No. of RNAs	Accession no.
105777	105	179,475	7,408,561	30	65.33	7,012	67	LODH000000000
105819	63	302,533	7,208,927	26	65.65	6,703	68	LOHH000000000
105880	86	215,191	6,914,271	17	65.98	6,490	60	LOHI000000000
105857	93	304,460	6,933,765	27	65.99	6,563	67	LOHJ000000000
105738	137	102,664	6,783,146	39	66.06	6,269	67	LOHK000000000

[a] Open reading frames.

Accession number(s). The whole-genome shotgun projects were deposited into GenBank under Bioproject ID PRJNA261239 with accession numbers listed in Table 1.

ACKNOWLEDGMENTS

This work was supported by funds from Miami University and the United States Department of Defense grant W81XWH-12-2-0035 awarded to L.A.A.

We are grateful to Daniel V. Zurawski from Walter Reed Army Institute of Research for providing the *P. aeruginosa* strains listed in Table 1. We would also like to thank Andor Kiss and the Miami University Center for Bioinformatics and Functional Genomics for assistance in sequence acquisition.

The findings and opinions expressed herein belong to the authors and do not necessarily reflect the official views of the WRAIR, the U.S. Army, or Department of Defense.

FUNDING INFORMATION

This work, including the efforts of Luis A Actis, was funded by U.S. Department of Defense (DOD) (W81XWH-12-2-0035).

REFERENCES

1. **Lyczak JB, Cannon CL, Pier GB.** 2000. Establishment of *Pseudomonas aeruginosa* infection: lessons from a versatile opportunist. Microbes Infect **2:**1051–1060. http://dx.doi.org/10.1016/S1286-4579(00)01259-4.
2. **Breidenstein EB, de la Fuente-Núñez C, Hancock RE.** 2011. *Pseudomonas aeruginosa*: all roads lead to resistance. Trends Microbiol **19:**419–426. http://dx.doi.org/10.1016/j.tim.2011.04.005.
3. **Hidron AI, Edwards JR, Patel J, Horan TC, Sievert DM, Pollock DA, Fridkin SK, National Healthcare Safety Network Team, Participating National Healthcare Safety Network Facilities.** 2008. Antimicrobial-resistant pathogens associated with health care-associated infections: annual summary of data reported to the National Healthcare Safety Network at the Centers for Disease Control and Prevention, 2006–2007. Infect Control Hosp Epidemiol **29:**996–1011. http://dx.doi.org/10.1086/591861.
4. **Rice L.** 2008. Federal funding for the study of antimicrobial resistance in nosocomial pathogens: no ESKAPE. J Infect Dis **197:**1079–1081. http://dx.doi.org/10.1086/533452.
5. **Arivett BA, Ream DC, Fiester SE, Mende K, Murray CK, Thompson MG, Kanduru S, Summers AM, Roth AL, Zurawski DV, Actis LA.** 2015. Draft genome sequences of *Klebsiella pneumoniae* clinical type strain ATCC 13883 and three multidrug-resistant clinical isolates. Genome Announc **3**(1):e01385-01314. http://dx.doi.org/10.1128/genomeA.01385-14.
6. **Seemann T.** 2014. Prokka: rapid prokaryotic genome annotation. BioInformatics **30:**2068–2069. http://dx.doi.org/10.1093/bioinformatics/btu153.